Isospin 0 and 2 two-pion scattering at physical pion mass using all-to-all propagators with periodic boundary conditions in lattice QCD

Thomas Blum,[1,2] Peter A. Boyle,[3] Mattia Bruno,[4,5] Daniel Hoying,[6] Taku Izubuchi,[2,3] Luchang Jin,[1,2] Chulwoo Jung,[3] Christopher Kelly,[7] Christoph Lehner,[8] Aaron S. Meyer,[9,10] Amarjit Soni,[3] and Masaaki Tomii[1]

(RBC and UKQCD Collaborations)

[1]*Physics Department, University of Connecticut, Storrs, Connecticut 06269, USA*
[2]*RIKEN-BNL Research Center, Brookhaven National Laboratory, Upton, New York 11973, USA*
[3]*Physics Department, Brookhaven National Laboratory, Upton, New York 11973, USA*
[4]*Dipartimento di Fisica, Universitá di Milano-Bicocca, Piazza della Scienza 3, I-20126 Milano, Italy*
[5]*INFN, Sezione di Milano-Bicocca, Piazza della Scienza 3, I-20126 Milano, Italy*
[6]*Albert Einstein Center, Institute for Theoretical Physics, University of Bern, CH-3012 Bern, Switzerland*
[7]*Computational Science Initiative, Brookhaven National Laboratory, Upton, New York 11973, USA*
[8]*Fakultät für Physik, Universität Regensburg, Universitätsstraße 31, 93040 Regensburg, Germany*
[9]*Department of Physics, University of California, Berkeley, California 94720, USA*
[10]*Nuclear Science Division, Lawrence Berkeley National Laboratory, Berkeley, California 94720, USA*

(Received 1 February 2023; accepted 28 April 2023; published 23 May 2023)

A study of two-pion scattering for the isospin channels, $I = 0$ and $I = 2$, using lattice QCD is presented. Möbius domain-wall fermions, on top of the Iwasaki-DSDR gauge action for gluons with periodic boundary conditions, are used for the lattice computations, which are carried out on two ensembles of gauge field configurations generated by the RBC and UKQCD Collaborations with physical masses, inverse lattice spacings of 1.023 and 1.378 GeV, and spatial extents of $L = 4.63$ and 4.58 fm, respectively. The all-to-all propagator method is employed to compute a matrix of correlation functions of two-pion operators. The generalized eigenvalue problem (GEVP) is solved for a matrix of correlation functions to extract phase shifts with multiple states—two pions with a nonzero relative momentum, as well as two pions at rest. Our results for phase shifts for both the $I = 0$ and $I = 2$ channels are consistent with the Roy equation and chiral perturbation theory, though at this preliminary stage our errors for $I = 0$ are large. An important outcome of this work is that we are successful in extracting two-pion excited states, which are useful for studying $K \to \pi\pi$ decay, on physical-mass ensembles using the GEVP.

DOI: 10.1103/PhysRevD.107.094512

I. INTRODUCTION

Understanding the interactions of two pions is an interesting endeavor for practitioners of nonperturbative QCD. Not only do we learn how the fundamental interactions of quarks and gluons give rise to the observable properties of hadrons, but these two particle systems also play an important role in Standard Model processes under intense investigation, such as $K \to \pi\pi$ decays [1–3] and the muon's anomalous magnetic moment $g-2$ [4,5]. Our focus in this study is primarily on isospins $I = 0$ and 2 for the former, while $I = 1$ is important for the latter. Isospin symmetry and Bose-Einstein statistics constrain the states that appear in these processes.

With Lüscher's technique [6] that relates two-pion energy in a finite box with the corresponding scattering phase shift, there have been many studies of two-pion scattering in lattice QCD at unphysical pion masses [7–20]. For these studies, a chiral extrapolation was needed to obtain physical results. The analytic evaluation of two-pion scattering in chiral perturbation theory [21,22] (ChPT) was employed in these works to perform the extrapolation of important parameters of two-pion scattering, such as the scattering length. While we can expect the extrapolation to be reasonable for the scattering length, which can be extracted near the two-pion threshold, the extrapolation of the scattering amplitudes or phase shifts might not be accurate at high energies.

Now, it is possible to perform a lattice calculation at the physical pion mass so that we can directly compute the two-pion phase shifts at relatively large energies without a chiral extrapolation. There was a study where the $I = 2$ scattering length was computed including the physical pion mass for the first time [23]. The $I = 0$ channel is challenging already at unphysical pion masses [7,15,17–19] because of the presence of disconnected diagrams and two-pion operators coupling with the vacuum state. This paper is part of a series of studies of two-pion scattering undertaken by the RBC and UKQCD Collaborations [24,25], where the challenging $I = 0$ channel is examined at physical pion mass. Here, we present results for phase shifts at various energy levels for $I = 2$ and $I = 0$ at physical pion mass using $2 + 1$ flavors of Möbius domain-wall fermions (MDWFs) with periodic boundary conditions.

The RBC and UKQCD Collaborations have reported results for CP violation in kaon decays and pion phase shifts at the physical point for the corresponding $I = 0$ and 2 final states [2,3,24]. Because the physical kinematics for such decays requires pions with back-to-back relative momenta, which is not the ground state achieved in ordinary lattice calculations where the pions are at rest [26], G-parity spatial boundary conditions (GPBCs) were employed in the simulations [27]. GPBCs forbid pions with zero momentum, and if the box size is adjusted appropriately, then the two-pion ground state computed on the lattice will have physical momenta satisfying $E_{\pi\pi} \approx M_K$. In the GPBC two-pion scattering work [24], we obtained the phase shifts of the $I = 0$ channel as well as the $I = 2$ channel at various two-pion energies with nonzero pion momenta that are consistent with the prediction from the dispersion theory [28–32] based on the Roy equation [33] with inputs obtained by a combination of chiral perturbation theory for the scattering lengths and experimental data for the high-energy regime. GPBCs are not implemented without extra cost, however. They are at least twice as expensive for measurements compared with periodic boundary conditions, because the G-parity Dirac operator is explicitly two-flavor, with mixing between the flavors occurring at the boundary, and they also require gauge ensembles with the same boundary conditions to be generated. In addition, an important future step is to include isospin-breaking effects in the calculation of ε', which is expected to be significant, but GPBCs may not be suitable due to the intrinsic role of the isospin symmetry.

The long-term aim of this study is to explore the use of periodic boundary conditions (PBCs) to answer the question of whether the decay amplitudes with physical kinematics can be extracted reliably from an *excited state* computed on the lattice. As a first step, we investigate pion scattering in this setup.

Two-pion states with a definite total momentum can vary their total energy not only by a standard excitation of a single pion, but also by changing the momenta of individual pions, or equivalently, the relative momentum. A finite box forces the momenta to be quantized in units of $2\pi/L$ for PBCs, implying that the typical interval among two-pion energies is in general of $O(2\pi/L)$. At the same time, simulations are carried out with typical values of $m_\pi L$ of approximately 3.3–4 to keep exponential finite-volume effects under control. Therefore, as we lower the pion mass toward the physical value, the box size grows, and it may become increasingly challenging to extract the signals of an excited state with the statistical and systematic errors under control. This is the case especially for $I = 0$, where there are disconnected diagrams, and corresponding operators couple with the vacuum state. In fact, we learned from our earlier works [2,3,24] with GPBCs that there is significant higher-state contamination in two-pion correlation functions.

The generalized eigenvalue problem (GEVP) method [34,35] provides us with a systematic procedure to decompose correlation functions into contributions from the several lightest states with the same quantum numbers, which have been widely used for hadron spectrum studies. In our particular case, it turned out from earlier works [2,3,17,24] that introducing a σ operator for $I = 0$ in the measurements plays a crucial role in removing the contamination from excited states, and that the introduction of the σ operator significantly reduces the statistical error. In this work, we introduce a σ operator as well as four two-pion operators with various pion momenta for our measurements and use GEVP analysis to extract the ground and excited states.

In addition, we propose a variant of the GEVP approach which we call the *rebased* GEVP (RGEVP). The eigenvectors of the GEVP obtained at a certain time slice give us a new basis of operators. In principle, each operator in the new basis couples well with one of the lowest-energy states considered in the GEVP. With limited statistics, since we could lose the signal from one or more of those states at large time separations, it may be reasonable to exclude such noisy states by removing the corresponding operators from the basis so that all the states included in the GEVP analysis have good statistical precision. The purpose of the RGEVP is to reduce the size of the GEVP by using fewer operators that couple well with states. We find that this approach gives us an improvement on statistical precision for the ground and first excited states of the $I = 0$ channel.

We perform a lattice calculation for two-pion scattering with 258 configurations on the $24^3 \times 64$ lattice with the lattice cutoff $a^{-1} = 1.023$ GeV and 107 configurations on the $32^3 \times 64$ lattice with $a^{-1} = 1.378$ GeV [36,37]. Both ensembles are generated with $2 + 1$-flavor Möbius domain-wall fermions and Iwasaki plus dislocation suppressed determinant ratio (DSDR) gauge action. See Table I for more detail. We employ several cutting-edge lattice methods—all-mode-averaging (AMA) [38,39] and all-to-all

TABLE I. Ensemble parameters. $2+1$ flavors of Möbius domain-wall fermions, generated by the RBC/UKQCD Collaborations [36,37]. Trajectories used for measurements are separated by 10 or 20 Monte Carlo time units. The last column refers to the number of configurations in each ensemble used for measurements.

m_π (MeV)	Lattice size	L_s	a^{-1} (GeV)	L (fm)	Trajectories (MD time units)	Configurations
142.6(3)	$24^3 \times 64$	24	1.023(2)	4.67	250–3860	258
143.6(9)	$32^3 \times 64$	12	1.378(5)	4.58	200–1320	107

(A2A) propagators [40], as well as the GEVP method [34,35]—to compute correlation functions and extract energy eigenvalues. While better statistical precision is desired, and we will update our results in the near future, we take the continuum limit of the scattering phase shifts and scattering lengths at this point. Our determination of the scattering length does not need a chiral extrapolation, which assumes the leading order as an input from ChPT and hence gives a precise value. Our results are meaningful as a pure lattice determination, though they have larger uncertainty. A companion paper [25] using distillation [41] will also be available soon.

Although the core of this study is the application to $K \to \pi\pi$ and the direct CP violation parameter, ε', the experience gained here will provide impetus to other applications of π-K scattering phases. Examples that we have in mind so far are direct CP violation in charm decays [42,43], possible CP violation in $\tau \to \nu K\pi$ [44], and three-body proton decays.

This paper is organized as follows: Section II describes the theoretical framework underlying the calculation. In Sec. III, we give the lattice details. Section IV gives results for the computed two-pion energies and the corresponding phase shifts. Here we also compare our results to recent data-driven studies [28]. In Sec. V, we compare the PBC calculation to the GPBC one [24]. Section VI summarizes the present work and future prospects.

II. THEORETICAL FRAMEWORK

A. Operator construction

In this subsection, we describe the operators and states used in this work.

We start with pion operators with definite spatial momentum

$$\pi^a(t,\vec{p}) = \sum_{\vec{x},\vec{y}} e^{-i(\vec{p}_1\cdot\vec{x}+\vec{p}_2\cdot\vec{y})} f_r(\|\vec{x}-\vec{y}\|) \times \bar{\psi}(t,\vec{x}) i\gamma_5 F^a \psi(t,\vec{y}), \tag{1}$$

which is defined with the Coulomb gauge fixing and the momentum $\vec{p} = \vec{p}_1 + \vec{p}_2$ of the pion operator. In this work, we consider pion operators whose momentum for a direction is zero or one unit. Thus, a natural way of assigning the inner momenta when $\vec{p}$ is nonzero is to say that $\vec{p}_1$ or $\vec{p}_2$ carries one unit of momentum and the other zero. We assign $\vec{p}_1 = \vec{0}$ and $\vec{p}_2 = \vec{p}$ in this work and add only $\vec{p}$ as the momentum argument of the single-pion operators. While there is no dependence on the relative momentum $\vec{p}_1 - \vec{p}_2$ without smearing, we introduce the exponential smearing function

$$f_r(\|\vec{x}-\vec{y}\|) = \exp(-\|\vec{x}-\vec{y}\|/r), \tag{2}$$

with smearing radius r and the periodic modulus $\|\vec{x}-\vec{y}\|$, the length of the shortest straight path from $\vec{y}$ to $\vec{x}$ in the periodic box. This hydrogen-like wave function has been used in our earlier works [3,24]. While the single-pion operator of course depends on the smearing radius, we drop r from the pion operator on the left-hand side of Eq. (1) for simplicity. The quark and antiquark isospin doublets are defined as

$$\psi = \begin{pmatrix} u \\ d \end{pmatrix}, \qquad \bar{\psi} = \begin{pmatrix} \bar{u} & \bar{d} \end{pmatrix}, \tag{3}$$

and

$$F^+ = \frac{1}{2}(\sigma_1 + i\sigma_2), \tag{4}$$

$$F^- = \frac{1}{2}(-\sigma_1 + i\sigma_2), \tag{5}$$

$$F^0 = \frac{1}{\sqrt{2}}\sigma_3, \tag{6}$$

with the Pauli matrices $\sigma_{1,2,3}$.

The two-pion operators are constructed by multiplying two single-pion ones:

$$\tilde{O}^{I,I_z}_{\pi\pi}(t_1,t_2,\vec{P},\vec{p}/2) = \sum_{a,b} c^{I,I_z}_{ab} \pi^a(t_1,(\vec{P}+\vec{p})/2) \times \pi^b(t_2,(\vec{P}-\vec{p})/2), \tag{7}$$

where $\vec{P}$ and $\vec{p}$ are the center of mass and relative momentum, respectively, of the two pseudoscalar operators, and $a,b \in \{+,-,0\}$. The coefficients c^{I,I_z}_{ab} project the two-pion operator to an isospin-definite channel labeled by (I,I_z). Appendix A gives the explicit forms of the $(I,I_z) = (2,0)$ and $(0,0)$ two-pion operators.

The discrete, finite lattice breaks the continuum rotational symmetry of angular momentum SO(3) down to a discrete subgroup, which depends on the center-of-mass momentum. The irreducible representations of such a discrete subgroup do not give rise to angular momentum eigenstates that appear as irreducible representations of SO(3). Instead, they are mixtures which can be classified in terms of the continuum irreducible representations.

It is fairly straightforward to make this classification based on fundamental group theory for one- and two-particle systems, both moving and at rest [14,45]. Our main targets are the s-wave two-pion states and their phase shifts. The corresponding interpolating operators are defined as

$$O^{I,I_z}_{\pi\pi}(t_1,t_2,\vec{P},\vec{p}/2)=\sum_{\hat{T}\in G}\chi_{A_1}(\hat{T})\tilde{O}^{I,I_z}_{\pi\pi}(t_1,t_2,\vec{P},\hat{T}[\vec{p}/2]), \tag{8}$$

where we sum over all elements $\hat{T}$ in the finite-volume symmetry group G, and the normalization factor $\chi_{A_1}(\hat{T})$ is the character of the group element $\hat{T}$ in the representation A_1 [14,45].

We can consider two-pion operators composed of two bilinear operators located at different time slices t_1 and t_2. As long as there is no other operator placed in between, the time-nonlocal two-pion operators still play a role in creating and annihilating two-pion states with corresponding quantum numbers, and we can discuss the spectrum at time slices outside the operator. It has been shown that placing the two bilinear operators on slightly different time slices is advantageous for reducing statistical noise, especially for $I=0$ [2,3,24], where the overlap of the two-particle operator with the vacuum state can be suppressed exponentially by the separation $\Delta\equiv|t_2-t_1|$.

In addition to these two-pion operators, we introduce a σ operator, or isosinglet scalar bilinear operator, for $I=0$:

$$\sigma(t,\vec{p})=\sum_{\vec{x},\vec{y}}e^{-i(\vec{p}_1\cdot\vec{x}+\vec{p}_2\cdot\vec{y})}f_r(\|\vec{x}-\vec{y}\|)\bar{\psi}(t,\vec{x})\psi(t,\vec{y}), \tag{9}$$

with $\vec{p}=\vec{p}_1+\vec{p}_2$. Again, we set $\vec{p}_1=\vec{0}$ and $\vec{p}_2=\vec{p}$ in this work. This operator has been found to play an important role in controlling the contamination from excited states [3,24].

In this work, we concentrate on the rest frame $\vec{P}=\vec{0}$ and s-wave operators and states. For $I=2$, $I_z=0$, we consider four values of relative pion momenta and use the following operator basis:

$$O^{2,0}(t)=\begin{pmatrix}O^{2,0}_{\pi\pi}(t,t+\Delta,\vec{0},(0,0,0)\times 2\pi/L)\\ O^{2,0}_{\pi\pi}(t,t+\Delta,\vec{0},(0,0,1)\times 2\pi/L)\\ O^{2,0}_{\pi\pi}(t,t+\Delta,\vec{0},(0,1,1)\times 2\pi/L)\\ O^{2,0}_{\pi\pi}(t,t+\Delta,\vec{0},(1,1,1)\times 2\pi/L)\end{pmatrix}. \tag{10}$$

Similarly, for $I=0$, $I_z=0$, we define

$$O^{0,0}(t)=\begin{pmatrix}O^{0,0}_{\pi\pi}(t,t+\Delta,\vec{0},(0,0,0)\times 2\pi/L)\\ \sigma(t,\vec{0})\\ O^{0,0}_{\pi\pi}(t,t+\Delta,\vec{0},(0,0,1)\times 2\pi/L)\\ O^{0,0}_{\pi\pi}(t,t+\Delta,\vec{0},(0,1,1)\times 2\pi/L)\\ O^{0,0}_{\pi\pi}(t,t+\Delta,\vec{0},(1,1,1)\times 2\pi/L)\end{pmatrix}. \tag{11}$$

The order of the operators in these bases matters when it comes to the $N\times N$ GEVP as described in Sec. II D. When we do not need to specify the isospin, we simply call the four two-pion operators $\pi\pi(000)$, $\pi\pi(001)$, $\pi\pi(011)$, and $\pi\pi(111)$.

B. Correlation functions

For the GEVP, a matrix correlation function is defined in the basis of operators given in the previous subsection:

$$C^{I,I_z}_{ij}(t)=\langle O^{I,I_z}_i(t)O^{I,I_z}_j(-\Delta_j)^\dagger\rangle, \tag{12}$$

where

$$\Delta_j=\begin{cases}\Delta & (I=2)\\ (1-\delta_{2,j})\Delta & (I=0)\end{cases} \tag{13}$$

translates the source two-pion operators by Δ but does nothing for the σ operator, so that the time variable t always indicates the minimum time separation between a bilinear of the source operator and that of the sink operator. While the measured correlator matrix is not exactly symmetric with finite statistics, we symmetrize it by averaging with the transposed partner.

The Wick contractions of the two-point functions are shown diagrammatically in Figs. 1 and 2. They are denoted

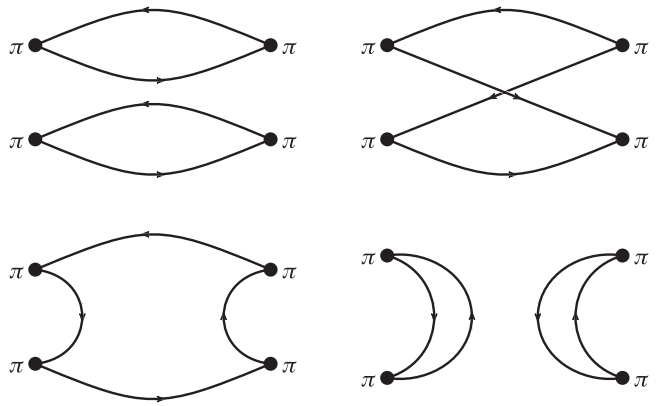

FIG. 1. Elemental Wick contractions. Clockwise from top-left: D (direct), C (cross), V (vacuum), and R (rectangle). Linear combinations of the four diagrams are used to construct pion-scattering correlation functions for $I=0$, 1, and 2 states with definite lattice hypercubic symmetry.

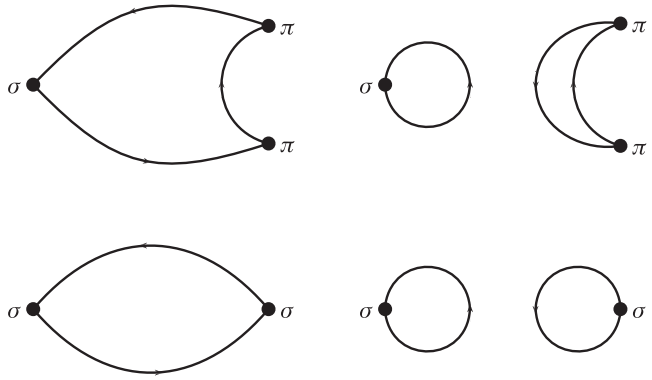

FIG. 2. Elemental Wick contractions with one (upper) or two (lower) scalar bilinear operators. These are analoguous to the R (left) and V (right) diagrams in Fig. 1 and relevant for only the $I = 0$ channel.

"direct" (D), "cross" (C), "rectangle" (R), and "vacuum" (V). By taking an appropriate linear combination of these elemental contractions, we construct a correlation function of operators carrying definite isospin. All diagrams in Figs. 1 and 2 contribute to the $I = 0$ channel, while only diagrams D and C contribute to the $I = 2$ channel. We compute the disconnected diagrams for every time translation and take the translation average, while the connected diagrams are computed after every several source time slices, which are specified in Sec. III. The complete formulas for the $I = 2$ and $I = 0$ channels are given in Appendix A.

For $I = 0$, there is an additional complication: in the rest frame, the ground state in this channel is the vacuum. This contribution dominates the correlation function and must be subtracted:

$$C_{ij}^{0,0}(t) = \langle O_i^{0,0}(t) O_j^{0,0}(-\Delta_j)^\dagger \rangle - \frac{1}{L_t} \sum_{t_{src}=0}^{L_t-1} \langle O_i^{0,0}(t+t_{src}) \rangle \langle O_j^{0,0}(t_{src}-\Delta_j)^\dagger \rangle, \tag{14}$$

where L_t stands for the time extent of the lattice ensemble in lattice units. While the second term on the right-hand side is independent of t in the limit of infinite statistics, we perform this subtraction time-slice by time-slice, as we have found it provides a minor statistical advantage [3,24].

C. Thermal effects

Due to the finite-time size of the lattice (L_t) and the pions satisfying periodic boundary conditions in time, unwanted contributions contaminate the correlation function. These so-called around-the-world (ATW), or thermal, effects arise when one of the source pions propagates forward in time while the other goes backwards through the boundary to reach the sink time slice. They can be seen by inserting a complete set of states into the two-point ("thermal") correlation function and translating the source and sink operators to equal times:

$$\begin{aligned} &\langle O_{\pi\pi}(t) O_{\pi\pi}(0)^\dagger \rangle \\ &= \sum_m \sum_n \langle m | O_{\pi\pi}(t) | n \rangle \langle n | O_{\pi\pi}^\dagger(0) | m \rangle \\ &= \sum_n (e^{-E_n^{\pi\pi} t} + e^{-E_n^{\pi\pi}(L_t - t)}) \langle 0 | O_{\pi\pi} | n \rangle \langle n | O_{\pi\pi}^\dagger | 0 \rangle \\ &\quad + e^{-E_{\pi(\vec{p})} t} e^{-E_{\pi(\vec{p})}(L_t - t)} \\ &\quad \times \langle \pi(\vec{p}) | O_{\pi\pi} | \pi(\vec{p}) \rangle \langle \pi(\vec{p}) | O_{\pi\pi}^\dagger | \pi(\vec{p}) \rangle + \cdots, \end{aligned} \tag{15}$$

where we omit the isospin superscripts and momentum arguments for simplicity, and the sum over m gives the thermal expectation value. The first term on the right-hand side contains the zero-temperature expectation value, while the last term is the thermal contribution, which vanishes as $L_t \to \infty$. Notice that when the rest frame is employed, the leading ATW contribution is time independent, while the ATW effects of an excited-state pion and those in a moving frame are time dependent. All thermal effects are suppressed exponentially with L_t.

Since we employ the rest frame, the leading ATW term, which is constant, can be removed simply by a "matrix" subtraction

$$C_{ij,subt}^{I,I_z}(t) \equiv C_{ij}^{I,I_z}(t) - C_{ij}^{I,I_z}(t + \delta_t), \tag{16}$$

where δ_t is an arbitrary time shift. This subtraction removes all constant contributions to the correlation functions, and therefore the vacuum subtraction [Eq. (14)] is in principle unnecessary if this subtraction is applied. In this work, we still apply the vacuum subtraction so that we can investigate the significance of the ATW effects with the absence of vacuum effects by analyzing both matrix-subtracted and unsubtracted correlators. As seen in Sec. IV A, the ATW effects are significant for two-pion states at rest, but they can be subtracted well by the matrix subtraction.

D. Generalized eigenvalue problem method

For the rest of the section, we omit the superscripts I and I_z and simplify our notation of the correlator matrix $C_{ij,subt}^{I,I_z}(t) \to C_{ij}(t)$, or $C(t)$ when the operator indices i and j can be dropped without confusion.

As is well known, Euclidean space correlation functions are a sum of exponential terms, each term corresponding to one state in a tower of states with fixed quantum numbers and increasing energies:

$$C_{ij}(t) = \sum_n A_{n,i} A_{n,j}^* e^{-E_n t}, \tag{17}$$

where we have neglected the backward-propagating contributions proportional to $e^{-E_n(L_t - t)}$, since $t \ll L_t$ in

our setup.[1] $A_{n,i} = \langle 0|O_i|n\rangle(1 - e^{-E_n\delta_t})^{1/2}$ is the overlap of the ith operator acting on the nth state and the vacuum multiplied with a normalization factor due to the matrix subtraction.

To extract the desired excited states in the correlator, we employ the variational method by solving a generalized eigenvalue problem (GEVP) [34,35]. For an $N \times N$ matrix $C(t)$, we solve the following GEVP:

$$C(t)V_n(t,t_0) = \lambda_n(t,t_0)C(t_0)V_n(t,t_0), \tag{18}$$

with eigenvalues $\lambda_n(t,t_0)$ and eigenvectors $V_n(t,t_0)$, where in principle we can choose t_0 in the range $0 < t_0 < t$. At asymptotically large time separations, the eigenvalue behaves as $\lambda_n(t,t_0) = e^{-E_n(t-t_0)}$, where E_n is the nth energy state in the GEVP. In Ref. [35], it was shown that the leading correction behaves like $e^{-(E_{N+1}-E_n)t}$ for $t_0 \geq t/2$. In this work, we use the first N operators of the bases in Eqs. (10) and (11) for the $I = 2$ and $I = 0$ channels, respectively, and solve GEVP with a t-independent value of $t - t_0 \equiv \Delta_t$. While the preferable inequality $t_0 \geq t/2$ is violated in the region $t < 2\Delta_t$, we do not use data at such short times relative to Δ_t for our final results.

Effective two-pion energies are defined as [34,35]

$$E_n^{\text{eff}}(t,t_0) = \ln\lambda_n(t,t_0) - \ln\lambda_n(t+1,t_0). \tag{19}$$

The corresponding eigenvector $V_n(t,t_0)$ at asymptotic time separation provides a new operator that couples to the nth state, but not with the other states in the GEVP[2] [35]:

$$\tilde{O}_n = \sum_i V_{n,i}O_i. \tag{20}$$

These eigenvectors play a key role in isolating the weak operator matrix elements between an excited two-pion state and the kaon in $K \to \pi\pi$ decays, for example.

In practice, the large statistical error of correlation functions at large time separations may cause the misordering of eigenvalues and eigenvectors for specific jackknife samples, resulting in incorrectly large errors in two-pion energies and GEVP eigenvectors. A brief description of our procedure to ensure the correct order of eigenvectors is given below:

(1) At small time separations, where correlators and hence eigenvectors are well resolved, ensure the descending order of eigenvalues. Then, the corresponding effective energies will be obtained in ascending order.

(2) At large time separations, where excited-state contamination is small, solve the GEVP with the correlators that are mostly diagonalized by Eq. (20) with the eigenvectors obtained one time slice earlier. The eigenvectors from such a GEVP are close to a unit vector for a certain direction, and the ordering is fairly trivial. Then, change the basis of these eigenvectors back into the original basis.

See Sec. B 1 of Appendix B for more detail.

In this work, we employ procedure 1 at $t_0 = 1$, 2 and procedure 2 at larger time separations $t_0 \geq 3$. The reason we switch the procedure at a certain value of t_0 rather than t is that the GEVP eigenvectors $V_n(t,t_0)$ receive contamination from the higher states by $O(e^{-(E_{N+1}-E_n)t_0})$ [35].

It is mathematically guaranteed that the GEVP eigenvalues and eigenvectors in Eq. (18) are real when $C(t_0)$ is a positive-definite real symmetric matrix, and some software functions to solve the GEVP have this assumption. While the correlator matrix at large time separations with limited statistics has zero-consistent eigenvalues, and it is inevitable that the correlator matrix will have negative eigenvalues at some time slices, that may not necessarily mean we cannot solve the GEVP or obtain any information from two-pion signals at those time separations. The positivity and real symmetry are sufficient but not necessary to give us real eigenvalues and eigenvectors of the GEVP. As shown in Sec. IV A, we find that the GEVP with $C(t_0)$ including a negative eigenvalue can still give us good signals of a few of the lowest-energy states with the ordering strategy explained above and in Sec. B 1 of Appendix B, as long as the GEVP eigenvalues and eigenvectors are real.

E. Rebased GEVP

The GEVP method provides a decomposition based on the N lightest states. It assumes sufficiently large time separations that the contamination of higher excited states ($n \geq N+1$) can be ignored. On the other hand, the GEVP becomes increasingly difficult with increasing time separation due to the exponentially deteriorating signal-to-noise ratio of the correlator matrix. For small N, we expect the plateau to start at larger time separations, where the signal-to-noise ratio is already poor. For large N, plateaus for the various energies move to earlier times, but the larger statistical errors on the higher-energy states in the GEVP might spoil the signal of the lower states. Thus, for any choice of N (or operator set), there is a chance that the signal loss will occur before a clear plateau is observed.

To address this problem, we propose a modified version of the GEVP, which we call the *rebased* GEVP (RGEVP), whereby we choose a new reduced basis of fewer operators that couple well with a few resolved low-energy states. The idea originates from the fact that the number of resolvable states which dictates the appropriate size of the GEVP decreases with increasing time separation, and that the

[1]This contribution is exponentially suppressed compared to the ATW effect considered earlier.

[2]The coupling is not perfect: in Ref. [35], it is shown that corrections are $O(e^{-(E_{N+1}-E_n)t_0})$.

GEVP at short time separations, even before reaching a plateau, provides a set of nearly diagonalized operators.

The simplest rebasing can be performed by Eq. (20) with a chosen number $N'(<N)$ of eigenvectors $V_{n(<N')}$ obtained at a chosen time slice $t_0 = t_0'$. The new basis provides an $N' \times N'$ correlator matrix with which we can perform GEVP without contamination from the states labeled by $N'+1$ to N.

The rebasing does not have to be a single step. When one is interested in the ground (first excited) state, the reduced GEVP size could minimally be one (two). Performing such a reduction of basis with a single step may not minimize both statistical and systematic errors. A multistep rebasing can be done by choosing multiple pairs of rebasing time $t_{0,\alpha}(>t_{0,\alpha-1})$ and reduced size $N_\alpha(<N_{\alpha-1})$ with the label α referring to rebasing steps and repeating the rebasing $N_{\alpha-1} \to N_\alpha$ at $t_0 = t_{0,\alpha}$ for each α. See Sec. B 2 of Appendix B for more detail.

In this work, we implement the rebasing with the central-values eigenvectors for all jackknife samples to maintain the configuration independence of the new operator basis.

F. Phase shifts

The Lüscher method [6] allows us to extract the scattering phase shifts from finite-volume energies on the lattice. The interaction region is supposed to be confined to a volume well contained inside a box of larger volume. Outside this region, the solution of the wave equation corresponds to free (noninteracting) particles, and the boundary conditions of the box impose a quantization condition on the complete solution, which necessarily relates the phase shifts to finite-volume energies.

While the extension to moving frames is straightforward [46], we limit our discussion to the case of the rest frame, where one obtains the two-pion s-wave scattering phase shift $\delta(E_{\pi\pi})$ corresponding to a given two-pion energy as follows:

$$k = \sqrt{\frac{E_{\pi\pi}^2}{4} - m_\pi^2}, \tag{21}$$

$$q = \frac{kL}{2\pi}, \tag{22}$$

$$\tan\phi(q) = \frac{\pi^{3/2} q}{Z_{00}(1;q^2)}, \tag{23}$$

$$\delta(E_{\pi\pi}) = -\phi(q) + \pi n, n \in \mathbb{Z}, \tag{24}$$

where $E_{\pi\pi}$ is the energy of the two-pion state in a finite box of size L^3, m_π is the pion mass, and $Z_{00}(1,q^2)$ is the Lüscher zeta function, which we compute via an efficient numerical implementation given in Ref. [47]. Equation (24) is used to compute all $I=0$ and 2 phase shifts.

The method outlined here for obtaining the phase shifts is strictly valid in the limited region $2m_\pi \le E_{\pi\pi} \le 4m_\pi$ and up to neglected higher partial waves. In the present work, we apply this method also to energies above the 4π inelastic threshold, and we neglect these sources of systematic errors. Numerical results presented in Sec. IV B suggest that these systematic errors may not be large within the energy range considered here.

G. The dispersion relation method

Up to small finite lattice spacing effects, Lüscher's method, explained above, gives an accurate prescription for obtaining the phase shift. With finite lattice spacing, Eq. (21) needs modification, since the appropriate dispersion relation for finite lattice spacing depends on the type of lattice fermion. While simulations at multiple lattice spacings enable the removal of these effects, we remove some of them for each lattice spacing separately [24].

The method is based on the cancellation of artifacts between interacting and noninteracting two-pion energies. The noninteracting two-pion energies, E_n^0, are determined from a product of two expectation values of single-pion correlators, $C^0(t)$, which is analogous to the D diagram in the interacting case. Since the correlation functions involving the σ operator do not contain the D diagram, they should be treated separately. We first explain the method for $I=2$, where the σ operator is absent, and then explain its generalization to the case including the σ operator.

The noninteracting correlator matrix $C^0(t)$ is diagonal with analogous two-pion effective energies, $E_1^{0,\mathrm{eff}}(t,t_0) < E_2^{0,\mathrm{eff}}(t,t_0) < \cdots < E_N^{0,\mathrm{eff}}(t,t_0)$. The energy shift of two-pion states due to interactions is

$$\Delta E_n^{\mathrm{eff}}(t,t_0) = E_n^{\mathrm{eff}}(t,t_0) - E_n^{0,\mathrm{eff}}(t,t_0), \tag{25}$$

where single-pion discretization errors largely cancel. Thus, we obtain an improved two-pion energy

$$E_n^{\mathrm{eff}\prime}(t,t_0) = E_n^{0,\mathrm{disp}} + \Delta E_n^{\mathrm{eff}}(t,t_0), \tag{26}$$

where we define

$$E_n^{0,\mathrm{disp}} = 2\sqrt{m_\pi^2 + |\vec{p}_n|^2}, \tag{27}$$

with a noninteracting pion momentum in the finite box $\vec{p}_n = (0,0,0), (0,0,2\pi/L), (0,2\pi/L,2\pi/L), \ldots$.

In addition to reducing the scaling violation in the dispersion relation, this method determines two-pion energies and phase shifts with other improvements as well. The first term on the right-hand side of Eq. (26), which is defined in Eq. (27), is as statistically precise as m_π. On the other hand, the second term on the right-hand side of Eq. (26), which is given in Eq. (25), is also expected to be more precise than $E_n^{\mathrm{eff}}(t,t_0)$ because of the correlation

between the first and second terms on the right-hand side of Eq. (25). Furthermore, the energy difference in Eq. (25) may also remove excited-state effects related to single pions and allow effective energies $E_n^{\text{eff}\prime}$ to plateau sooner. We find these to be the case, especially for the $I = 2$ channel, as discussed in Sec. IV.

For the $I = 0$ channel, the statistical errors are dominated by the disconnected diagram, which cannot be improved by this method, though we still find some improvement for the combination of diagrams by applying the following procedure with the σ operator. The $I = 0$ channel is more complicated, not only because of the inclusion of the σ operator, but also because the interaction between the two pions makes the finite-volume two-pion energies quite unlike the energies of two noninteracting pions—i.e., $|\Delta E_n^{\text{eff}}(t, t_0)|$ for $I = 0$ is much larger than that for $I = 2$. Therefore, it is less meaningful to identify the one-to-one correspondence between the interacting and noninteracting two-pion energies as in Eq. (25). In this work, instead of matching the state label n of the interacting and noninteracting two-pion energies, the first and second terms in Eq. (25), we choose the noninteracting two-pion energy as the one closest to the interacting nth-state energy $E_n^{\text{eff}}(t, t_0)$ for the procedure explained above.

III. ENSEMBLE DETAILS AND COMPUTATIONAL SETUP

Our computations are carried out on two ensembles of $2 + 1$ flavors of Möbius domain-wall fermions (MDWFs) with physical masses generated by the RBC/UKQCD Collaborations [36,37]. Both use the Iwasaki-DSDR gauge action [48] and correspond to inverse lattice spacings of about 1.0 and 1.4 GeV, respectively, with similar physical volumes ($L \sim 5$ fm). The parameters of each ensemble are listed in Table I.

Correlation functions are computed in an all-to-all propagator (A2A) [40] framework using 2000 low modes of the preconditioned, squared Dirac operator and spin-color-time diluted random source propagators for the high modes.

We employ all-mode averaging (AMA) [38,39] to save the computational cost for the conjugate gradient (CG). While the traditional AMA is to perform fewer exact measurements (e.g., with fewer source locations) for all the configurations with which sloppy measurements are performed, we instead reduce the number of configurations for the exact measurements, keeping the A2A procedure as it is. We first perform both exact and sloppy measurements with N_{exact} configurations and create corresponding jackknife samples of the difference between exact and sloppy correlators, which would correct the bias due to the sloppy CG. In the case of bin size 1,

$$\Delta C^{(l)}(t) = \frac{1}{N_{\text{exact}} - 1} \sum_{k \neq l} \left(C^{\mathcal{E}_k}_{\text{exact}}(t) - C^{\mathcal{E}_k}_{\text{sloppy}}(t) \right), \quad (28)$$

where $\mathcal{E}$ is the list of configurations with which both exact and sloppy measurements are performed and $C^{\mathcal{E}_k}_{\text{exact/sloppy}}(t)$ stands for an exact/sloppy sample of the correlator matrix calculated with a configuration $\mathcal{E}_k$. The average of the difference is defined as

$$\Delta C(t) = \frac{1}{N_{\text{exact}}} \sum_{l=1}^{N_{\text{exact}}} \Delta C^{(l)}(t). \quad (29)$$

We also perform sloppy measurements with N_{sloppy} additional configurations in the list $\mathcal{S}$ and create corresponding jackknife samples. If we set the bin size to 1, they are written as

$$C^{(l)}_{\text{sloppy}}(t) = \frac{1}{N_{\text{sloppy}} - 1} \sum_{k \neq l} C^{\mathcal{S}_k}_{\text{sloppy}}(t), \quad (30)$$

and the average is given as

$$C_{\text{sloppy}}(t) = \frac{1}{N_{\text{sloppy}}} \sum_{l=1}^{N_{\text{sloppy}}} C^{(l)}_{\text{sloppy}}(t). \quad (31)$$

With these jackknife samples and averages, we define super-jackknife samples as

$$C^{(l)}_{\text{AMA}}(t) = \begin{cases} C_{\text{sloppy}}(t) + \Delta C^{(l)}(t) & (1 \leq l \leq N_{\text{exact}}) \\ C^{(l - N_{\text{exact}})}_{\text{sloppy}}(t) + \Delta C(t) & (l > N_{\text{exact}}) \end{cases}. \quad (32)$$

In this work, the sloppy (high-mode) propagators are computed with 400 and 330 iterations of CG, and the exact propagators are computed to the CG residual of 10^{-8} with 14 and 17 configurations for the 24^3 and 32^3 lattices, respectively. For the sloppy part of the measurements on the 24^3, 1.023 GeV ensemble, we employ the zMöbius approximation [49] of the Möbius Dirac operator, reducing the size of the fifth dimension by a factor of 2.

As described in Sec. II A, the two-pion operators are defined as a product of two single-pion operators separated by a parameter Δ. We choose $\Delta = 3$ and 4 for the 24^3 and 32^3 lattices, respectively, so the separation in physical units is about the same. The smearing radius r of the single-pion and the sigma operators is set to 1.5 and 2.0 in lattice units for the 24^3 and 32^3 lattices, respectively. We average the correlation functions over the time location of the source operator t_{src}. The disconnected diagrams are computed at $t_{src} = 0, 1, \ldots, 63$, while the connected diagrams are computed at $t_{src} = 0, 8, \ldots, 56$ for the 24^3 lattice and at $t_{src} = 0, 10, \ldots, 50$ for the 32^3 lattice.

IV. RESULTS

A. Energies

Single-pion energies with the four lowest momenta are summarized in Table II. The results from single-pion correlation functions with respective momenta and from the continuum dispersion relation are listed. The noninteracting two-pion energies can be estimated as the double of these values. The difference between the values from the two approaches corresponds to the discretization effect on the two-pion energies that can be removed by the dispersion relation (DR) method explained in Sec. II G. By definition, the results for zero-momentum energy from the two approaches are identical. One can recognize the discretization effect in the results for the nonzero momenta on the 24^3 lattice, while the results on the 32^3 are not sufficiently resolved to see the difference.

Interacting two-pion energies are tabulated and plotted for several values of Euclidean times t_0, $t - t_0$, δ_t, and various types ($N \times N$ or RGEVP) of GEVP, with and without the dispersion relation method, in Tables XXXIV–LI and Figs. 33–50 in Appendix C. The parameters for rebasing are found in the captions of their respective figures and tables throughout this subsection, and tables in Appendix C. Some general patterns are apparent. For short times, the statistical errors are subpercent, even down to the per mille level in some cases. The effect of increasing $t - t_0$ is small, and likewise for δ_t. The DR method greatly enhances statistical precision, especially for the $I = 2$ ground state, but gains are seen generally. It also lessens (single-pion) excited-state contamination. In the next two subsections, we discuss the results in detail, including comparisons in a range of t and for both lattice spacings to assess residual excited-state contamination and lattice artifacts, respectively.

Our guiding principle throughout this analysis is to stick to as short times as possible, where statistics are better and ATW effects are smaller, taking advantage of the GEVP and the DR method that reduce excited-state contamination. In this section, the state label n begins with 0, so the ground state is labeled with $n = 0$, the first excited state with $n = 1$, and so on.

TABLE II. Summary of single-pion energies with the four lowest momenta on the 24^3 and 32^3 lattices. The three-digit number in the first column specifies the spatial momentum of the single pion. Results from correlated χ^2 fits to single-pion correlators with the cosh function [lattice] and dispersion relation [DR, half of Eq. (27)] are shown in lattice units. The values of χ^2/d.o.f. are displayed in the square brackets.

Momentum	Lattice	DR
	24^3 lattice	
(000)	0.13944(17)[1.2]	0.13944(17)
(001)	0.29572(30)[0.9]	0.296621(80)
(011)	0.39431(66)[1.2]	0.395630(60)
(111)	0.4685(18)[1.0]	0.474407(50)
	32^3 lattice	
(000)	0.10422(20)[1.1]	0.10422(20)
(001)	0.22190(44)[1.1]	0.222293(94)
(011)	0.2954(10)[1.5]	0.296593(71)
(111)	0.3559(28)[1.2]	0.355697(59)

1. $I = 2$

We begin with the ground state for the 24^3 ensemble. Figure 33 shows the ground-state energy for several GEVP types and representative values of $\delta_t = 2, 5, 8$, $t - t_0 = 1, 2, 3, 4$, and $t = 4, 6, 8$. Similar patterns of behavior emerge for the various GEVP types. Without the DR method, increasing either δ_t or $t - t_0$ tends to decrease the energy, suggesting smaller excited-state effects (the statistical errors are relatively large, so we do not draw a strong conclusion). For larger times, the effect is smaller. For fixed t, we often observe smaller statistical errors as δ_t increases, though after $\delta_t = 5$ the improvement is slight. Increasing $t - t_0$ has little effect. The DR method, on the other hand, shows a dramatic reduction in statistical error but little change after that for the other variables. In either case, there is little dependence on the GEVP type. This is because, in Eq. (26), $E_0^{0,\mathrm{disp}} = 2m_\pi$ dominates the statistical error, and $\Delta E_0^{\mathrm{eff}}(t, t_0)$, which is dependent on GEVP type, is much more precise for the ground state in our measurements.

Figure 3 shows the effective ground-state energy for the 4×4 GEVP (our largest basis for $I = 2$) with $t - t_0 = 1$ and matrix subtractions in the range $4 \le \delta_t \le 11$, both with (lower panel) and without (upper panel) the DR method. There are several interesting features. First, a clear and stable plateau sets in between $t = 4$ and 5 for all nonzero δ_t. Both statistical uncertainties and excited-state contamination are significantly reduced by the DR method. In the

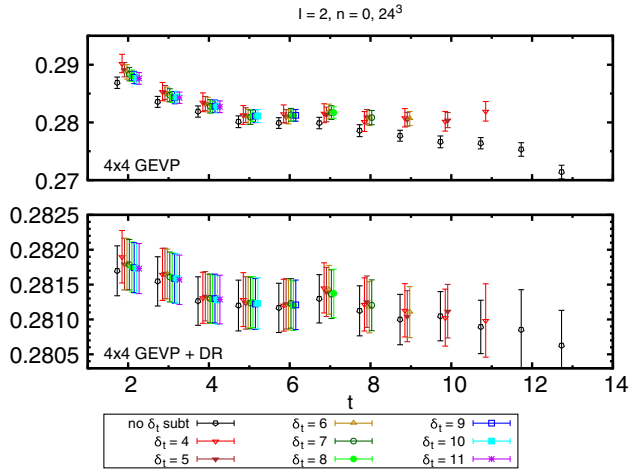

FIG. 3. The $I = 2$ effective ground-state energy with the dispersion relation method (lower) and without (upper). 24^3, 4×4 GEVP, $t - t_0 = 1$. Without matrix subtraction, there is an evident downward shift in the energy, an indication of the ATW effect, for the non-DR result.

TABLE III. Fit results for two-pion energy of the $I = 2$ ground state on the 24^3 lattice with various fit ranges and GEVP methods. We choose parameters $\delta_t = 5$ and $t - t_0 = 1$. The values of χ^2/d.o.f. are shown in the square brackets. The rebasing matrix is calculated as $4 \times 4 \to 3 \times 3$ at $t_0 = 4$.

	Fit range		
GEVP type	4–10	5–10	6–10
2×2	0.28132(34)[0.7]	0.28129(34)[0.8]	0.28129(34)[1.0]
3×3	0.28131(34)[0.7]	0.28129(34)[0.7]	0.28129(34)[0.9]
4×4	0.28128(34)[0.6]	0.28126(34)[0.7]	0.28126(34)[0.9]
RGEVP	0.28130(34)[0.6]	0.28128(34)[0.7]	0.28128(34)[0.9]

TABLE IV. Fit results for two-pion energy of the $I = 2$ first excited state on the 24^3 lattice with various fit ranges and GEVP methods. We choose parameters $\delta_t = 5$ and $t - t_0 = 1$. The values of χ^2/d.o.f. are shown in the square brackets. The rebasing matrix is calculated as $4 \times 4 \to 3 \times 3$ at $t_0 = 4$.

	Fit range		
GEVP type	4–9	5–9	6–9
2×2	0.60859(27)[1.3]	0.60824(31)[0.3]	0.60824(43)[0.4]
3×3	0.60821(27)[0.9]	0.60793(31)[0.3]	0.60799(43)[0.4]
4×4	0.60817(27)[0.8]	0.60789(31)[0.3]	0.60797(43)[0.3]
RGEVP	0.60816(27)[0.9]	0.60789(31)[0.3]	0.60797(43)[0.3]

upper panel (no matrix subtraction), there is a systematic downward shift for each time slice, which grows with increasing t. This is a clear indication of the ATW effect, which is eliminated by the matrix subtraction. Perhaps somewhat surprisingly, the shift is also eliminated by the DR method. This can be understood as follows: A very similar ATW effect occurs in the single-pion case, so the observed cancellation implies that in the interacting case, the two pions do not interact very much. We also observe a small reduction in statistical error as δ_t increases in the absence of the dispersion method, while there is no difference when it is used, as the dominant error on the ground-state energy after DR is from the error on m_π. Since contractions were only computed for $t \leq 16$ to reduce computational cost, the maximum value of t for the effective energy in each case is $t_{\max,\delta_t} = 15 - \delta_t$, as seen in the figure (15 and not 16 appears because the effective energy depends on GEVP eigenvalues at t and $t + 1$).

In Table III, we tabulate the fit results for the ground-state energy using the dispersion relation method for different fit ranges and GEVP types and display them in Fig. 19. In this work, all fits are correlated fit to a constant (t-independent) parameter, performed separately for each individual effective energy. The stability of the fits is quite robust for all values of t and GEVP types considered in the figure.

The behavior of the first excited state is similar to that of the ground state. In Fig. 4, we again observe a stable plateau beginning with $t = 5$; however, an ATW effect cannot be seen. But we do see excited-state effects, especially without the DR method, and statistical errors are reduced significantly by the DR method. There is little dependence on δ_t. The small deviation visible at $t_{\min} = 4$ in the fit results in Table IV and Fig. 20 may be associated with the slight blip observed in the effective energy at $t = 4$ in Fig. 4. The 2×2 GEVP may be systematically high, especially for $t = 4$.

The second and third excited-state energies are shown in Fig. 5 and listed for various fit ranges and GEVP types in Tables V and VI (see also Figs. 21 and 22). In the upper panel, the energy fluctuates down at $t = 4$, which leads to

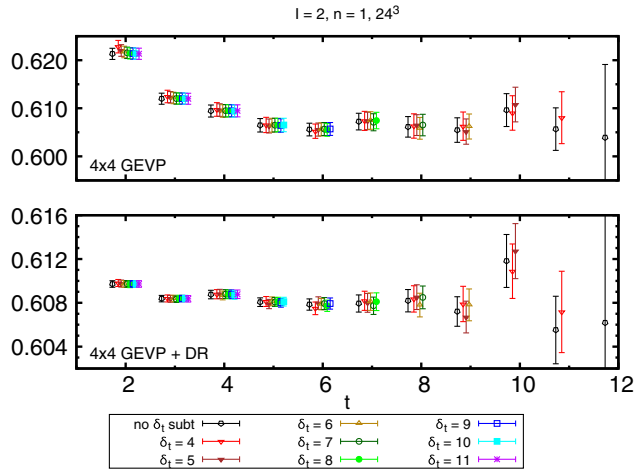

FIG. 4. The $I = 2$ effective first excited-state energy with (lower) and without (upper) the dispersion relation method. 24^3, 4×4 GEVP, $t - t_0 = 1$. The ATW effect is not observed; cf. Fig. 3.

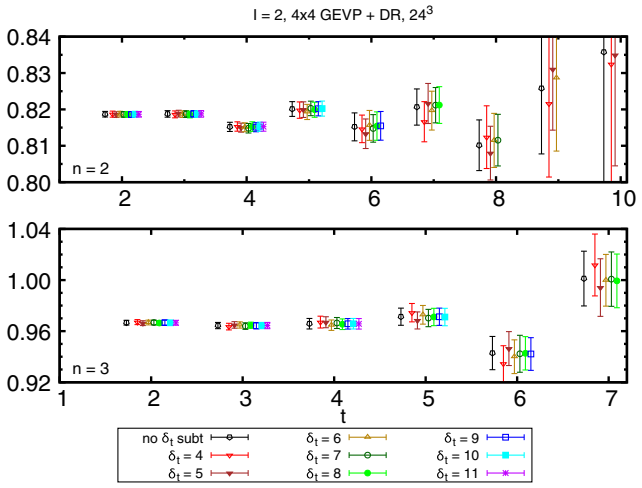

FIG. 5. The $I = 2$ effective second (upper) and third (lower) excited-state energies with the dispersion relation method. 24^3, 4×4 GEVP, $t - t_0 = 1$. The ATW effect is not observed; cf. Fig. 3.

TABLE V. Fit results for two-pion energy of the $I = 2$ second excited state on the 24^3 lattice with various fit ranges and GEVP methods. We choose parameters $\delta_t = 5$ and $t - t_0 = 1$. The values of χ^2/d.o.f. are shown in the square brackets. The rebasing matrix is calculated as $4 \times 4 \to 3 \times 3$ at $t_0 = 4$.

	Fit range		
GEVP type	3–9	4–9	5–9
3×3	0.81855(58)[1.5]	0.81743(92)[1.3]	0.8183(15)[1.5]
4×4	0.81743(56)[1.5]	0.81637(89)[1.3]	0.8178(15)[1.3]
RGEVP	0.81753(56)[1.4]	0.81665(87)[1.3]	0.8185(15)[1.0]

TABLE VI. Fit results for two-pion energy of the $I = 2$ third excited state on the 24^3 lattice with various fit ranges and GEVP methods. We choose parameters $\delta_t = 5$ and $t - t_0 = 1$. The values of χ^2/d.o.f. are shown in the square brackets.

	Fit range	
GEVP type	3–5	4–5
4×4	0.9658(17)[0.1]	0.9674(36)[0.0]

an elevated χ^2 in the fit. The same happens at $t = 6$ for the third excited state. Again, there is little dependence on δ_t or GEVP type, except that the 3×3 GEVP is a bit high for small t_{min} in the fit (Figs. 21 and 22). With four interpolating operators for $I = 2$, the third excited state is as far as we can go.

The effective ground-state energy computed on the 32^3 lattice is shown in Fig. 6. The ATW effect is even more pronounced, as expected, since the physical time extent is smaller compared to the 24^3 lattice, and it is significantly

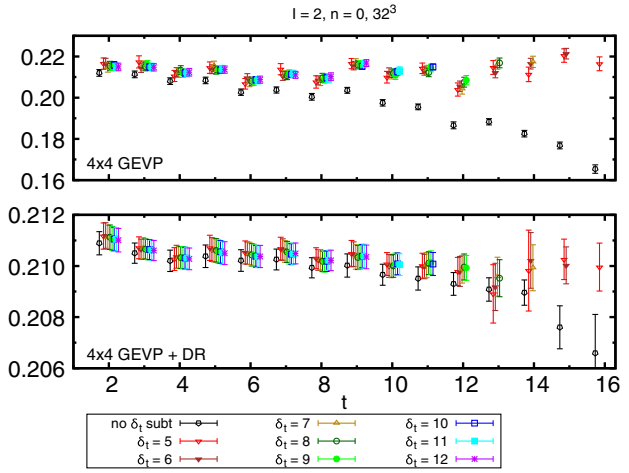

FIG. 6. The $I = 2$ effective ground-state energy with (lower) and without (upper) the dispersion relation method. 32^3, 4×4 GEVP, $t - t_0 = 1$. There is a pronounced ATW effect without matrix subtraction (upper panel). The dispersion relation method reduces, but does not entirely eliminate the effect (lower panel).

TABLE VII. Fit results for two-pion energy of the $I = 2$ ground state on the 32^3 lattice with various fit ranges and GEVP methods. We choose parameters $\delta_t = 8$ and $t - t_0 = 1$. The values of χ^2/d.o.f. is shown in the square brackets. The rebasing matrix is calculated as $4 \times 4 \to 3 \times 3$ at $t_0 = 5$.

	Fit range		
GEVP type	4–9	5–9	6–9
2×2	0.21041(38)[0.8]	0.21041(38)[0.9]	0.21039(38)[0.7]
3×3	0.21041(37)[0.8]	0.21042(37)[1.0]	0.21039(37)[0.7]
4×4	0.21039(37)[0.8]	0.21039(37)[1.0]	0.21036(37)[0.7]
RGEVP	0.21041(37)[0.8]	0.21041(37)[1.0]	0.21038(37)[0.7]

TABLE VIII. Fit results for two-pion energy of the $I = 2$ first excited state on the 32^3 lattice with various fit ranges and GEVP methods. We choose parameters $\delta_t = 8$ and $t - t_0 = 1$. The values of χ^2/d.o.f. are shown in the square brackets. The rebasing matrix is calculated as $4 \times 4 \to 3 \times 3$ at $t_0 = 5$.

	Fit range		
GEVP type	4–10	5–10	6–10
2×2	0.45698(37)[0.7]	0.45669(41)[0.4]	0.45665(47)[0.5]
3×3	0.45654(36)[0.3]	0.45639(41)[0.3]	0.45638(47)[0.3]
4×4	0.45648(36)[0.3]	0.45636(41)[0.2]	0.45638(47)[0.3]
RGEVP	0.45648(36)[0.3]	0.45637(41)[0.3]	0.45639(46)[0.3]

reduced again, but not completely eliminated, by the DR method. The lower panel indicates that the effective energy even with the matrix subtraction might decrease with increasing time from $t = 10$, and it could mean that there are also higher-order ATW effects that cannot be removed by the matrix subtraction in Eq. (16). Since this tendency is not statistically significant and it is still possible that this is

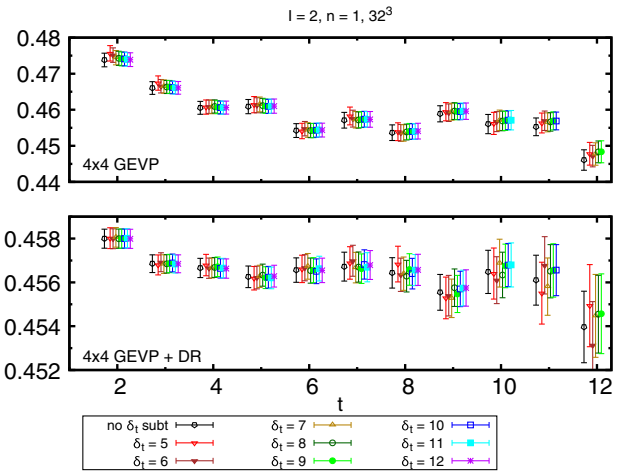

FIG. 7. The $I = 2$ effective first excited-state energy with (lower) and without (upper) the dispersion relation method. 32^3, 4×4 GEVP, $t - t_0 = 1$.

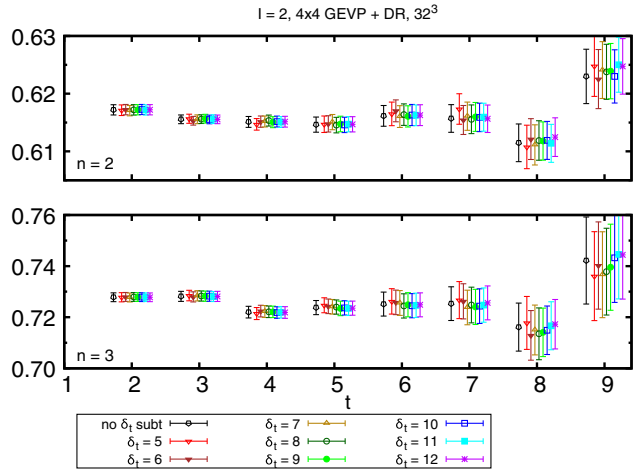

FIG. 8. The $I = 2$ effective second (upper) and third (lower) excited-state energies with the dispersion relation method. 32^3, 4×4 GEVP, $t - t_0 = 1$.

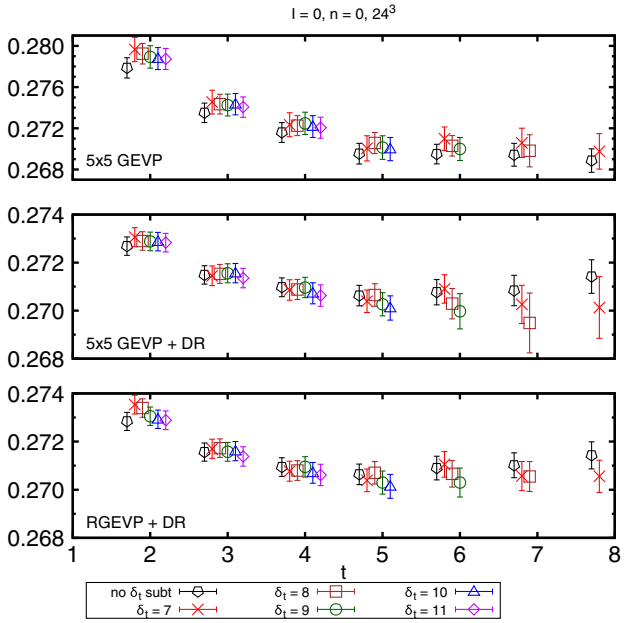

FIG. 9. The $I = 0$ effective ground-state energy. 24^3, 5×5 GEVP, $t - t_0 = 1$ with (middle, lower) and without (upper) the dispersion relation method. The RGEVP result is shown in the lower panel. The rebasing from $5 \times 5 \to 3 \times 3$ uses GEVP eigenvectors at $t_0 = 4$.

due to statistical fluctuation, we will conclude this point after increasing statistics, but we do not use data points at $t \geq 10$ for our fits. Again, a large reduction in the statistical error and excited-state contamination occurs with the dispersion relation method where a plateau emerges beginning at $t = 4$. Figure 23 shows fits for several ranges and GEVP types. Results are tabulated in Table VII. There is little dependence on t_{min} or GEVP type.

The situation is similar for the first excited-state energy (see Fig. 7), except that the ATW effect is not detectable, the same as we saw for the 24^3 lattice. The plateau begins at $t = 4$ or 5 with the DR method. The DR method removes a bit of jitter as well, which is probably due to poor statistics. Fit results are summarized in Table VIIIand Fig. 24.

The energies for higher excited states are shown in Fig. 8. Fits are summarized in Tables IX and X and shown in Figs. 25 and 26.

TABLE IX. Fit results for two-pion energy of the $I = 2$ second excited state on the 32^3 lattice with various fit ranges and GEVP methods. We choose parameters $\delta_t = 8$ and $t - t_0 = 1$. The values of χ^2/d.o.f. are shown in the square brackets. The rebasing matrix is calculated as $4 \times 4 \to 3 \times 3$ at $t_0 = 5$.

	Fit range		
GEVP type	3–7	4–7	5–7
3×3	0.61671(59)[0.5]	0.61605(83)[0.3]	0.6158(12)[0.4]
4×4	0.61548(59)[0.3]	0.61523(80)[0.3]	0.6151(12)[0.4]
RGEVP	0.61552(58)[0.3]	0.61522(81)[0.3]	0.6151(12)[0.4]

TABLE X. Fit results for two-pion energy of the $I = 2$ third excited state on the 32^3 lattice with various fit ranges and GEVP methods. We choose parameters $\delta_t = 8$ and $t - t_0 = 1$. The values of χ^2/d.o.f. are shown in the square brackets.

	Fit range		
GEVP type	4–7	5–7	6–7
4×4	0.7230(17)[0.1]	0.7241(25)[0.0]	0.7245(43)[0.0]

2. $I = 0$

This case is statistically noisier than $I = 2$ due to the disconnected diagrams of the correlation function, as well as the coupling with the vacuum state. In Fig. 37, the effective energies for the ground state are shown for several GEVP types computed on the 24^3 ensemble. Values of $t - t_0$ range from 1 to 4 with $3 \leq t \leq 7$ and $\delta_t = 2$, 5, 8. Like $I = 2$, there is little dependence on GEVP type.

TABLE XI. Fit results for two-pion energy of the $I = 0$ ground state on the 24^3 lattice with various fit ranges and GEVP methods. We choose parameters $\delta_t = 7$ and $t - t_0 = 1$. The values of χ^2/d.o.f. are shown in the square brackets. The rebasing matrix is calculated as $5 \times 5 \to 3 \times 3$ at $t_0 = 4$.

	Fit range		
GEVP type	3–8	4–8	5–8
3×3	0.27116(38)[1.8]	0.27082(41)[0.9]	0.27058(47)[0.8]
4×4	0.27115(38)[1.5]	0.27087(41)[0.9]	0.27067(46)[0.9]
5×5	0.27104(38)[1.6]	0.27074(41)[1.0]	0.27054(46)[1.1]
RGEVP	0.27122(38)[3.6]	0.27069(41)[1.1]	0.27053(46)[1.3]

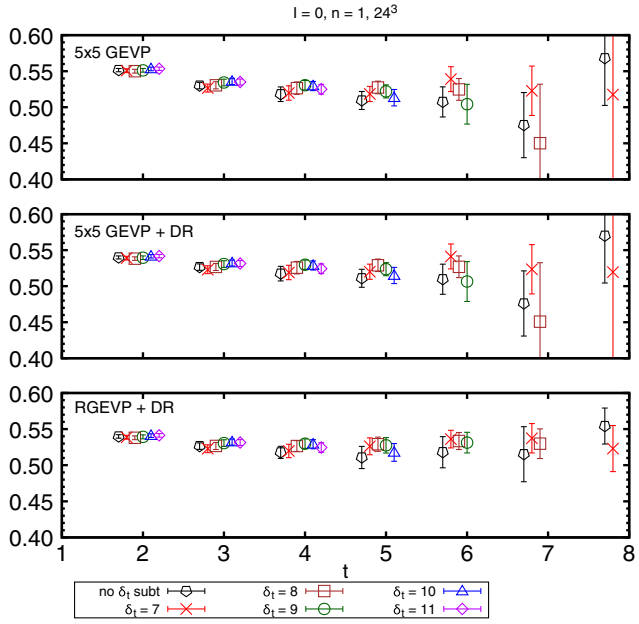

FIG. 10. The $I = 0$ effective first excited-state energy with (middle, lower) and without (upper) the dispersion relation method. 24^3, 5×5 (middle, upper) and 3×3 (lower) GEVP, $t - t_0 = 1$. Note the significant jump from $t = 6$ to 7 for $\delta_t = 8$ in the upper two panels.

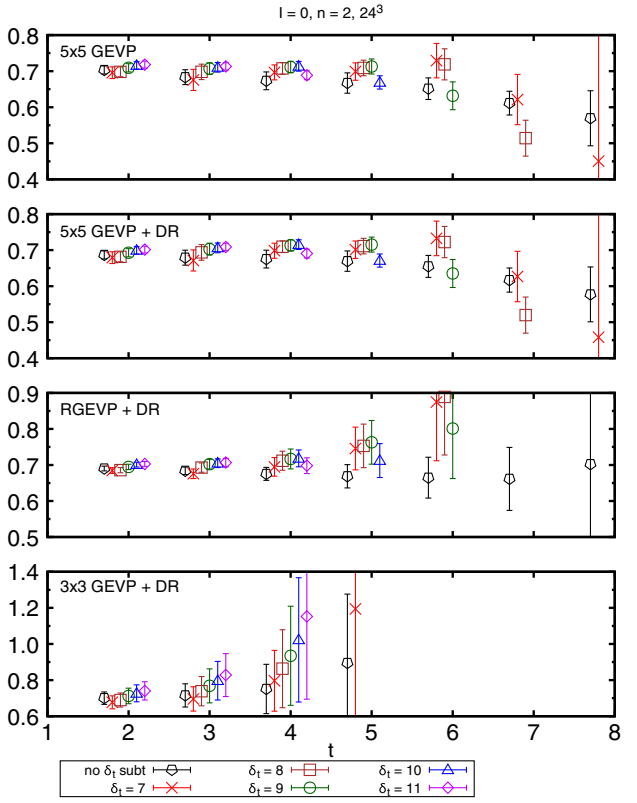

FIG. 11. The $I = 0$ effective second excited-state energy with (second, third, fourth panels) and without (first panel) the dispersion relation method. 24^3, 5×5 GEVP (first, second), 3×3 RGEVP (third) and 3×3 pure GEVP (fourth), $t - t_0 = 1$. Note the significant jump from $t = 6$ to 7 for $\delta_t = 8$ in the upper two panels. Statistical error on 3×3 GEVP is significantly large compared to the others.

The dispersion relation method reduces excited-state contamination and statistical errors, as does increasing δ_t. The effect of $t - t_0$ is less clear, though it appears it may also reduce excited-state effects.

Figure 9 shows the effective ground-state energy for the 5×5 GEVP with $t - t_0 = 1$ and matrix subtractions in the range $7 \le \delta_t \le 11$, both with and without the dispersion relation method and for the RGEVP. A small ATW effect may be visible in the upper panel when no matrix subtraction is performed, and it is largely absent in the middle and lower panels, showing again that the dispersion relation method largely eliminates it. We also observe that the RGEVP makes a moderate improvement on the statistical errors for larger times (lower panel).

Fit results are summarized in Table XI and Fig. 27. There appears to be a small systematic shift with the minimum time separation in the fit, t_{min}, but it is within the statistical uncertainty.

The first excited-state energies are summarized in Table XXXIX and Fig. 38 for a wide range of parameters. In Fig. 10, we show the first excited-state energy for the 5×5 GEVP and $t - t_0 = 1$. A plateau begins at $t = 3$ or 4, and an interesting systematic begins to emerge as well, which is even more pronounced for the second excited

TABLE XII. Fit results for two-pion energy of the $I = 0$ first excited state on the 24^3 lattice with various fit ranges and GEVP methods. We choose parameters $\delta_t = 9$ and $t - t_0 = 1$. The values of χ^2/d.o.f. are shown in the square brackets. The rebasing matrix is calculated as $5 \times 5 \to 3 \times 3$ at $t_0 = 3$.

	Fit range		
GEVP type	3–6	4–6	5–6
3×3	0.5319(45)[0.1]	0.5306(59)[0.1]	0.5298(72)[0.1]
4×4	0.5302(45)[0.4]	0.5296(64)[0.6]	0.5255(94)[0.8]
5×5	0.5304(45)[0.3]	0.5296(61)[0.5]	0.5262(83)[0.6]
RGEVP	0.5308(44)[0.1]	0.5302(65)[0.1]	0.528(11)[0.1]

TABLE XIII. Fit results for two-pion energy of the $I = 0$ second excited state on the 24^3 lattice with various fit ranges and GEVP methods. We choose parameters $\delta_t = 9$ and $t - t_0 = 1$. The values of χ^2/d.o.f. are shown in the square brackets. The rebasing matrix is calculated as $5 \times 5 \to 3 \times 3$ at $t_0 = 1$.

	Fit range	
GEVP type	3–5	4–5
3×3	0.713(40)[1.4]	0.841(89)[0.1]
4×4	0.709(14)[0.4]	0.714(15)[0.0]
5×5	0.710(13)[0.3]	0.714(14)[0.0]
RGEVP	0.695(12)[0.7]	0.699(23)[1.3]

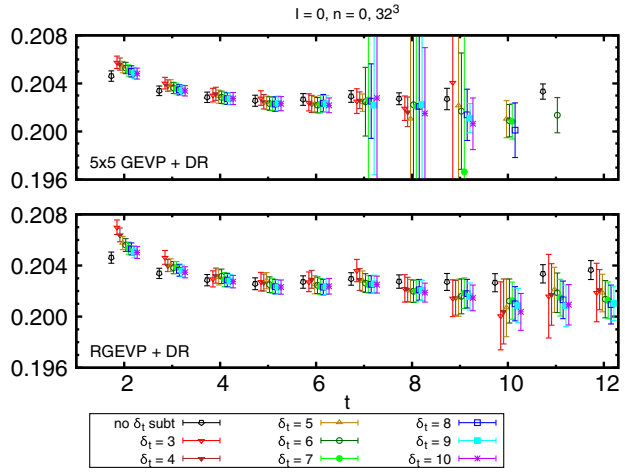

FIG. 12. The $I = 0$ effective ground-state energy with the dispersion relation method. 32^3, 5×5 GEVP (upper) and 2×2 RGEVP (lower), $t - t_0 = 1$. A multistep RGEVP is performed at $t_0 = 1$, 2, and 4 to go from $5 \times 5 \to 2 \times 2$.

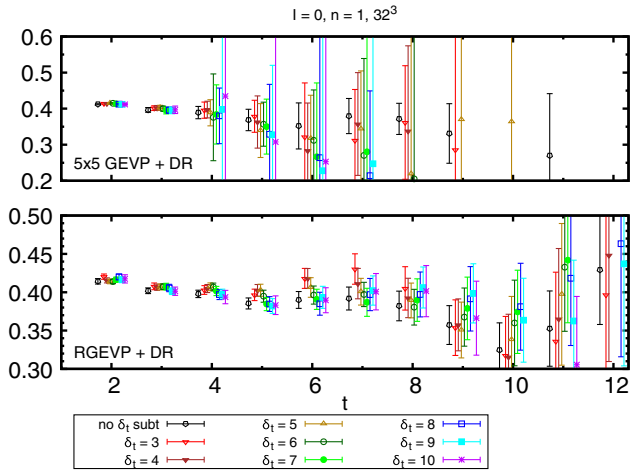

FIG. 13. The $I = 0$ effective first excited-state energy for the 5×5 GEVP (upper) and 2×2 RGEVP (lower) with the dispersion relation method. 32^3, $t - t_0 = 1$.

state, as we see shortly. A careful inspection of Fig. 10 shows a systematic downward drift of the energy for each $t_{\max,\delta_t}$. It is most visible between $t = 6$ and 7 for $\delta_t = 8$, but a smaller shift appears at smaller times for large values of δ_t. The effect is absent for the RGEVP (lower panel), and this leads us to believe it is due to a breakdown of the GEVP at large t due to large statistical errors in the correlation matrix.

Fit results are given in Table XII and displayed in Fig. 28. There is no detectable difference as $t_{\min}$ or the GEVP type varies.

The second excited state is less well resolved statistically, so we restrict our focus to relatively small times (see Fig. 11). There is little difference without or with the DR method (upper and middle panels); however, the downward trend observed for the first excited state is even more visible here and is also removed by the RGEVP, although the statistical errors increase significantly. Fit results are listed in Table XIII and plotted in Fig. 29.

TABLE XIV. Fit results for two-pion energy of the $I = 0$ ground state on the 32^3 lattice with various fit ranges and GEVP methods. We choose parameters $\delta_t = 5$ and $t - t_0 = 1$. The values of χ^2/d.o.f. are shown in the square brackets. The rebasing matrix is calculated as $5 \times 5 \to 4 \times 4$ at $t_0 = 1$, $4 \times 4 \to 3 \times 3$ at $t_0 = 2$, and $3 \times 3 \to 2 \times 2$ at $t_0 = 4$.

	Fit range		
GEVP type	4–9	5–9	6–9
3×3	0.20268(44)[0.4]	0.20252(48)[0.3]	0.20225(57)[0.2]
4×4	0.20279(48)[0.4]	0.20259(52)[0.3]	0.20234(62)[0.2]
5×5	0.20288(50)[0.4]	0.20265(55)[0.2]	0.20237(67)[0.1]
RGEVP	0.20272(51)[0.5]	0.20248(56)[0.4]	0.20235(66)[0.5]

Another dramatic difference happens when we reduce the GEVP to 3×3 (4×4 is essentially the same as 5×5) without rebasing (see the lower panel of Fig. 11). The noise increases dramatically because of the significant coupling between the second excited state and the $\pi\pi(011)$ operator, which is excluded in the 3×3 analysis. This is similar to the effect observed in Refs. [3,24], where adding a noisy scalar bilinear operator reduced the statistical error of (and excited state contamination in) the ground state, although it is the $\pi\pi(011)$ operator that is not included in the 3×3 but in the 4×4 and 5×5 analyses in this case.

The GEVP eigenvalues are too noisy even for short times to extract meaningful energies for the higher-energy states. They will have to wait for better statistics in the future.

On the 32^3 ensemble, the pattern repeats, except that the effective energies are even noisier, as seen in Fig. 12. It is interesting to note that the statistical error in the latter case is smaller at large time when no matrix subtraction is performed. Fits are summarized in Table XIV and Fig. 30.

After $t = 3$ or 4, the statistical errors get very large for the first excited state even with the DR method (see Fig. 13). However, we observe a large reduction in the statistical error using the RGEVP compared to the standard GEVP in this case. Rebasings to go from 5×5 down to 2×2 are implemented at $t_0 = 1$, $t_0 = 2$, and $t_0 = 4$. Presumably, the improvement occurs because the overlap of the higher states with the lower states is more and more unresolved with increasing t, adding only noise to the GEVP. Fit results are summarized in Table XV and Fig. 31.

The second excited state is shown in Fig. 14, where again there is a large reduction in statistical error with the RGEVP. A drift downwards with increasing time is

TABLE XV. Fit results for two-pion energy of the $I = 0$ first excited state on the 32^3 lattice with various fit ranges and GEVP methods. We choose parameters $\delta_t = 5$ and $t - t_0 = 1$. The values of χ^2/d.o.f. are shown in the square brackets. The rebasing matrix is calculated as $5 \times 5 \to 4 \times 4$ at $t_0 = 1$, $4 \times 4 \to 3 \times 3$ at $t_0 = 2$, and $3 \times 3 \to 2 \times 2$ at $t_0 = 4$.

	Fit range		
GEVP type	3–8	4–8	5–8
3×3	0.3989(60)[0.2]	0.399(12)[0.3]	0.394(24)[0.4]
4×4	0.3998(57)[0.1]	0.399(14)[0.2]	0.390(41)[0.2]
5×5	0.3997(59)[0.2]	0.398(17)[0.2]	0.392(28)[0.2]
RGEVP	0.4054(28)[0.5]	0.4052(41)[0.6]	0.3989(66)[0.3]

TABLE XVI. Fit results for two-pion energy of the $I = 0$ second excited state on the 32^3 lattice with various fit ranges and GEVP methods. We choose parameters $\delta_t = 5$ and $t - t_0 = 1$. The values of χ^2/d.o.f. are shown in the square brackets. The rebasing matrix is calculated as $5 \times 5 \to 4 \times 4$ at $t_0 = 1$ and $4 \times 4 \to 3 \times 3$ at $t_0 = 2$.

	Fit range		
GEVP type	3–6	4–6	5–6
3×3	0.428(19)[0.2]	0.426(26)[0.3]	0.417(32)[0.4]
4×4	0.442(44)[0.0]	0.450(66)[0.0]	0.445(80)[0.1]
5×5	0.417(26)[0.1]	0.414(32)[0.1]	0.414(35)[0.3]
RGEVP	0.5296(65)[0.5]	0.524(11)[0.4]	0.523(19)[0.9]

observed for larger values of δ_t for the 3×3 RGEVP, though it is not easy to investigate the systematic error at this point because of the accompanied large statistical errors. Fit results are summarized in Table XVI and Fig. 32.

In preparation for the next subsection, we now summarize in Table XVII the energies and corresponding time-slice fit ranges and GEVP types that we will use to compute the phase shifts. In all cases except the third excited state for $I = 2$, which is only accessible with the 4×4 GEVP, we choose the RGEVP, since the noise is usually reduced or unchanged from the ordinary GEVP. In addition, we believe it is more robust at large times, since poorly resolved elements of the correlation function are avoided. As mentioned already, we stick to small time slices where the signal is better resolved, and we use the results of the DR method throughout. With the DR method, we see negligible dependence on $t - t_0$, so we take it to be 1 in all cases.

For the $I = 2$ ground state, we choose 4–10 (24^3) and 4–9 (32^3) for the fit range. From Figs. 19 and 23, one can see that the results are very stable with both the range and GEVP type.

Similarly, for the first excited state we choose 5–9 and 4–10 (in the case of 24^3, a small excited-state effect may be visible at $t = 4$). In both cases, the 2×2 GEVP appears to be a little high. For the second excited state we take 3–9 and 3–7. Finally, for the third excited state our ranges are 3–5 and 4–7.

For $I = 0$, it is not as straightforward to choose central values due to larger statistical errors, especially for the 32^3 ensemble, and as we have seen already, small times comprise the set of usable time slices.

From Figs. 27 (24^3 lattice) and 30 (32^3 lattice), one sees small variations with t_{min} for the ground states. We choose fit ranges 4–8 and 5–9, respectively. On the 24^3 lattice, we see no significant variation for the first excited state, so we take 3–6. For 32^3, the errors are large for all but the RGEVP, and we take 4–8. Finally, for the second excited state, the fit ranges are chosen to be 3–6 and 4–6. In the latter case, we use $\delta_t = 3$, since we observed a flatter plateau and smaller statistical errors for this choice. Higher excited states cannot be extracted from our data; improved statistics are needed.

In Fig. 15, two-pion energies and energy shifts due to pion-pion interactions in a finite box are plotted. The error is statistical only. The results for the $I = 2$ third excited state ($n = 3$) show smaller energy shifts than that for the second excited state ($n = 2$). This may indicate that there are significant systematic effects.

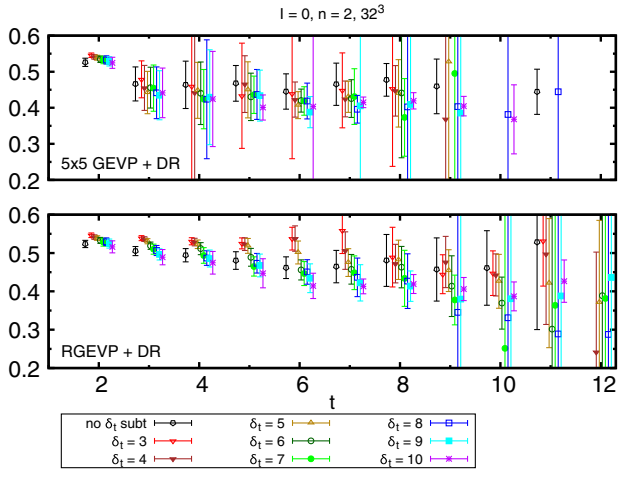

FIG. 14. The $I = 0$ effective second excited-state energy for the 5×5 GEVP (upper) and 3×3 RGEVP (lower) with the dispersion relation method. 32^3, $t - t_0 = 1$.

B. Phase shifts

The phase shifts are computed using the fitted energies described in the previous subsections. Specifically, we take fit values corresponding to Eq. (26) and insert them into Eq. (24). For the $I = 2$ ground state with pions at rest, the interacting two-pion energy is above the $2m_\pi$ threshold, since the interaction is repulsive, and a phase shift is readily calculated using Eq. (24). For $I = 0$, the ground state is below the threshold, so the phase shift is purely imaginary.

TABLE XVII. Summary of two-pion energies and phase shifts (δ). The energies are determined by correlated χ^2 fits to the effective energies with the DR method. The last column gives the scattering length in units of the pion mass. The first error is statistical, and the second (δ, $m_\pi a_0$) a systematic error, which is estimated by varying fit range as well as δ_t in the range shown in the square brackets. See text for more detail.

I	n	GEVP type	Fit range	δ_t	χ^2/d.o.f.	Energy	δ_0 (deg)	$m_\pi a_0^I$
				24^3 lattice				
2	0	RGEVP	4–10	5[4–8]	0.6	0.28130(34)	−0.374(13)(4)	−0.0496(11)(5)
2	1	RGEVP	5–9	5[4–8]	0.3	0.60789(31)	−12.33(22)(20)	
2	2	RGEVP	3–9	5[4–8]	1.4	0.81753(56)	−20.18(43)(54)	
2	3	4×4	3–5	5[4–8]	0.1	0.9658(17)	−26.5(2.4)(4)	
0	0	RGEVP	4–8	7[5–9]	1.1	0.27069(41)		0.2038(70)(160)
0	1	RGEVP	3–6	9[6–9]	0.1	0.5308(44)	45.1(2.9)(2.1)	
0	2	RGEVP	3–5	9[7–9]	0.7	0.695(12)	83(11)(15)	
				32^3 lattice				
2	0	RGEVP	4–9	8[4–8]	0.8	0.21041(37)	−0.424(51)(23)	−0.0537(42)(22)
2	1	RGEVP	4–10	8[4–8]	0.3	0.45648(36)	−13.37(32)(11)	
2	2	RGEVP	3–7	8[4–8]	0.3	0.61552(58)	−22.90(59)(34)	
2	3	4×4	4–7	8[4–8]	0.1	0.7230(17)	−24.2(3.2)(2.1)	
0	0	RGEVP	5–9	5[5–8]	0.4	0.20248(56)		0.1947(150)(126)
0	1	RGEVP	4–8	5[5–8]	0.6	0.4052(41)	38.6(3.6)(10.1)	
0	2	RGEVP	4–6	5[4–6]	0.4	0.5304(91)	71(12)(16)	

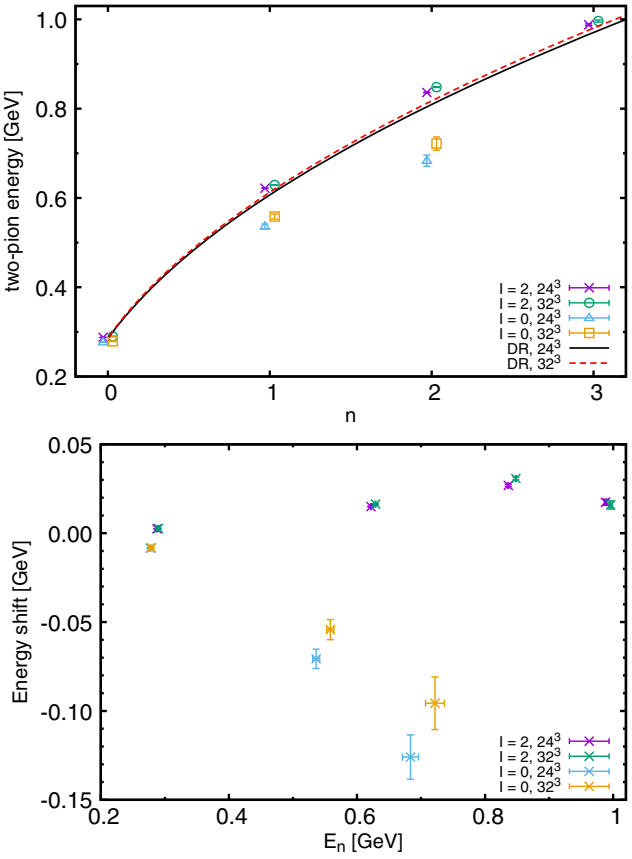

FIG. 15. Summary of two-pion energies obtained by correlated fits to DR effective energies (top) and their difference from the corresponding noninteracting energies given by Eq. (27) (bottom). In the top panel, the noninteracting energy is also drawn using the continuum dispersion relation [Eq. (27)] with $|\vec{p}_n|^2 = n(2\pi/L)^2$ for both 24^3 and 32^3 lattices.

The phase shifts for each state and various fit ranges for the energies are summarized in Tables XVIII–XXIX.

Results corresponding to the energies (fit ranges) chosen at the end of the last section are shown in Fig. 16 and given in Table XVII for both ensembles. Agreement with the Roy equation result[3] [28,30] is observed up to the third (second) excited state for $I = 2(0)$. Even though, strictly speaking, Lüscher's method [6] is not valid above the inelastic scattering threshold ($4m_\pi$), which is shown for each ensemble by the vertical gray lines in Fig. 16, we see no evidence of a dramatic breakdown above this threshold (or higher pion multiplicities, $K\bar{K}$, and so on). It will be interesting to see in future works with more precision if a signal of such a breakdown emerges.

In addition to statistical errors, we also estimate a systematic error due to choice of fit range for the energy and δ_t in the matrix subtraction to remove the ATW effect. The error is estimated by comparing phase shifts for various fit ranges and δ_t values, and taking half the difference between minimum and maximum central values for a given state. For the comparison of the systematic error, we use the fit ranges shown in Tables XVIII–XXIX and a range of δ_t values shown in the square brackets in Table XVII. We remove the fit results that have more than twice as large a statistical error as the fit result shown in Table XVII from the estimation of the systematic error. In all cases, we do not vary the GEVP type and choose the RGEVP except for

[3]In the figures displaying Roy equation results, we always use the formulas in Ref. [28], for technical reasons. In later papers, we will switch to the update in Ref. [30].

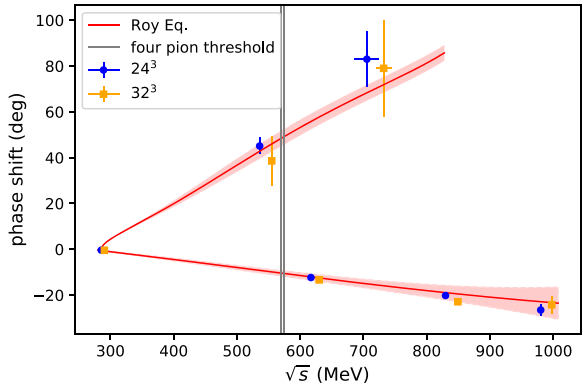

FIG. 16. Pion-scattering phase shifts for ground and higher excited states; $I = 0$ (upper) and $I = 2$ (lower). Bars denote statistical and systematic errors added in quadrature (see Table XVII). The Roy equation results [28] are shown by solid lines and corresponding error bands. Vertical gray lines denote $4m_\pi$ thresholds for 24^3 and 32^3 ensembles, above which the method of determining phase shifts [6] in this work is no longer strictly valid.

the $I = 2$ third excited state, where we need to use the full-size 4×4 GEVP. This is because only the RGEVP appears to give reasonable results for the $I = 0$ excited states on the 32^3 lattice, while the other results are less dependent on GEVP type than fit range. The systematic errors are small for the ground state (less than the statistical error) and become comparable to, and even larger than, the statistical error with increasing energy. Since the $I = 0$ energies are noisier than their $I = 2$ counterparts, so too are their phase shifts.

The physical energies corresponding to the various states differ slightly on the two ensembles, so to compare the phase shifts at fixed energy, we do a piecewise linear interpolation of the phase shifts in discrete energy at fixed lattice spacing and then extrapolate the interpolated phase shifts to the continuum, $a \to 0$, at fixed energy. The extrapolation is performed linearly in a^2. The results are shown in Fig. 17. In each panel, the $a \to 0$ extrapolation is shown with a green band. The values are compatible with the Roy equation, albeit within relatively large uncertainties, especially for $I = 0$. For this study, we calculate error bands for the dispersive results using Ref. [28], and we defer a more comprehensive study—including, for example, the more accurate results of Ref. [30]—to a future publication.

Lastly, we discuss the two-pion scattering length. Since the relation between the two-pion phase shift δ_0 and scattering length a_0 is given as[4]

$$k \cot \delta_0(k) = \frac{1}{a_0} + \frac{1}{2} r_0 k^2 + O(k^4), \tag{33}$$

with the effective range parameter r_0, we can calculate the scattering length by

[4]The subscript refers to the s-wave channel.

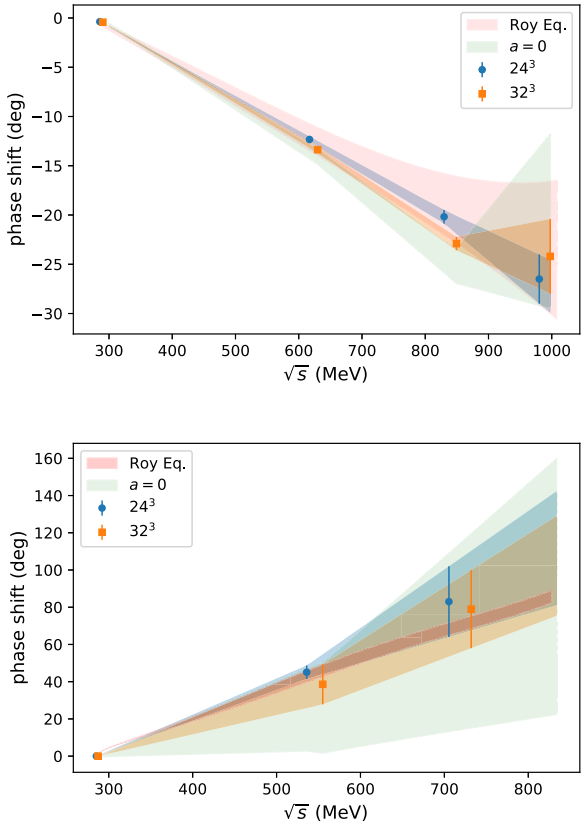

FIG. 17. Continuum limit of the pion-scattering phase shifts for ground and higher excited states (light green bands) for $I = 2$ (upper panel) and $I = 0$ (lower). The continuum extrapolation is performed linearly in a^2 after linear interpolation in the energy at fixed lattice spacing. The Roy equation results [28] are shown by the light-red error bands.

$$a_0 = \frac{\tan \delta_0(k)}{k} + O(k^2), \tag{34}$$

with a sufficiently small value of k, which can be obtained with the ground state straightforwardly for the $I = 2$ channel. For the $I = 0$ channel, k is a pure imaginary number for the ground state, and we cannot directly use Eq. (33) and the formulas given in Sec. II F for this case. It is known [19] that these formulas can be analytically continued with pure imaginary values of k. With that, we obtain the scattering length as a real number. The values for the scattering lengths for various ranges of fits to the ground-state energies are given in Tables XXX–XXXIII. In Table XVII, central values are displayed; systematic errors are computed as before for the phase shifts. A simple linear extrapolation in a^2, after combining statistical and systematic errors in quadrature, yields

$$m_\pi a_0^2 = -0.058(11), \tag{35}$$

$$m_\pi a_0^0 = 0.184(47) \tag{36}$$

for $I = 2$ and $I = 0$, respectively.

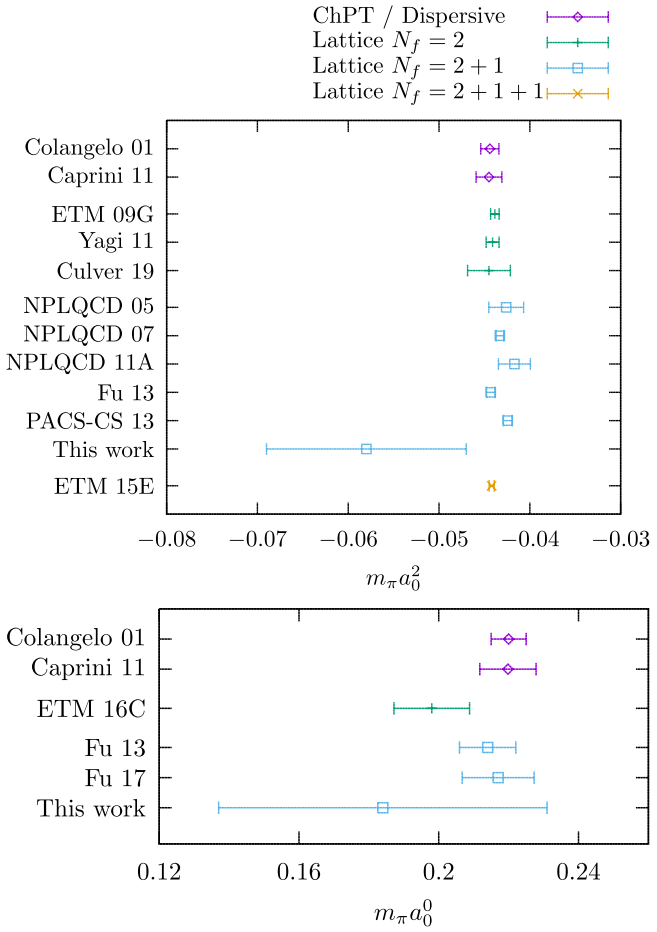

FIG. 18. Summary plot of two-pion scattering length $m_\pi a_0^I$ for $I = 2$ (upper) and $I = 0$, comparing with results from earlier phenomenology and lattice studies summarized by FLAG [50]. Earlier lattice results quoted with statistical error only are not plotted. The plotted earlier results are all obtained by a chiral extrapolation [Eqs. (37) and (38)] to the physical pion mass using an inputted value of f_π and lattice results at unphysical pion masses, while the result from this work is a purely lattice result at the physical pion mass.

Figure 18 shows a comparison of these numbers with results from earlier works, including phenomenology and lattice QCD. The figure indicates our results are consistent with ChPT prediction and earlier lattice calculations [29,50] within 1.3σ for $I = 2$ and 1σ for $I = 0$. The errors on our results are somewhat larger, because the earlier works at unphysical pion masses performed a chiral extrapolation with the assumption

$$m_\pi a_0^2 = -\frac{m_\pi^2}{8\pi f_\pi^2}\left\{1 + \frac{m_\pi^2}{16\pi^2 f_\pi^2}\left[3\ln\frac{m_\pi^2}{f_\pi^2} - 1 - l_{\pi\pi}^2\right]\right\}, \quad (37)$$

$$m_\pi a_0^0 = \frac{7m_\pi^2}{16\pi f_\pi^2}\left\{1 - \frac{m_\pi^2}{16\pi^2 f_\pi^2}\left[9\ln\frac{m_\pi^2}{f_\pi^2} - 5 - l_{\pi\pi}^0\right]\right\}, \quad (38)$$

where the leading order with the pion decay constant f_π was inputted independently of lattice calculation. They only used lattice results for determination of the energy constants $l_{\pi\pi}^I$, which is associated with the subleading contribution to the scattering length. Our results, on the other hand, are pure lattice results obtained without assuming the leading contribution. Another work [23] carried out at physical pion mass gave $m_\pi a_0^2 = -0.0481(86)$, which is omitted from the plot because of the absence of the systematic error but certainly has a larger error than others, even without the continuum extrapolation.

V. COST COMPARISON WITH G-PARITY BOUNDARY CONDITIONS

One of the main goals of this study is to extract the signal of an excited state that has an energy near the kaon mass and is useful for calculation of $K \to \pi\pi$ decay matrix elements and ε', the measure of direct CP violation. We find from the previous section that the energy of the first excited state is close to the kaon mass and well resolved. We have carried out the same kind of studies with G-parity boundary conditions (GPBCs) [2,3,24], in which pions are antiperiodic in space and therefore must have nonzero spatial momentum, and realized the on-shell $K \to \pi\pi$ kinematics with the corresponding $I = 0$ ground two-pion state. It is valuable to compare the effectiveness of GPBCs against the conventional periodic boundary conditions (PBCs). In this section, we carry out an efficiency comparison between the GPBC ground state and PBC first excited state.

In Ref. [24], measurements were carried out on an ensemble of 741 gauge field configurations with identical parameters to those used in the 32^3 ensemble, except that GPBCs were used. Nine hundred low modes and twenty-four (spin-color-flavor diluted) random source fields on each time slice comprised the A2A [40] measurement setup. The high-mode part is double for GPBCs—1536 vs 768 modes in this work because of no need of flavor dilution with PBC. The low-mode part also differs—900 exact eigenvectors (GPBCs) vs 2000 approximate coarse-grained eigenvectors based on local coherence (PBCs) [51]. It is not easy to estimate a quantitative difference between this and the GPBC calculation, since different setups (low modes, AMA, solvers, etc.) have been used in the two cases. However, assuming similar solver performances, we expect the cost of GPBCs being roughly twice as much, for the same quark mass and lattice volume, because of the doubled size of the Dirac operator. Taking the two-pion energy at the kaon mass as the goal of our calculation, this cost has to be contrasted with a possibly easier extraction of energy levels in GPBCs compared to PBCs. Another difference is the time-translation interval of connected diagrams. Most of the connected diagrams are calculated with six source locations in this work and eight source locations in the earlier work. One exception is the connected diagram of the σ-σ two-point function, which is

computed, again, with six source locations in this work, but with 64 source locations in the earlier work. This difference in σ-σ measurement detail would not affect computational cost, as it is very cheap, though it might make an impact on the precision.

We will focus on the zero-total-momentum rest frame. For $I = 2$, Table X in Ref. [24] lists the energy (in lattice units) as 0.41528(46) with $t_0 = 11$, $t - t_0 = 1$. In this study, the corresponding value is 0.45549(160). Recall that the momentum, in units of $2\pi/L$, of the pions is slightly smaller in the GPBC case, $\sqrt{3 \times (\frac{1}{2})^2}$ instead of 1, and therefore we do not expect the central values to agree. In fact, both the number in our present study and that of Ref. [24] agree with the dispersive results at their corresponding momenta. Accounting for the increased error growth due to this slight mismatch in the energy [52] and the difference in the number of measurements expects the GPBC result to be more precise than the PBC by a factor of $\approx 1.6 \times \sqrt{741/107} = 4.2$, which implies that the efficiency is about the same for the two methods in this case.

The more salient comparison is for the $I = 0$ case, since that is the main reason for using GPBCs. In Table X in Ref. [24], the energy of the two-pion state is given as 0.3479(11)[10], where the first error is statistical and the second is excited-state systematic. It is determined from a three-operator, two-state fit with fit range 6–15. A GEVP analysis with $t_0 = 5$, $t - t_0 = 1$, without matrix subtraction, gives 0.3489(11), where the error is statistical. The matrix subtraction was not performed for this analysis, as the ATW effects with GPBCs are due to a long-time propagation of moving pions, and the estimates of the size of the dominant ATW contribution gave values 10 times smaller than the statistical errors on the data, and separate multioperator fits with the ATW term included gave results consistent with zero. The corresponding result for PBC is 0.406(16), where a matrix subtraction was performed to remove ATW contamination. While accounting again for the mismatch in energies and number of measurements expects that the GPBC result should be more precise by a factor of about 3.5, we do not see a significant shift by the matrix subtraction for $I = 0$, and it would be interesting to study and understand how significant the ATW effect on $I = 0$ is. In any case, the factor 3.5 is not big enough to explain the difference in the statistical error, which is about 4 times bigger in the PBC case for equivalent statistics and energies. Of course, the argument about exponential growth of errors is not perfect, since the prefactors may differ between the two cases.

In the GPBC case, the boundary conditions lead to cubic symmetry breaking at the quark level, which is suppressed by averaging pairs of single-pion interpolating operators with different quark and antiquark momentum assignments, but with the same total pion momentum [24,27]. For the ground state, eight pairs (averages) of pion interpolating operators are used to construct 64 correlation functions, which most strongly overlap with the s-wave G-parity ground state. Here, we use six single-pion operators with momentum $(\pm 1, 0, 0)$ (plus permutations), or 36 correlators, for the corresponding s-wave excited state. While it is difficult to quantify the improvement gained from averaging over more combinations due to correlations, we do expect some benefit and will study this question in future calculations in both setups.

While not as direct, it is interesting and useful to compare the 24^3 ensemble to the GPBC case. Here, the PBC setup is the same as before, but the statistics are based on 258 configurations. The relevant two-pion energy ($t = 4$) is 0.5298(64) in lattice units. Converting the errors to GeV and accounting for the different number of measurements yields a factor ≈ 2.5, by which the GPBC result is expected to be more precise than the PBC result. Accounting for the different number of pion momentum combinations as before, this factor is further reduced to somewhere between 1 and 2. (These factors are based on an assumption of statistical independence between the momentum orientations that may not be borne out in practice.) The exponential factor is roughly 1 in this case, which we ignore. A more thorough comparison between the GPBC and PBC approaches will be performed when we have measurements performed on an equivalent statistical sample.

VI. CONCLUSION

In this work, we have carried out a study of pion scattering at the physical point using $2 + 1$ flavor Möbius domain-wall fermion ensembles with inverse lattice spacings of 1.023 and 1.378 GeV using periodic boundary conditions (PBCs). The main focus was to extract the first excited-state energies in the rest frame, in both $I = 0$ and 2 channels, and their corresponding phase shifts, using the finite-volume Lüscher formalism [6]. The first excited-state energy (roughly) corresponds to the important case of on-shell $K \to \pi\pi$ decay, which is our longer-term goal [53].

The energies were computed using the GEVP method [34,35]. In order to extract the desired first excited state and control excited-state contamination, several two-pion interpolating operators were used, including a simple scalar bilinear. The other operators were constructed from pions with equal and opposite momenta. The single-pion momentum took values (0, 0, 0), $(\pm 1, 0, 0)$, $(\pm 1, \pm 1, 0)$, $(\pm 1, \pm 1, \pm 1)$ (and permutations) in units of $2\pi/L$. As found in Refs. [3,24], the inclusion of the scalar bilinear with the quantum numbers of the vacuum is crucial to disentangle the first and second excited-state energies.

The GEVP, or matrix correlation function, size ranged from 2×2 to 5×5. We found in most cases that the size did not have a large effect after 2×2 for $I = 2$ and 3×3 for $I = 0$. However, in some cases, the noise of the higher states in the correlation matrix at large times adversely impacted the lower energies. In these cases, the overlap of

higher states with lower states was small, and the extra states only contributed noise to the lower states. This problem led to a modification of the method: as time increases, the operator basis of the GEVP is changed ("rebased") using the eigenvectors of the GEVP from earlier times. While this method gives similar results in most cases studied here, it had a dramatic improvement for the $I = 0$ first excited state on the 32^3 ensemble, where the statistics were relatively poor (see Figs. 30–32). This RGEVP then allowed a relatively precise phase-shift determination (see Fig. 16).

We started this series of $K \to \pi\pi$ studies with G-parity boundary conditions (GPBCs) [2,3,24] because we anticipated it would be challenging to extract the signal of an excited two-pion state, which is necessary for the $K \to \pi\pi$ study using PBCs. After seeing the successful calculation of two-pion scattering and $K \to \pi\pi$ decay amplitudes with GPBCs [3,24], we launched this PBC project to find a practical alternative, as a further check, and to enable calculations with isospin corrections. We note once again that we have been successful in extracting signals of multiple states: the four lowest-energy states for $I = 2$, and the three lowest ones (at least on the 24^3 lattice with better statistics) for $I = 0$, despite the anticipated difficulty of extracting the excited-state signals.

In this first study, we have focused on two important systematic effects. First, by computing energies and phase shifts on ensembles with different lattice spacings, we find no statistically significant discretization errors for $I = 0$ and small, but statistically significant, effects for $I = 2$. Second, we studied the time dependence of the effective energies and observed noticeable excited-state contamination for short times. We also saw that many of the effects arising from single-pion excited states could be removed with the dispersion relation method, which also removes leading discretization errors. Moreover, we expect the systematic uncertainties for PBCs to be similar to GPBCs. In that case, statistical and systematic errors on the energies were estimated to be roughly equal [24].

Another important motivation of employing PBCs is that it appears difficult to use GPBCs to compute QED and strong-interaction isospin-breaking effects, since they explicitly enforce isospin symmetry, though isospin symmetry breaking is expected to significantly impact the value of the direct CP violation parameter ε' (20%–30%) [54]. Controlling such effects precisely is important for the next generation of ε' calculations.

We are currently improving the statistics on both ensembles for our companion $K \to \pi\pi$ calculation, and when that is complete, we will have an even better comparison with G-parity and estimates of systematic errors. These results and the ones so far from the kaon decay project leave us optimistic for the PBC method.

ACKNOWLEDGMENTS

We thank the U.S. Department of Energy (DOE) for partial support under Awards No. DE-FG02-92ER40716 (T. B., D. H.), No. DE-SC0010339 (T. B., L. J., M. T.), No. DE-SC0046548 (A. S. M.), No. DE-SC0012704 (P. A. B., T. I., C. J., A. S.), and No. DE-SC001704 (A. S.). L. J. and M. T. were also supported in part by the U.S. DOE under Early Career Award No. DE-SC002114. The work of C. K. was supported by the U.S. DOE Exascale Computing Project. P. B., T. I., and C. J. acknowledge support under DOE Grant No. SciDAC-5 LAB 22-2580. T. I. is also supported by the Department of Energy, Laboratory Directed Research and Development (LDRD No. 23-051) of BNL and RIKEN BNL Research Center. The research of M. B. was funded through the MUR program for young researchers, "Rita Levi Montalcini." The work of D. H. was supported by the Swiss National Science Foundation (SNSF) through Grant No. 200020_208222. The software used for this work is based on `CPS`, `Grid`, and `Hadrons`. We thank the collaborators in the RBC and UKQCD Collaborations, especially N. H. Christ, for fruitful discussions. Computations were carried out with USQCD resources funded by the U.S. DOE at BNL and JLab.

APPENDIX A: WICK CONTRACTIONS

We write down the explicit forms of two-pion operators and the Wick contractions of two-point functions of these operators to clarify the convention used in this paper.

$$\tilde{O}^{2,0}_{\pi\pi}(X_1, X_2) = \frac{1}{\sqrt{6}}(\pi^+(X_1)\pi^-(X_2) + 2\pi^0(X_1)\pi^0(X_2) + \pi^-(X_1)\pi^+(X_2)), \tag{A1}$$

$$\tilde{O}^{0,0}_{\pi\pi}(X_1, X_2) = \frac{1}{\sqrt{3}}(\pi^+(X_1)\pi^-(X_2) - \pi^0(X_1)\pi^0(X_2) + \pi^-(X_1)\pi^+(X_2)), \tag{A2}$$

where X_i denotes the 4D position x_i, or the set of the time coordinate and spatial momentum, $(t_i, \vec{p}_i)$, of the operator labeled by i. Wick contractions for two-point functions of these operators yield

$$\langle \tilde{O}^{2,0}_{\pi\pi}(X_1, X_2)\tilde{O}^{2,0}_{\pi\pi}(X_3, X_4)^\dagger \rangle = 2D(X_1, X_2, X_3, X_4) - 2C(X_1, X_2, X_3, X_4), \tag{A3}$$

$$\langle \tilde{O}^{0,0}_{\pi\pi}(X_1, X_2)\tilde{O}^{0,0}_{\pi\pi}(X_3, X_4)^\dagger \rangle = 2D(X_1, X_2, X_3, X_4) + C(X_1, X_2, X_3, X_4) - 6R(X_1, X_2, X_3, X_4) + 3V(X_1, X_2, X_3, X_4), \tag{A4}$$

where we define the contributions of the diagrams D, C, R, and V by

$$D(x_1,x_2,x_3,x_4) = \frac{1}{2}\langle \mathrm{Tr}[\gamma_5 S_l(x_1,x_3)\gamma_5 S_l(x_3,x_1)] \cdot \mathrm{Tr}[\gamma_5 S_l(x_2,x_4)\gamma_5 S_l(x_4,x_2)] + \mathrm{Tr}[\gamma_5 S_l(x_1,x_4)\gamma_5 S_l(x_4,x_1)] \cdot \mathrm{Tr}[\gamma_5 S_l(x_2,x_3)\gamma_5 S_l(x_3,x_2)]\rangle, \tag{A5}$$

$$\begin{aligned} C(x_1,x_2,x_3,x_4) &= \frac{1}{2}\langle \mathrm{Tr}[\gamma_5 S_l(x_1,x_3)\gamma_5 S_l(x_3,x_2)\cdot\gamma_5 S_l(x_2,x_4)\gamma_5 S_l(x_4,x_1)] \\ &\quad + \mathrm{Tr}[\gamma_5 S_l(x_1,x_4)\gamma_5 S_l(x_4,x_2)\cdot\gamma_5 S_l(x_2,x_3)\gamma_5 S_l(x_3,x_1)]\rangle \\ &= \langle \mathrm{Tr}[\gamma_5 S_l(x_1,x_3)\gamma_5 S_l(x_3,x_2)\cdot\gamma_5 S_l(x_2,x_4)\gamma_5 S_l(x_4,x_1)]\rangle, \end{aligned} \tag{A6}$$

$$\begin{aligned} R(x_1,x_2,x_3,x_4) &= \frac{1}{4}\langle \mathrm{Tr}[\gamma_5 S_l(x_1,x_2)\gamma_5 S_l(x_2,x_3)\cdot\gamma_5 S_l(x_3,x_4)\gamma_5 S_l(x_4,x_1)] \\ &\quad + \mathrm{Tr}[\gamma_5 S_l(x_1,x_4)\gamma_5 S_l(x_4,x_3)\cdot\gamma_5 S_l(x_3,x_2)\gamma_5 S_l(x_2,x_1)] \\ &\quad + \mathrm{Tr}[\gamma_5 S_l(x_1,x_2)\gamma_5 S_l(x_2,x_4)\cdot\gamma_5 S_l(x_4,x_3)\gamma_5 S_l(x_3,x_1)] \\ &\quad + \mathrm{Tr}[\gamma_5 S_l(x_1,x_3)\gamma_5 S_l(x_3,x_4)\cdot\gamma_5 S_l(x_4,x_2)\gamma_5 S_l(x_2,x_1)]\rangle \\ &= \frac{1}{2}\langle \mathrm{Tr}[\gamma_5 S_l(x_1,x_2)\gamma_5 S_l(x_2,x_3)\cdot\gamma_5 S_l(x_3,x_4)\gamma_5 S_l(x_4,x_1)] \\ &\quad + \mathrm{Tr}[\gamma_5 S_l(x_1,x_3)\gamma_5 S_l(x_3,x_4)\cdot\gamma_5 S_l(x_4,x_2)\gamma_5 S_l(x_2,x_1)]\rangle, \end{aligned} \tag{A7}$$

$$V(x_1,x_2,x_3,x_4) = \langle \mathrm{Tr}[\gamma_5 S_l(x_1,x_2)\gamma_5 S_l(x_2,x_1)] \cdot \mathrm{Tr}[\gamma_5 S_l(x_3,x_4)\gamma_5 S_l(x_4,x_3)]\rangle \tag{A8}$$

for $X_i = x_i$. For our actual calculation with the A2A quark propagators proposed in Ref. [40], we define the pion meson field $\Pi^{\pi}_{ij}(t,\vec{p})$, which is projected to a certain spatial momentum and spin-color singlet but has mode indices that label the low and high modes. In our calculation, there are 2000 low modes and $4\times 3\times 64 = 768$ high modes from the spin-color-time dilution, and therefore each mode index runs for 1, 2, …, 2768. The expressions of the contractions in Eqs. (A5)–(A8) in time-momentum space with the pion meson fields are then given as follows:

$$D(X_1,X_2,X_3,X_4) = \frac{1}{2}\left\langle \sum_{i,j}\Pi^{\pi}_{ij}(X_1)\Pi^{\pi}_{ji}(X_3)\cdot\sum_{k,l}\Pi^{\pi}_{kl}(X_2)\Pi^{\pi}_{lk}(X_4) + \sum_{i,j}\Pi^{\pi}_{ij}(X_1)\Pi^{\pi}_{ji}(X_4)\cdot\sum_{k,l}\Pi^{\pi}_{kl}(X_2)\Pi^{\pi}_{lk}(X_3)\right\rangle, \tag{A9}$$

$$C(X_1,X_2,X_3,X_4) = \left\langle \sum_{i,j,k,l}\Pi^{\pi}_{ij}(X_1)\Pi^{\pi}_{jk}(X_3)\Pi^{\pi}_{kl}(X_2)\Pi^{\pi}_{li}(X_4)\right\rangle, \tag{A10}$$

$$R(X_1,X_2,X_3,X_4) = \frac{1}{2}\left\langle \sum_{i,j,k,l}\Pi^{\pi}_{ij}(X_1)\Pi^{\pi}_{jk}(X_2)\Pi^{\pi}_{kl}(X_3)\Pi^{\pi}_{li}(X_4) + \sum_{i,j,k,l}\Pi^{\pi}_{ij}(X_1)\Pi^{\pi}_{jk}(X_3)\Pi^{\pi}_{kl}(X_4)\Pi^{\pi}_{li}(X_2)\right\rangle, \tag{A11}$$

$$V(X_1,X_2,X_3,X_4) = \left\langle \sum_{i,j}\Pi^{\pi}_{ij}(X_1)\Pi^{\pi}_{ji}(X_2)\cdot\sum_{k,l}\Pi^{\pi}_{kl}(X_3)\Pi^{\pi}_{lk}(X_4)\right\rangle, \tag{A12}$$

with $X_i = (t_i,\vec{p}_i)$.

Wick contractions for two-point functions including one or two sigma operators read

$$\langle \tilde{O}^{2,0}_{\pi\pi}(X_1,X_2)\sigma(X_3)^{\dagger}\rangle = -\sqrt{6}R_{\sigma}(X_1,X_2,X_3) + \sqrt{6}V_{\sigma}(X_1,X_2,X_3), \tag{A13}$$

$$\langle \sigma(X_1)\sigma(X_3)^{\dagger}\rangle = -R_{\sigma\sigma}(X_1,X_3) + 2V_{\sigma\sigma}(X_1,X_3). \tag{A14}$$

Here, we define

$$\begin{aligned} R_{\sigma}(x_1,x_2,x_3) &= \frac{1}{2}\langle \mathrm{Tr}[\gamma_5 S_l(x_1,x_2)\gamma_5 S_l(x_2,x_3)S_l(x_3,x_1)] + \mathrm{Tr}[\gamma_5 S_l(x_2,x_1)\gamma_5 S_l(x_1,x_3)S_l(x_3,x_2)]\rangle \\ &= \langle \mathrm{Tr}[\gamma_5 S_l(x_1,x_2)\gamma_5 S_l(x_2,x_3)S_l(x_3,x_1)]\rangle, \end{aligned} \tag{A15}$$

$$V_\sigma(x_1,x_2,x_3) = \langle \mathrm{Tr}[\gamma_5 S_l(x_1,x_2)\gamma_5 S_l(x_2,x_3)] \cdot \mathrm{Tr}[S_l(x_3,x_1)]\rangle, \quad \text{(A16)}$$

$$R_{\sigma\sigma}(x_1,x_3) = \langle \mathrm{Tr}[S_l(x_1,x_3)S_l(x_3,x_1)]\rangle, \quad \text{(A17)}$$

$$V_{\sigma\sigma}(x_1,x_3) = \langle \mathrm{Tr}[S_l(x_1,x_1)S_l(x_3,x_3)]\rangle, \quad \text{(A18)}$$

which can be expressed in terms of the pion Π^π_{ij} and sigma Π^σ_{ij} meson fields as

$$R_\sigma(X_1,X_2,X_3) = \left\langle \sum_{i,j,k} \Pi^\pi_{ij}(X_1)\Pi^\pi_{jk}(X_2)\Pi^\sigma_{ki}(X_3) \right\rangle, \quad \text{(A19)}$$

$$V_\sigma(X_1,X_2,X_3) = \left\langle \sum_{i,j} \Pi^\pi_{ij}(X_1)\Pi^\pi_{ji}(X_2) \cdot \sum_k \Pi^\sigma_{kk}(X_3) \right\rangle, \quad \text{(A20)}$$

$$R_{\sigma\sigma}(X_1,X_3) = \left\langle \sum_{i,j} \Pi^\sigma_{ij}(X_1)\Pi^\sigma_{ji}(X_3) \right\rangle, \quad \text{(A21)}$$

$$V_{\sigma\sigma}(X_1,X_3) = \left\langle \sum_i \Pi^\sigma_{ii}(X_1) \cdot \sum_j \Pi^\sigma_{jj}(X_3) \right\rangle \quad \text{(A22)}$$

for $X_i = (t_i, \vec{p}_i)$.

APPENDIX B: DETAILS OF GEVP PROCEDURE

1. Ordering of GEVP eigenvectors

While a simple description of how we order GEVP eigenvectors was made in Sec. II D, it is valuable to address the exact procedure using equations.

Since we fix $t - t_0$ to a constant Δ_t, we can drop t or t_0 from the arguments of eigenvalues and eigenvectors, and it is valuable for the following discussion. We drop t rather than t_0, since the contamination from excited states in eigenvalues and eigenvectors is measured by t_0. The GEVP equation is then rewritten as

$$C(t)V_n(t_0) = \lambda_n(t_0)C(t_0)V_n(t_0). \quad \text{(B1)}$$

At short time separations where the statistical errors are small enough, we simply sort eigenvalues into descending order. This will give us the ascending order of effective energies and ensure. Since this approach for short times is trivial and has no ambiguity, we spend the rest of the subsection for the ordering at larger time separations where the statistical error is large, but the excited-state contamination is expected to be small.

At long distances, we employ a recursive approach using the eigenvectors obtained one time slice earlier. As explained in Sec. II D, the idea is to use eigenvectors at one time slice earlier to construct a near diagonal correlator matrix, with which it is very easy to obtain the correct order of eigenvectors at the current time slice. The exact procedure is given as follows.

We now suppose the ordering of the eigenvectors $V_n(t_0-1)$ at t_0-1 is successful and give a recipe to obtain the correct order of the eigenvectors $V_n(t_0)$ at t_0 using $V_n(t_0-1)$. We define an $N \times N$ matrix

$$T(t_0-1) = (V_1(t_0-1)V_2(t_0-1)\ldots V_N(t_0-1)), \quad \text{(B2)}$$

using the set of the GEVP eigenvectors $V_n(t_0-1)$ obtained at one time slice earlier. Then we can calculate approximately diagonal matrices

$$C'(t,t_0-1) = T(t_0-1)^\dagger C(t) T(t_0-1), \quad \text{(B3)}$$

$$C'(t_0,t_0-1) = T(t_0-1)^\dagger C(t_0) T(t_0-1). \quad \text{(B4)}$$

Here, the second argument of C' on the left-hand sides corresponds to the argument of T on the right-hand sides. The off-diagonal elements of these matrices are associated only with the statistical fluctuation and systematic effect from excited states. With these near-diagonal matrices, we can express the GEVP [Eq. (B1)] as

$$C'(t,t_0-1)V'_n(t_0) = \lambda_n(t_0)C'(t_0,t_0-1)V'_n(t_0), \quad \text{(B5)}$$

where $V'_n(t_0)$ satisfies

$$V_n(t_0) = T(t_0-1)V'_n(t_0). \quad \text{(B6)}$$

If we can obtain the correct order of $V'_n(t_0)$ when solving the modified GEVP [Eq. (B5)], we can also obtain the corresponding GEVP eigenvectors $V_n(t_0)$ with the original basis through Eq. (B6). In fact, eigenvectors $V'_n(t_0)$ are mostly a unit vector for a certain direction, and it is easy to recognize their correct order at sufficiently large t_0 where the contamination from the $(N+1)$th and higher states is small, and therefore the correlator matrices in the GEVP [Eq. (B5)] are mostly diagonal.

2. RGEVP

In this work, we consider the RGEVP with fixed $t - t_0 \equiv \Delta_t$, and we continue to omit t from the arguments of V_n in this subsection. In this subsection, we give the recipe for finding a new basis of fewer operators.

(1) Choose the GEVP size N_{t_0} at each time slice

$$N_1 \geq N_2 \geq \ldots. \quad \text{(B7)}$$

Note that N_{t_0} here has a different meaning than N_α used in Sec. II E.

(2) Solve the $N_1 \times N_1$ GEVP at the beginning time slice $t_0 = 1$ and order the eigenvectors $V_n(1)$, ensuring the descending order of the corresponding eigenvalues.

(3) For $t_0 \geq 2$, suppose we have obtained the eigenvectors $V_n(t_0-1)$ at t_0-1 for $n = 1, 2, \ldots, N_{t_0-1}$ and calculate the $N_{t_0} \times N_{t_0}$ rebased correlator matrices

by Eqs. (B3) and (B4) with the modified $N_1 \times N_{t_0}$ rebasing matrix

$$T(t_0-1) = (V_1(t_0-1)V_2(t_0-1)\ldots V_{N_{t_0}}(t_0-1)). \tag{B8}$$

(4) Solve the GEVP [Eq. (B5)] with the rebased correlators in Eqs. (B3) and (B4) and obtain the eigenvectors $V_n(t)$ by Eq. (B6) for $n = 1, 2, \ldots, N_t$ using the ordering procedure described in the previous subsection.

Note that, in step 3, the number N_{t_0} of columns of $T(t_0-1)$ despite $N_{t_0-1}(\geq N_{t_0})$ eigenvectors $V_n(t_0-1)$ obtained at time slice t_0-1 plays a role in reducing the size of the GEVP at time slice t_0 when $N_{t_0-1} \neq N_{t_0}$.

While repeating steps 3 and 4 and applying the results to Eq. (19) gives us a new series of effective two-pion energies, they are identical to the normal GEVP results at small t_0 that satisfy $N_{t_0} = N_1$. On the other hand, it is interesting to investigate how the GEVP with the reduced new basis behaves at smaller time slices. Therefore, we perform the following additional steps:

(5) Repeat steps 3 and 4 to obtain $T(\tilde{t}_0)$ with a chosen time $\tilde{t}_0$ where the final rebasing is performed—i.e., $N_{\tilde{t}_0-1} > N_{\tilde{t}_0} = N_{\tilde{t}_0+1} = \ldots$.

(6) Perform the GEVP analysis with the rebased correlator matrices $T(\tilde{t}_0)^\dagger C(t) T(\tilde{t}_0)$ for all available time slices.

The $N_1 \times N_{\tilde{t}_0}$ matrix $T(\tilde{t}_0)$ is the matrix to define the new operator basis. These steps can be parametrized by the pairs of t_0 and N_{t_0} that satisfy $N_{t_0-1} > N_{t_0}$. A single pair gives us a single-step RGEVP, while multiple pairs correspond to a multistep RGEVP. We present the RGEVP results with these parameters in Sec. IV.

APPENDIX C: SUPPLEMENTAL FIGURES AND TABLES

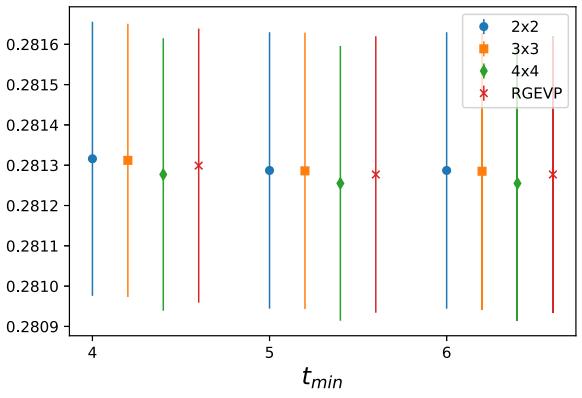

FIG. 19. $I = 2$ $\pi\pi$ ground-state energy on the 24^3 ensemble obtained from fits to a constant for various fit ranges and GEVP types plotted in lattice units.

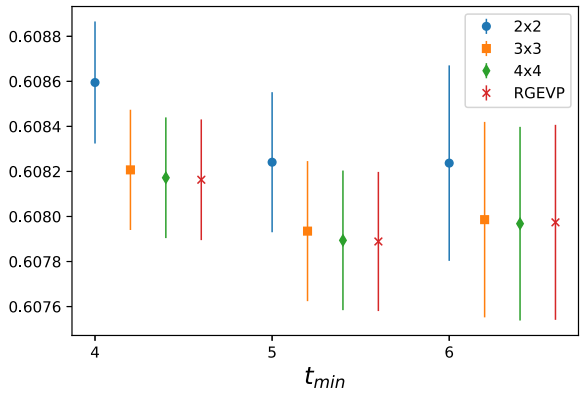

FIG. 20. Same as Fig. 19, but results for the $I = 2$ first excited state on the 24^3 ensemble.

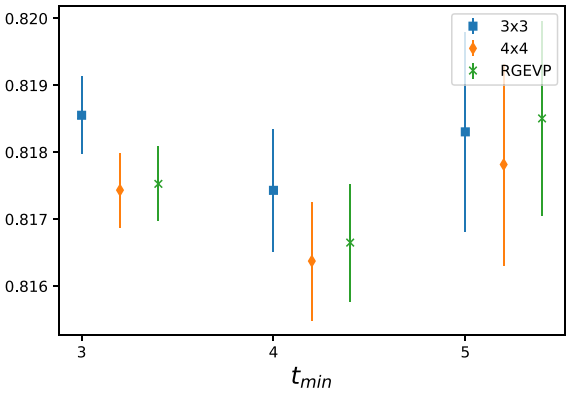

FIG. 21. Same as Fig. 19, but results for the $I = 2$ second excited state on the 24^3 ensemble.

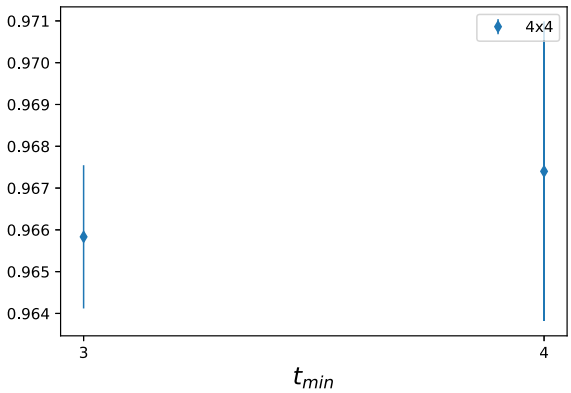

FIG. 22. Same as Fig. 19, but results for the $I = 2$ third excited state on the 24^3 ensemble.

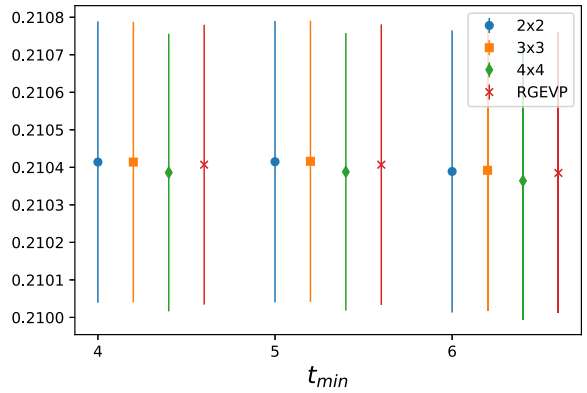

FIG. 23. Same as Fig. 19, but results for the $I = 2$ ground state on the 32^3 ensemble.

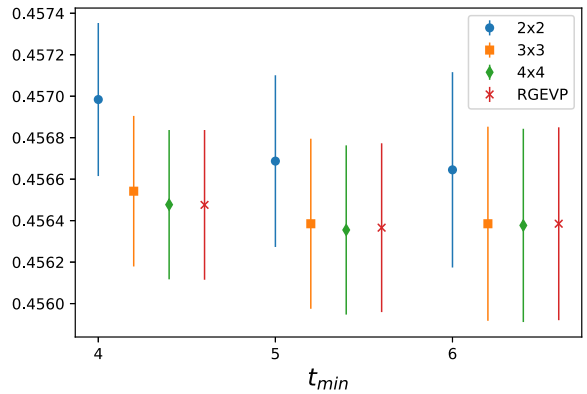

FIG. 24. Same as Fig. 19, but results for the $I = 2$ first excited state on the 32^3 ensemble.

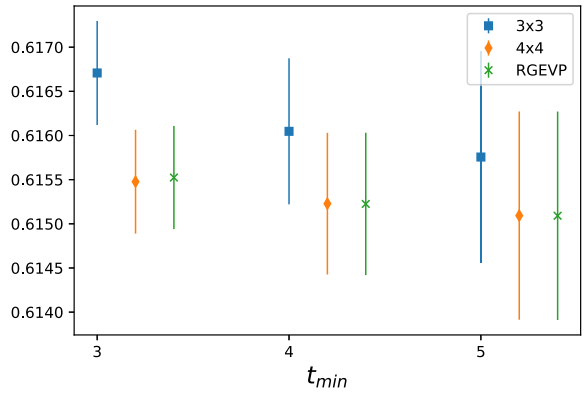

FIG. 25. Same as Fig. 19, but results for the $I = 2$ second excited state on the 32^3 ensemble.

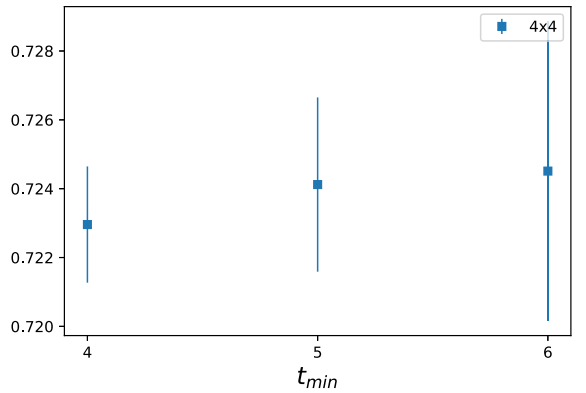

FIG. 26. Same as Fig. 19, but results for the $I = 2$ third excited state on the 32^3 ensemble.

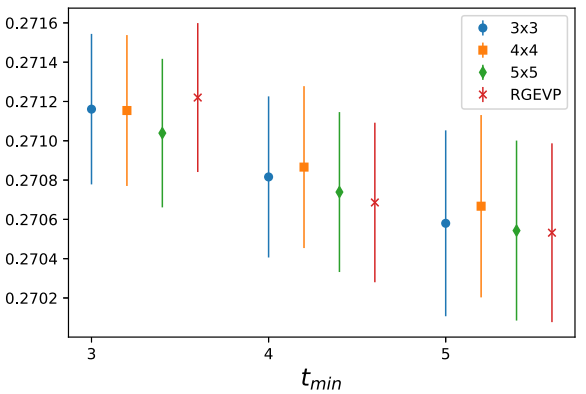

FIG. 27. Same as Fig. 19, but results for the $I = 0$ ground state on the 24^3 ensemble.

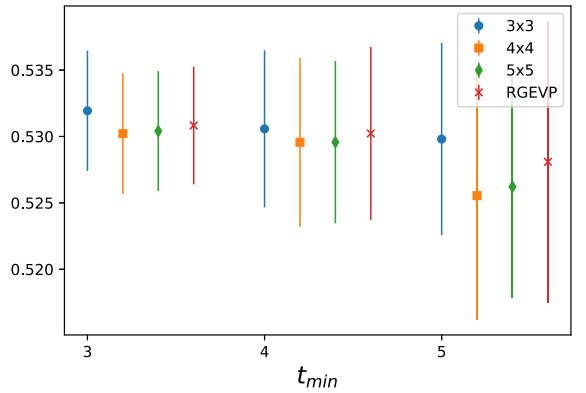

FIG. 28. Same as Fig. 19, but results for the $I = 0$ first excited state on the 24^3 ensemble.

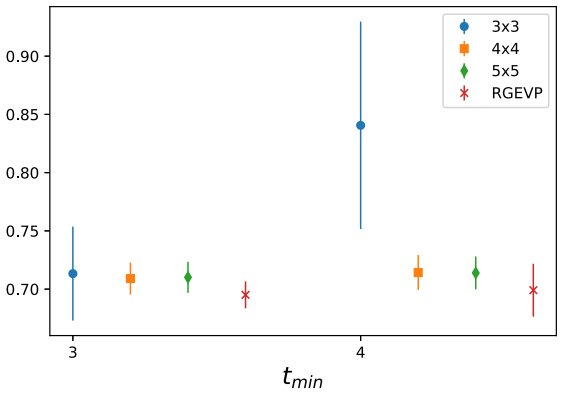

FIG. 29. Same as Fig. 19, but results for the $I = 0$ second excited state on the 24^3 ensemble.

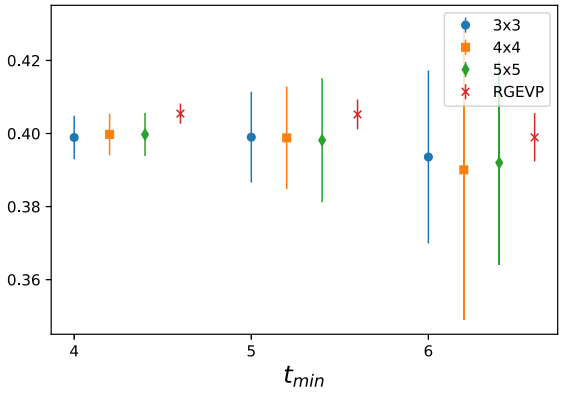

FIG. 31. Same as Fig. 19, but results for the $I = 0$ first excited state on the 32^3 ensemble.

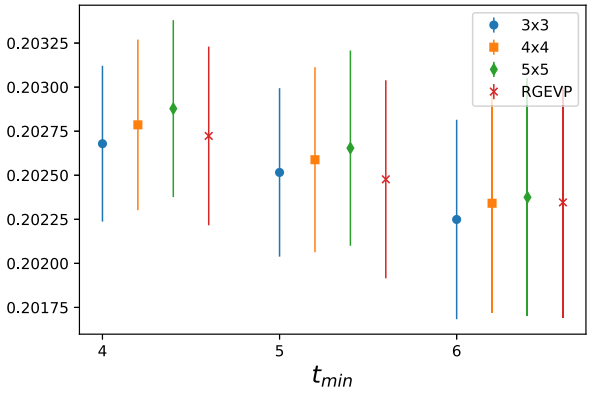

FIG. 30. Same as Fig. 19, but results for the $I = 0$ ground state on the 32^3 ensemble.

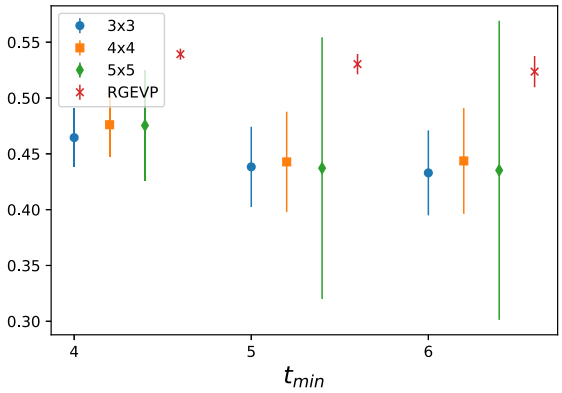

FIG. 32. Same as Fig. 19, but results for the $I = 0$ second excited state on the 32^3 ensemble.

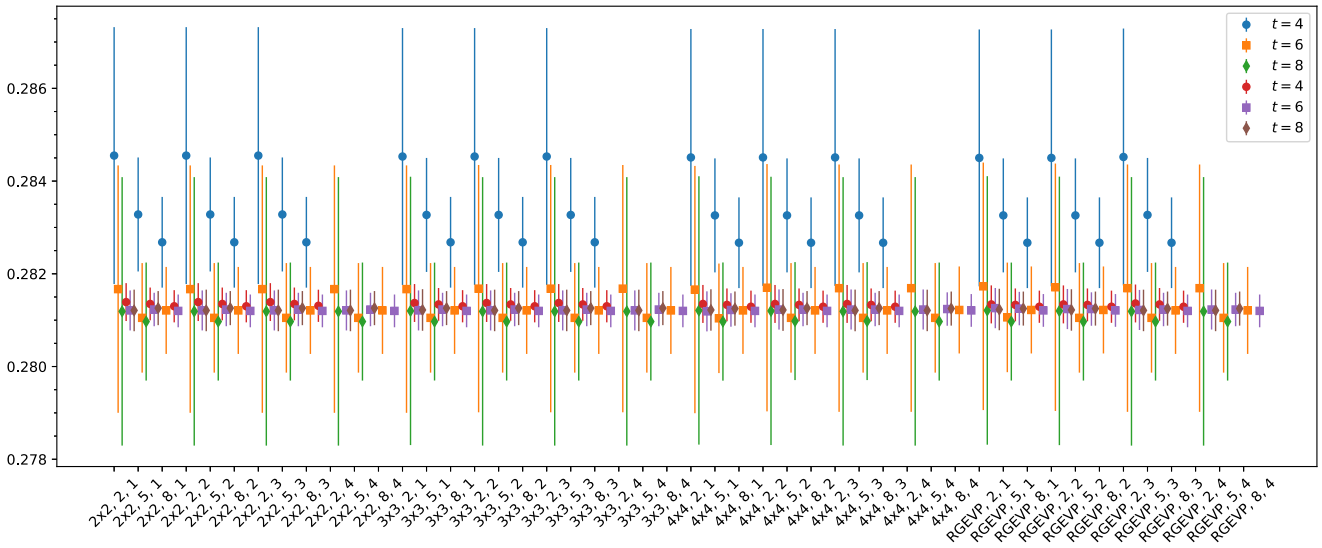

FIG. 33. $I = 2$ effective ground-state $\pi\pi$ energies on the 24^3 lattice plotted in lattice units. X-axis labels correspond to GEVP type, δ_t (matrix subtraction), and $t - t_0$. For each label, there are up to six values, corresponding to two sets of $t = 4$ (circle), 6 (square), and 8 (diamond), one set each for the nondispersion relation method and dispersion relation method, respectively.

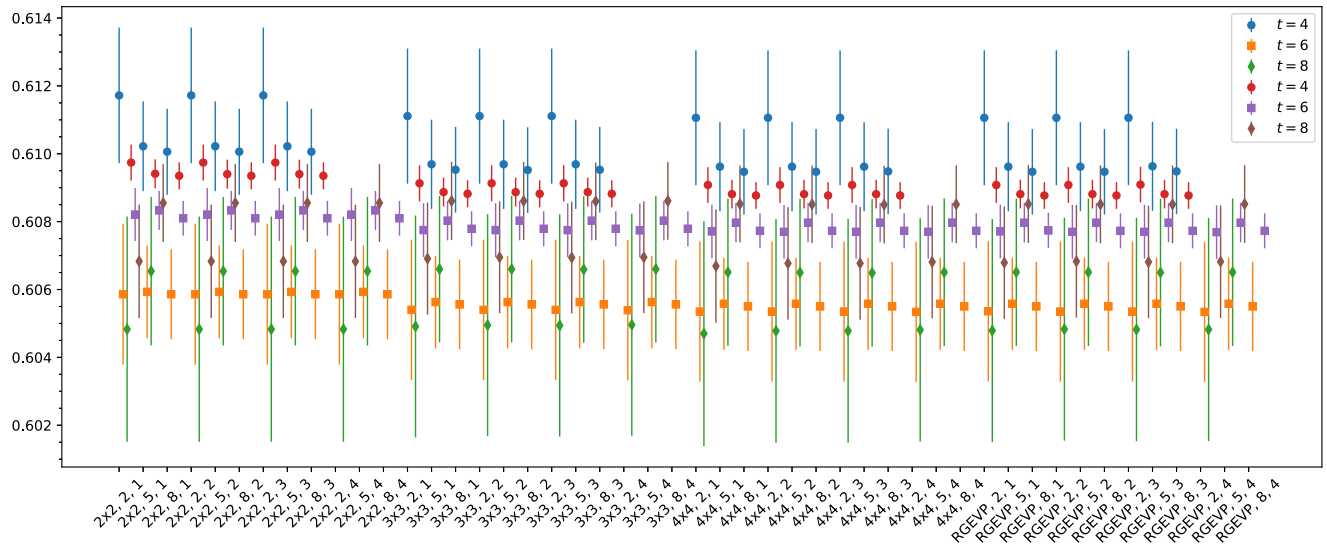

FIG. 34. $I = 2$ effective first excited-state $\pi\pi$ energies on the 24^3 lattice plotted in lattice units. X-axis labels correspond to GEVP type, δ_t (matrix subtraction), and $t - t_0$. For each label, there are up to six values, corresponding to two sets of $t = 4$ (circle), 6 (square), and 8 (diamond), one set each for the nondispersion relation method and dispersion relation method, respectively.

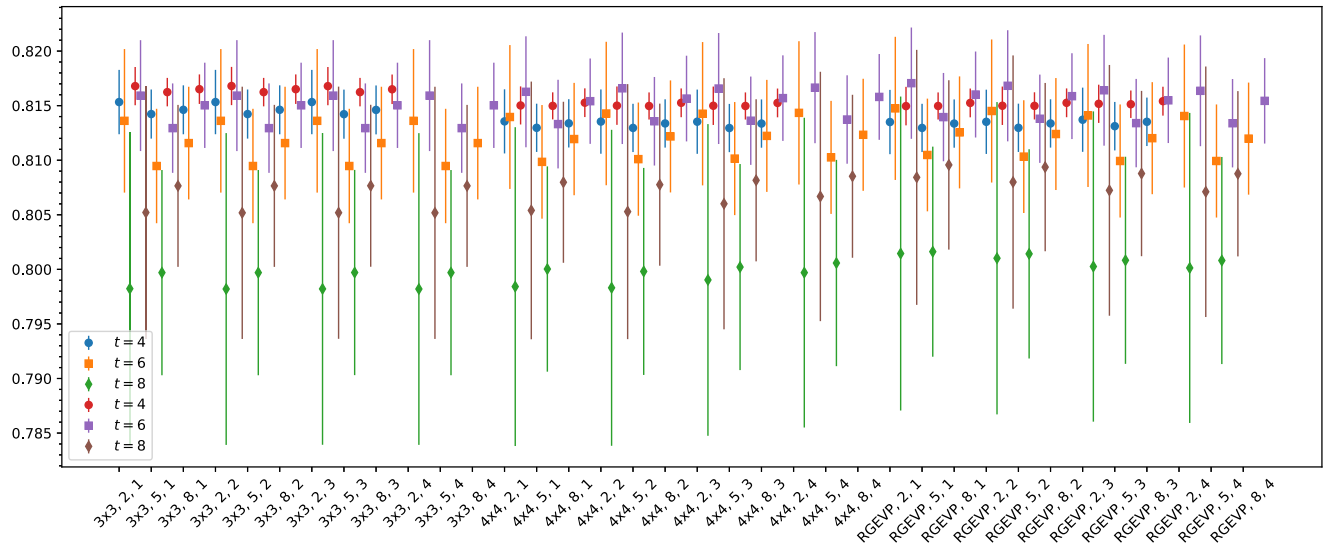

FIG. 35. $I = 2$ effective second excited-state $\pi\pi$ energies on the 24^3 lattice plotted in lattice units. X-axis labels correspond to GEVP type, δ_t (matrix subtraction), and $t - t_0$. For each label, there are up to six values, corresponding to two sets of $t = 4$ (circle), 6 (square), and 8 (diamond), one set each for the nondispersion relation method and dispersion relation method, respectively.

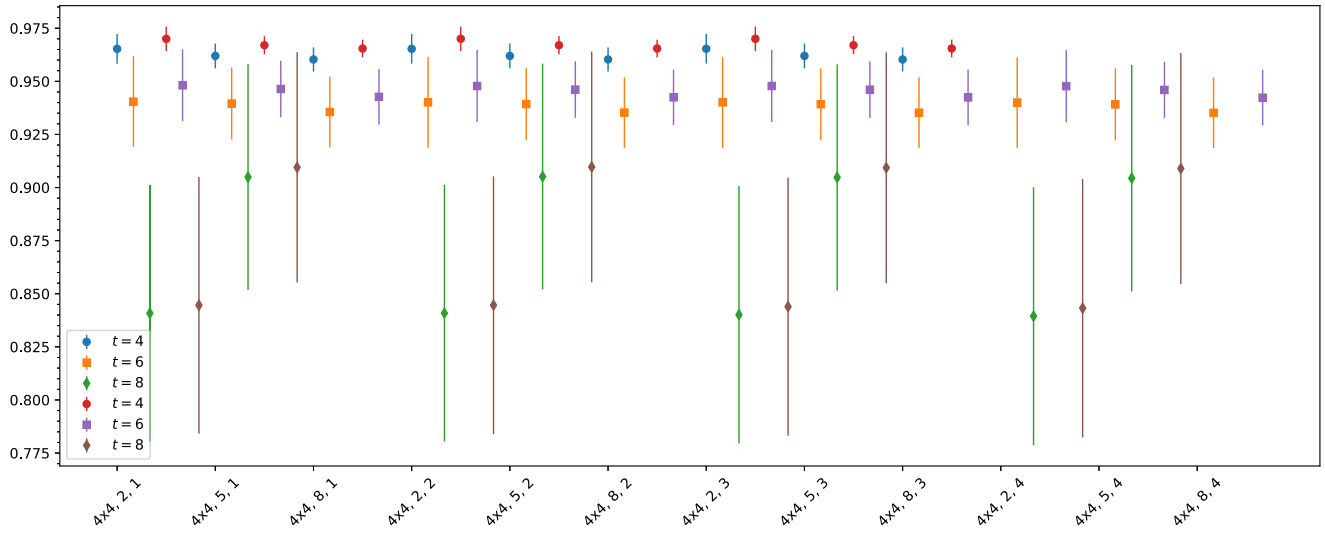

FIG. 36. $I = 2$ effective third excited-state $\pi\pi$ energies on the 24^3 lattice plotted in lattice units. X-axis labels correspond to GEVP type, δ_t (matrix subtraction), and $t - t_0$. For each label, there are up to six values, corresponding to two sets of $t = 4$ (circle), 6 (square), and 8 (diamond), one set each for the nondispersion relation method and dispersion relation method, respectively.

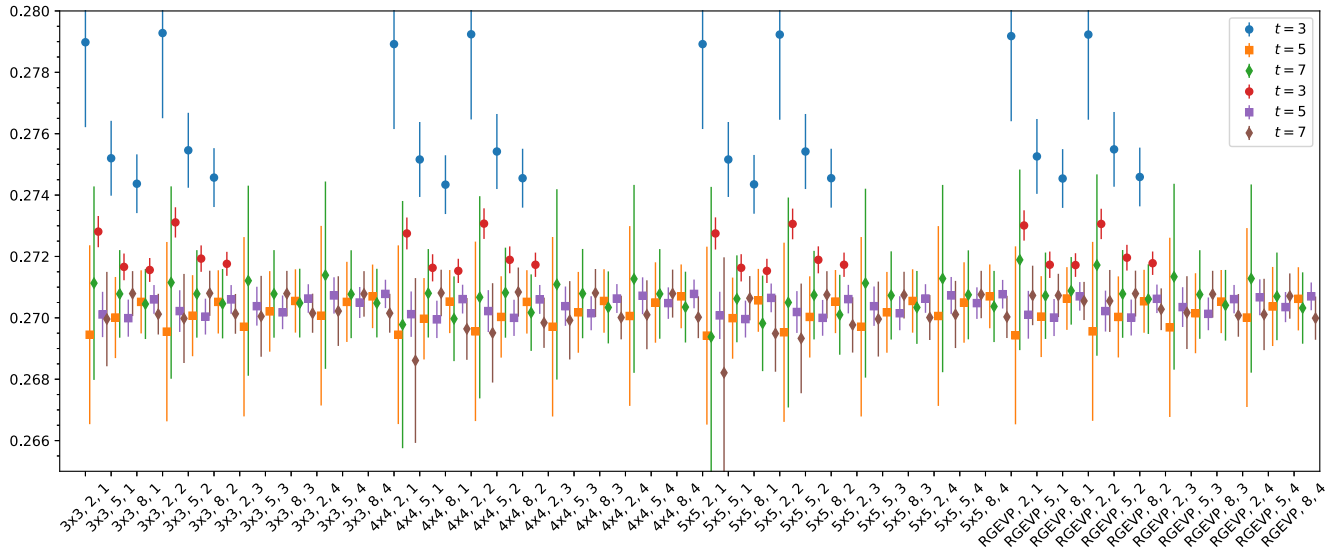

FIG. 37. $I = 0$ effective ground-state $\pi\pi$ energies on the 24^3 lattice plotted in lattice units. X-axis labels correspond to GEVP type, δ_t (matrix subtraction), and $t - t_0$. For each label, there are up to six values, corresponding to two sets of $t = 4$ (circle), 6 (square), and 8 (diamond), one set each for the nondispersion relation method and dispersion relation method, respectively.

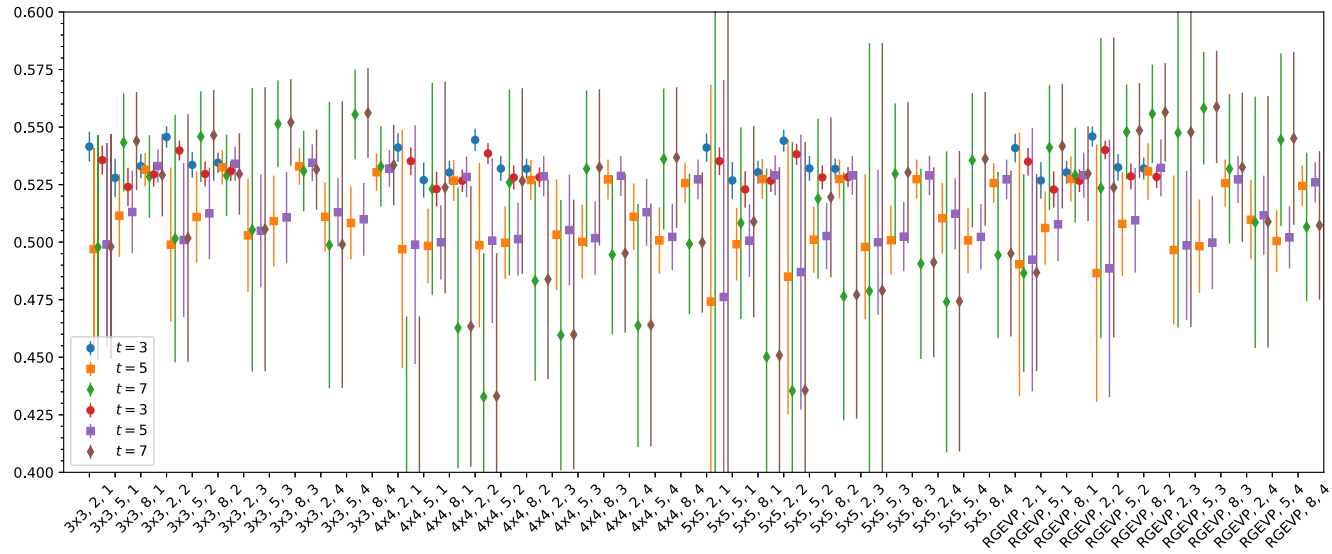

FIG. 38. $I = 0$ effective first excited-state $\pi\pi$ energies on the 24^3 lattice plotted in lattice units. X-axis labels correspond to GEVP type, δ_t (matrix subtraction), and $t - t_0$. For each label, there are up to six values, corresponding to two sets of $t = 3$ (circle), 5 (square), and 7 (diamond), one set each for the nondispersion relation method and dispersion relation method, respectively.

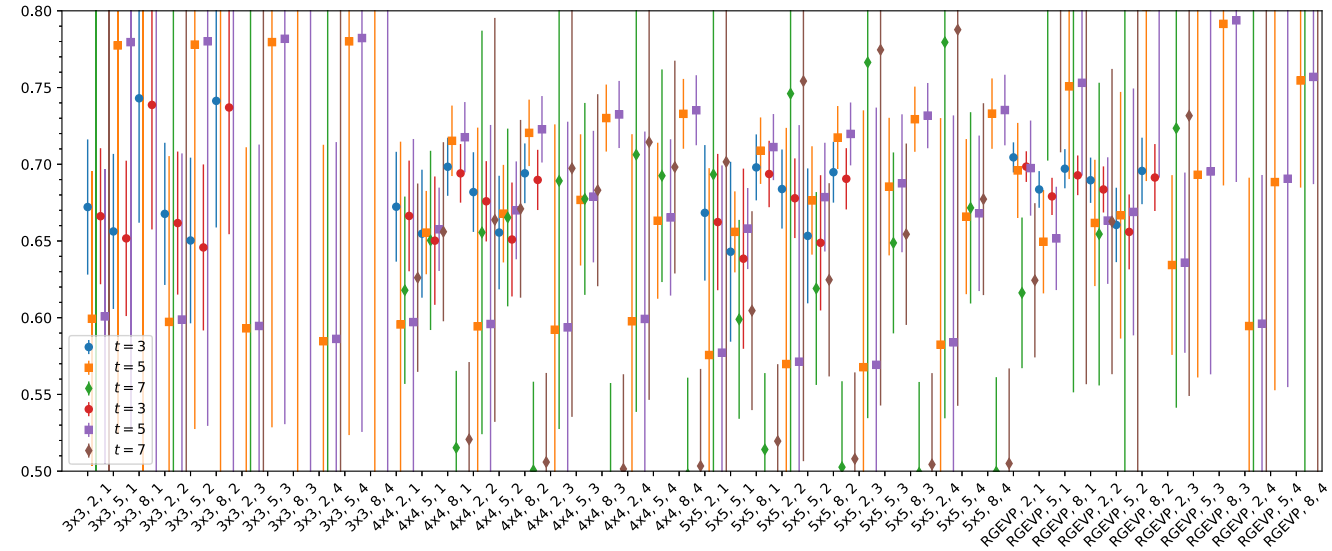

FIG. 39. $I = 0$ effective second excited-state $\pi\pi$ energies on the 24^3 lattice plotted in lattice units. X-axis labels correspond to GEVP type, δ_t (matrix subtraction), and $t - t_0$. For each label, there are up to six values, corresponding to two sets of $t = 3$ (circle), 5 (square), and 7 (diamond), one set each for the nondispersion relation method and dispersion relation method, respectively.

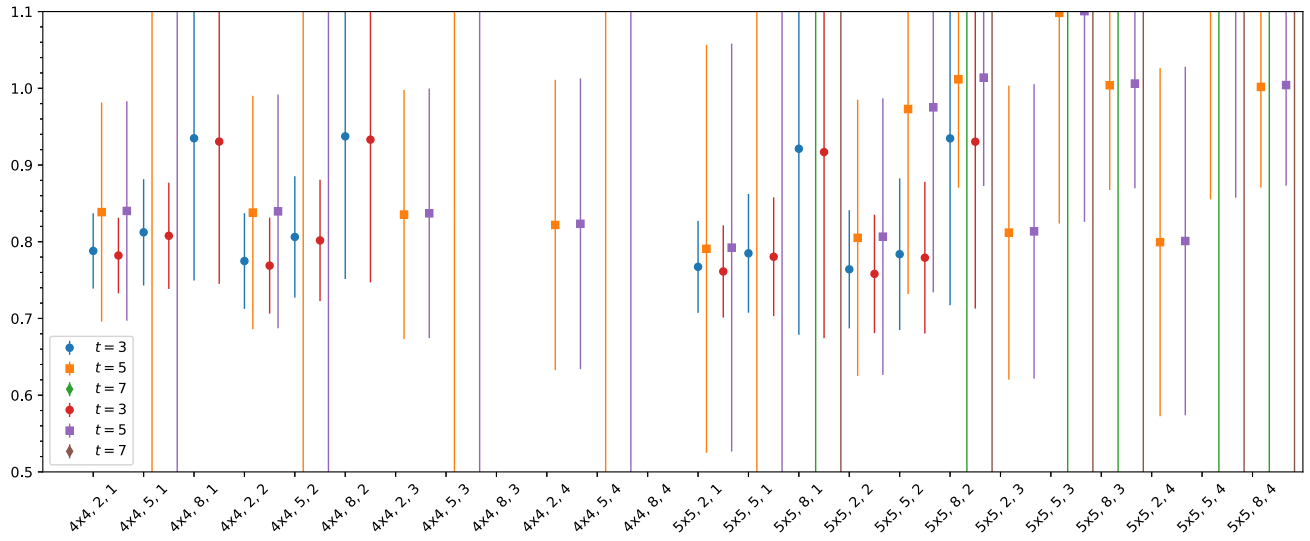

FIG. 40. $I = 0$ effective third excited-state $\pi\pi$ energies on the 24^3 lattice plotted in lattice units. X-axis labels correspond to GEVP type, δ_t (matrix subtraction), and $t - t_0$. For each label, there are up to six values, corresponding to two sets of $t = 3$ (circle), 5 (square), and 7 (diamond), one set each for the nondispersion relation method and dispersion relation method, respectively.

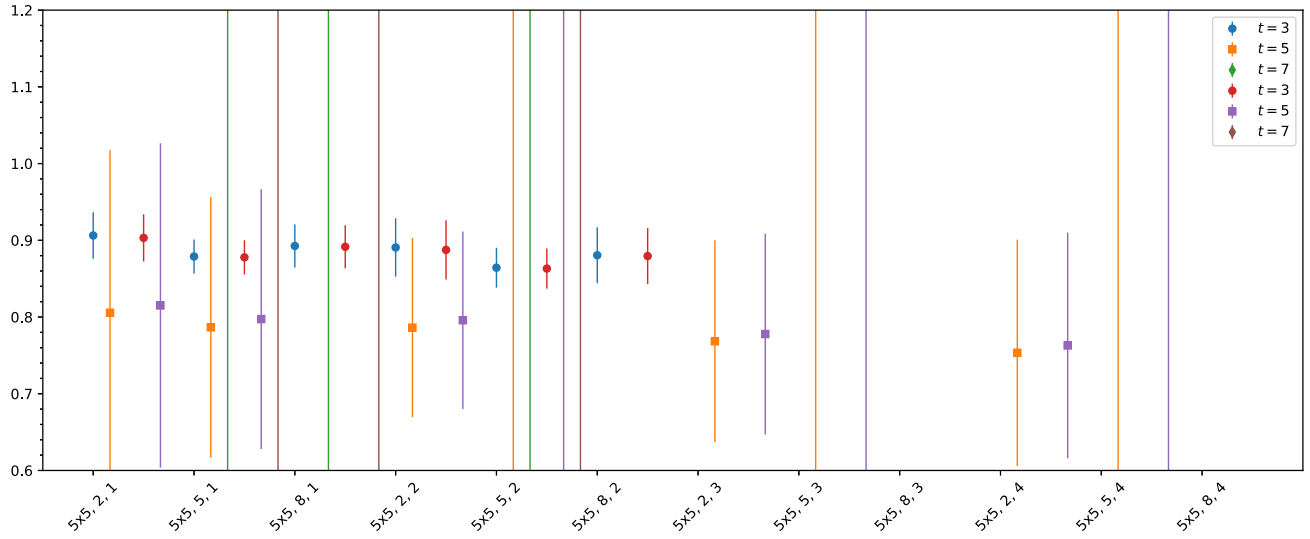

FIG. 41. $I = 0$ effective fourth excited-state $\pi\pi$ energies on the 24^3 lattice plotted in lattice units. X-axis labels correspond to GEVP type, δ_t (matrix subtraction), and $t - t_0$. For each label, there are up to six values, corresponding to two sets of $t = 3$ (circle), 5 (square), and 7 (diamond), one set each for the nondispersion relation method and dispersion relation method, respectively.

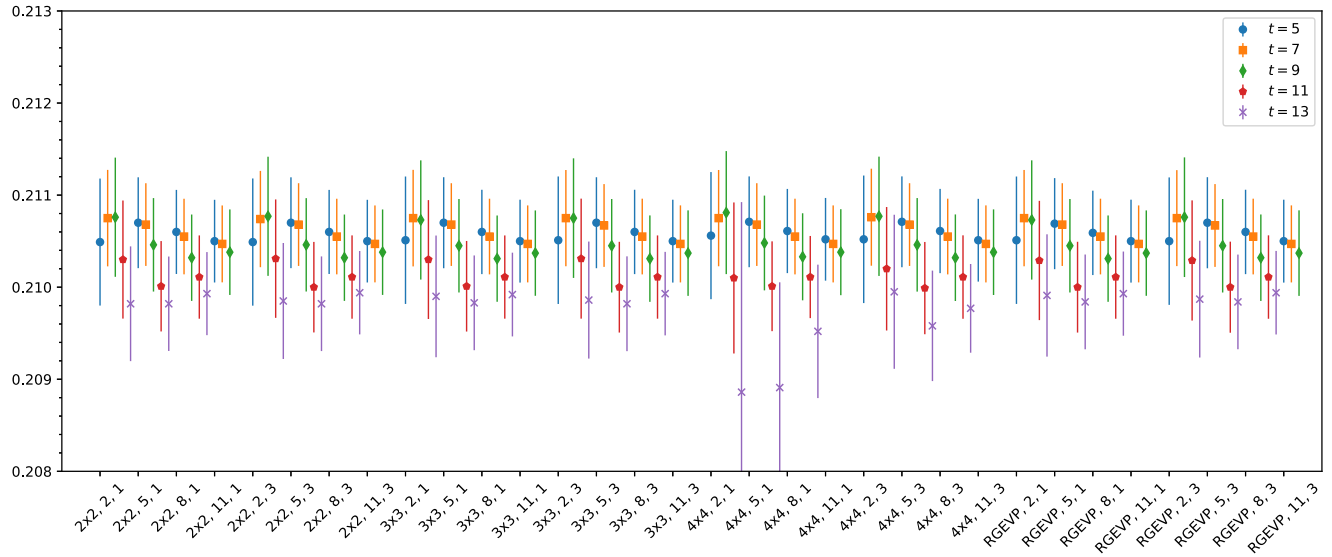

FIG. 42. $I = 2$ effective ground-state $\pi\pi$ energies on the 32^3 lattice plotted in lattice units. X-axis labels correspond to GEVP type, δ_t (matrix subtraction), and $t - t_0$. For each label, there are results for five values of $t = 5$ (circle), 7 (square), 9 (diamond), 11 (pentagon), and 13 (cross).

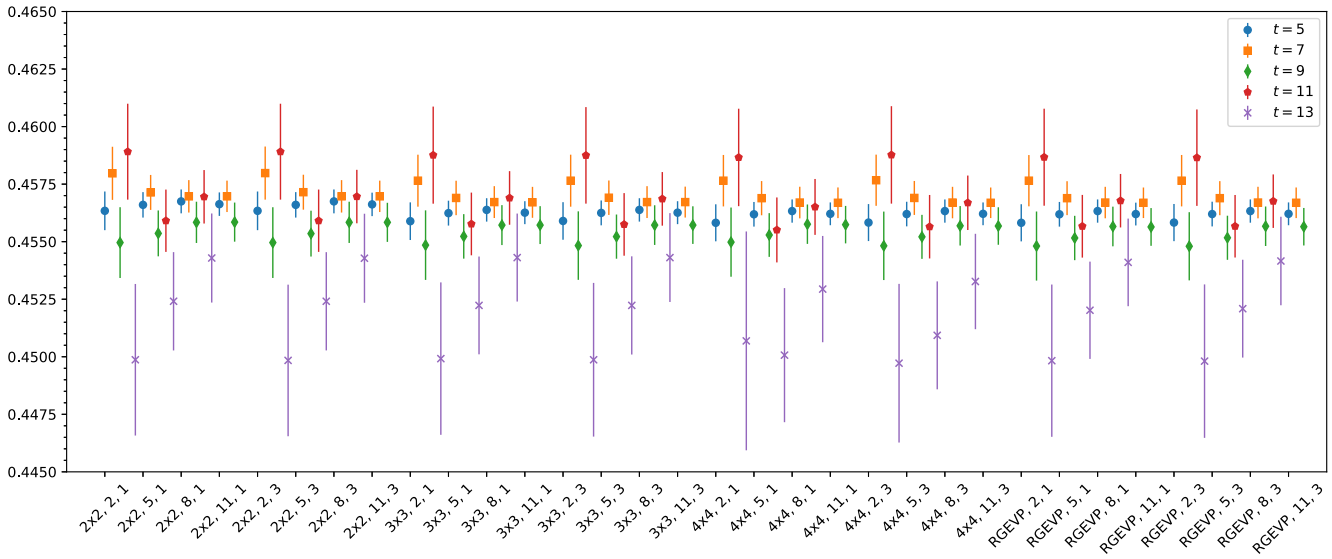

FIG. 43. $I = 2$ effective first excited-state $\pi\pi$ energies on the 32^3 lattice plotted in lattice units. X-axis labels correspond to GEVP type, δ_t (matrix subtraction), and $t - t_0$. For each label, there are results for five values of $t = 5$ (circle), 7 (square), 9 (diamond), 11 (pentagon), and 13 (cross).

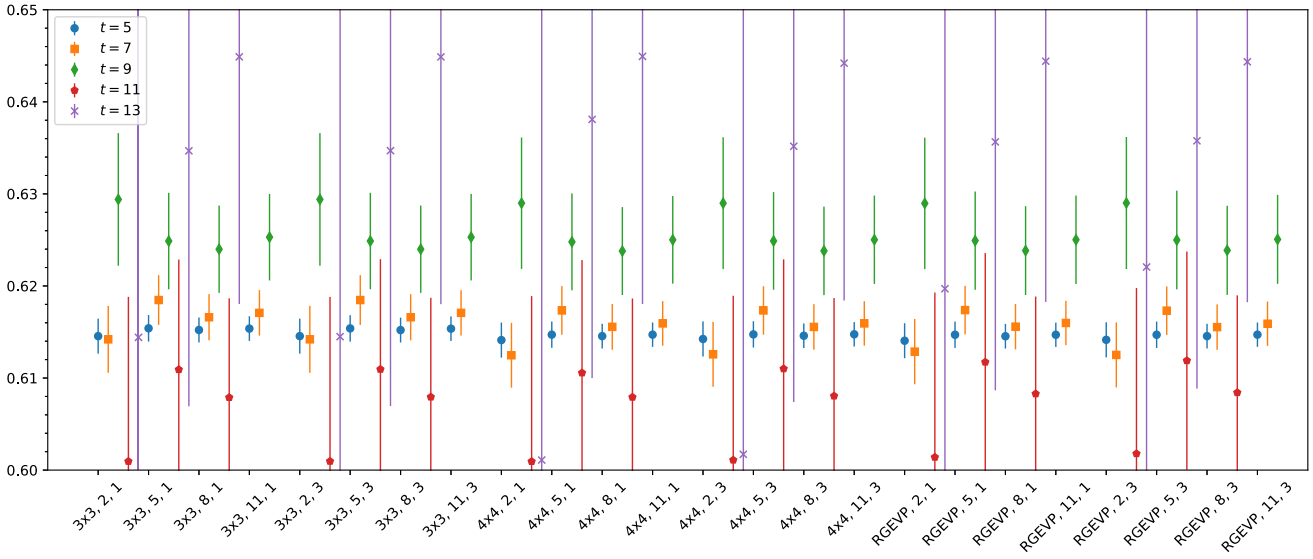

FIG. 44. $I = 2$ effective second excited-state $\pi\pi$ energies on the 32^3 lattice plotted in lattice units. X-axis labels correspond to GEVP type, δ_t (matrix subtraction), and $t - t_0$. For each label, there are results for five values of $t = 5$ (circle), 7 (square), 9 (diamond), 11 (pentagon), and 13 (cross).

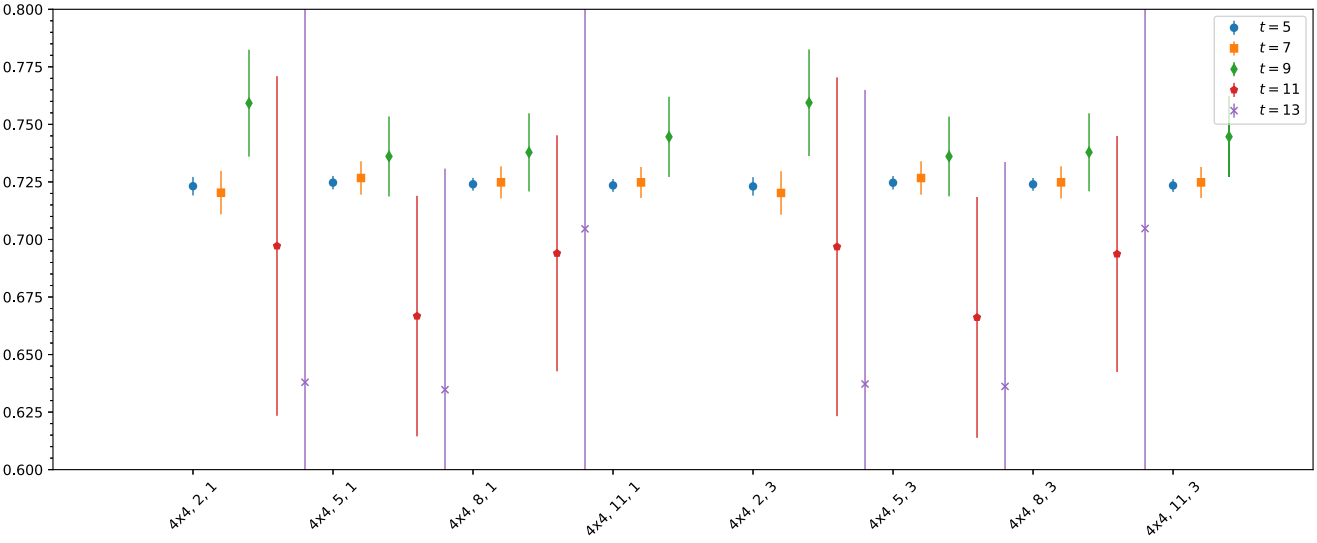

FIG. 45. $I = 2$ effective third excited-state $\pi\pi$ energies on the 32^3 lattice plotted in lattice units. X-axis labels correspond to GEVP type, δ_t (matrix subtraction), and $t - t_0$. For each label, there are results for five values of $t = 5$ (circle), 7 (square), 9 (diamond), 11 (pentagon), and 13 (cross).

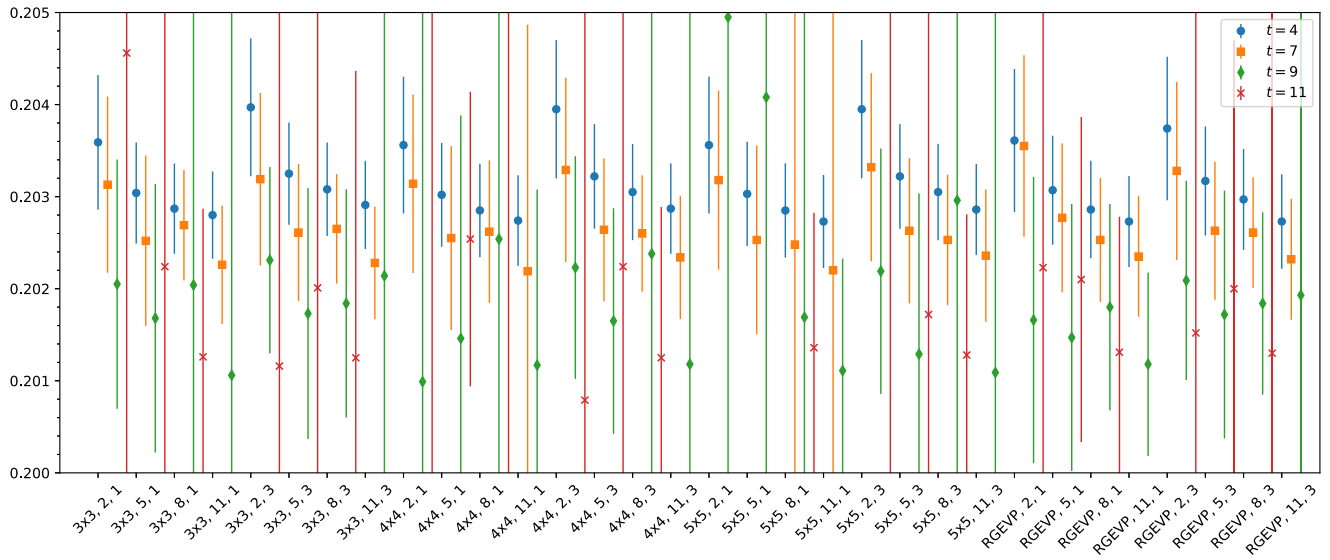

FIG. 46. $I = 0$ effective ground-state $\pi\pi$ energies on the 32^3 lattice plotted in lattice units. X-axis labels correspond to GEVP type, δ_t (matrix subtraction), and $t - t_0$. For each label, there are results for four values of $t = 4$ (circle), 7 (square), 9 (diamond), and 11 (cross).

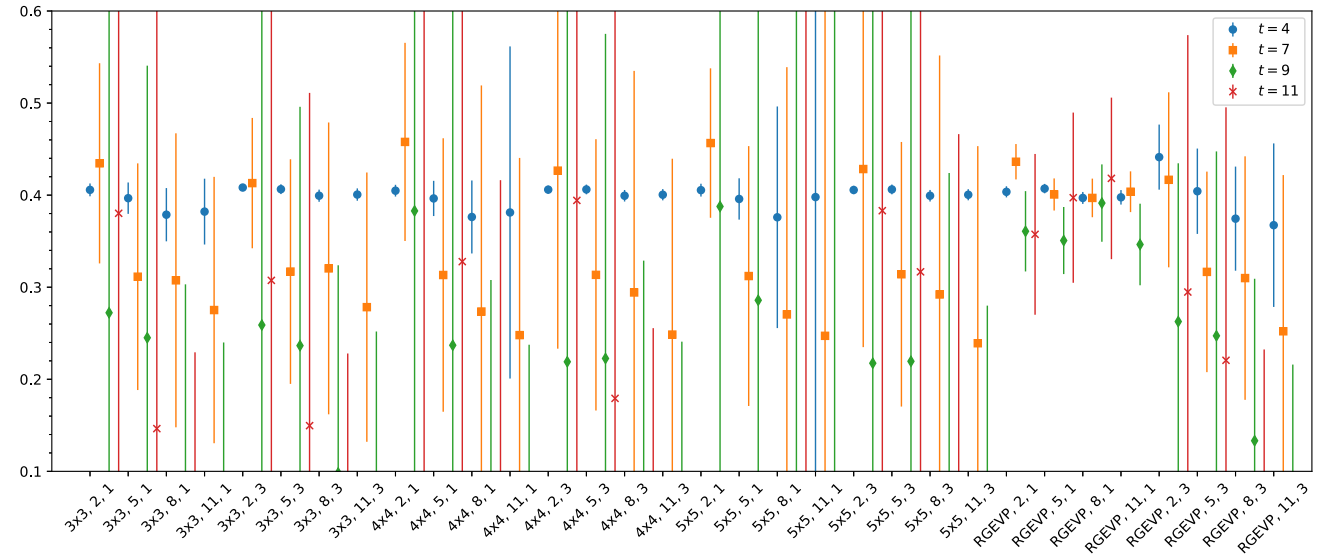

FIG. 47. $I = 0$ effective first excited-state $\pi\pi$ energies on the 32^3 lattice plotted in lattice units. X-axis labels correspond to GEVP type, δ_t (matrix subtraction), and $t - t_0$. For each label, there are results for four values of $t = 4$ (circle), 7 (square), 9 (diamond), and 11 (cross).

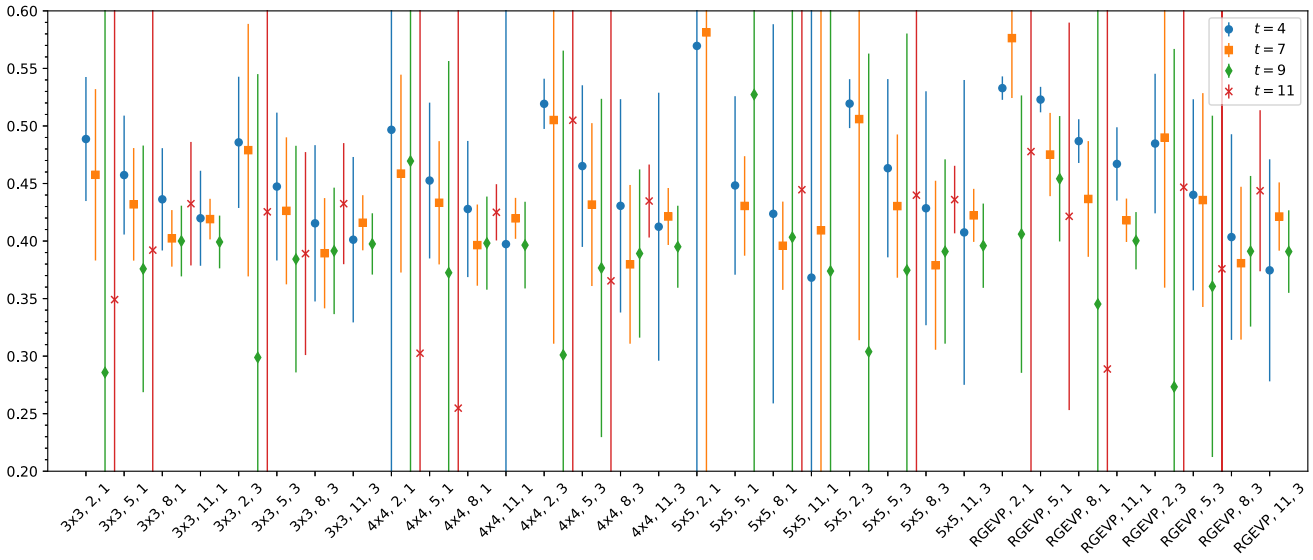

FIG. 48. $I = 0$ effective second excited-state $\pi\pi$ energies on the 32^3 lattice plotted in lattice units. X-axis labels correspond to GEVP type, δ_t (matrix subtraction), and $t - t_0$. For each label, there are results for four values of of $t = 4$ (circle), 7 (square), 9 (diamond), and 11 (cross).

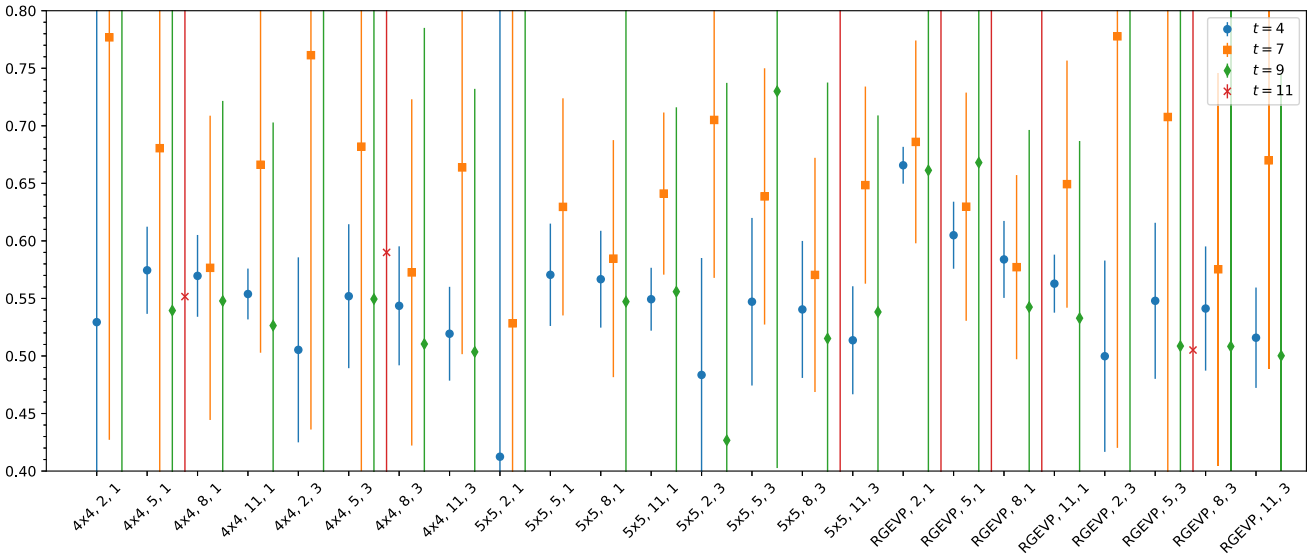

FIG. 49. $I = 0$ effective third excited-state $\pi\pi$ energies on the 32^3 lattice plotted in lattice units. X-axis labels correspond to GEVP type, δ_t (matrix subtraction), and $t - t_0$. For each label, there are results for four values of $t = 4$ (circle), 7 (square), 9 (diamond), and 11 (cross).

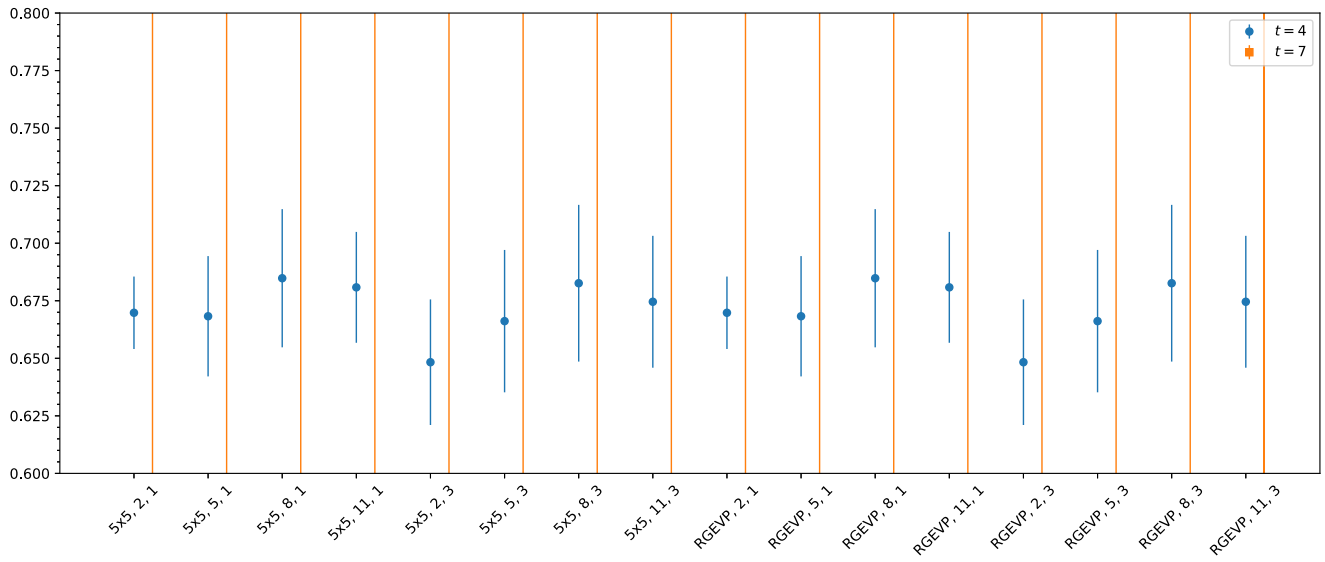

FIG. 50. $I = 0$ effective fourth excited-state $\pi\pi$ energies on the 32^3 lattice plotted in lattice units. X-axis labels correspond to GEVP type, δ_t (matrix subtraction), and $t - t_0$. For each label, there are results for two values of $t = 4$ (circle) and 7 (square).

TABLE XVIII. Results for the $I = 2$ phase shift on the 24^3 lattice for two-pion energy of the ground state shown in Table III.

	Fit range		
GEVP type	4–10	5–10	6–10
2×2	−0.378(13)°	−0.372(14)°	−0.372(13)°
3×3	−0.377(13)°	−0.371(14)°	−0.371(14)°
4×4	−0.369(13)°	−0.364(14)°	−0.364(14)°
RGEVP	−0.374(13)°	−0.369(14)°	−0.369(13)°

TABLE XIX. Results for the $I = 2$ phase shift on the 24^3 lattice for two-pion energy of the first excited state shown in Table IV.

	Fit range		
GEVP type	4–9	5–9	6–9
2×2	−12.94(19)°	−12.64(23)°	−12.63(34)°
3×3	−12.61(18)°	−12.37(23)°	−12.41(34)°
4×4	−12.58(18)°	−12.33(23)°	−12.40(34)°
RGEVP	−12.57(18)°	−12.33(23)°	−12.40(34)°

TABLE XX. Results for the $I = 2$ phase shift on the 24^3 lattice for two-pion energy of the second excited state shown in Table V.

	Fit range		
GEVP type	3–9	4–9	5–9
3×3	−20.97(44)°	−20.10(71)°	−20.8(1.2)°
4×4	−20.11(42)°	−19.29(68)°	−20.4(1.2)°
RGEVP	−20.18(43)°	−19.50(67)°	−20.9(1.1)°

TABLE XXI. Results for the $I = 2$ phase shift on the 24^3 lattice for two-pion energy of the third excited state shown in Table VI.

	Fit range	
GEVP type	3–5	4–5
4×4	−26.5(2.4)°	−28.7(5.0)°

TABLE XXII. Results for the $I = 2$ phase shift on the 32^3 lattice for two-pion energy of the ground state shown in Table VII.

	Fit range		
GEVP type	4–9	5–9	6–9
2×2	−0.427(50)°	−0.427(51)°	−0.419(52)°
3×3	−0.426(51)°	−0.427(51)°	−0.420(52)°
4×4	−0.418(53)°	−0.418(53)°	−0.411(54)°
RGEVP	−0.424(51)°	−0.424(52)°	−0.417(53)°

TABLE XXIII. Results for the $I = 2$ phase shift on the 32^3 lattice for two-pion energy of the first excited state shown in Table VIII.

	Fit range		
GEVP type	4–10	5–10	6–10
2×2	−13.96(32)°	−13.61(40)°	−13.57(47)°
3×3	−13.45(32)°	−13.26(39)°	−13.26(47)°
4×4	−13.37(32)°	−13.23(39)°	−13.25(47)°
RGEVP	−13.37(32)°	−13.24(39)°	−13.26(46)°

TABLE XXIV. Results for the $I = 2$ phase shift on the 32^3 lattice for two-pion energy of the second excited state shown in Table IX.

	Fit range		
GEVP type	3–7	4–7	5–7
3×3	−24.13(59)°	−23.44(83)°	−23.1(1.2)°
4×4	−22.85(59)°	−22.59(81)°	−22.5(1.2)°
RGEVP	−22.90(59)°	−22.59(81)°	−22.4(1.2)°

TABLE XXV. Results for the $I = 2$ phase shift on the 32^3 lattice for two-pion energy of the third excited state shown in Table X.

	Fit range		
GEVP type	4–7	5–7	6–7
4×4	−24.2(3.2)°	−26.4(4.7)°	−27.1(8.1)°

TABLE XXVI. Results for the $I = 0$ phase shift on the 24^3 lattice for two-pion energy of the first excited state shown in Table XII.

	Fit range		
GEVP type	3–6	4–6	5–6
3×3	44.4(3.0)°	45.3(3.8)°	45.8(4.7)°
4×4	45.5(3.0)°	45.9(4.1)°	48.5(6.0)°
5×5	45.4(2.9)°	45.9(3.9)°	48.1(5.3)°
RGEVP	45.1(2.9)°	45.5(4.2)°	46.9(6.8)°

TABLE XXVII. Results for the $I = 0$ phase shift on the 24^3 lattice for two-pion energy of the second excited state shown in Table XIII.

	Fit range	
GEVP type	3–5	4–5
3×3	65(38)°	141(72)°
4×4	69(13)°	64(14)°
5×5	68(13)°	65(13)°
RGEVP	83(11)°	79(22)°

TABLE XXVIII. Results for the $I = 0$ phase shift on the 32^3 lattice for two-pion energy of the first excited state shown in Table XV.

	Fit range		
GEVP type	3–8	4–8	5–8
3×3	44.1(5.2)°	44(11)°	49(20)°
4×4	43.4(5.0)°	44(12)°	52(34)°
5×5	43.4(5.2)°	45(15)°	50(24)°
RGEVP	38.4(2.5)°	38.6(3.6)°	44.1(5.7)°

TABLE XXIX. Results for the $I = 0$ phase shift on the 32^3 lattice for two-pion energy of the second excited state shown in Table XVI.

	Fit range		
GEVP type	3–6	4–6	5–6
3×3	17(19)°	20(25)°	28(30)°
4×4	40(680)°	140(690)°	80(860)°
5×5	28(24)°	30(30)°	31(33)°
RGEVP	71.6(8.4)°	79(14)°	80(24)°

TABLE XXX. Results for the $I = 2$ scattering length times pion mass $m_\pi a_0$ calculated on the 24^3 lattice using the phase shift of the ground state shown in Table XVIII and Eq. (34).

	Fit range		
GEVP type	4–10	5–10	6–10
2×2	−0.0499(11)	−0.0494(12)	−0.0494(12)
3×3	−0.0499(12)	−0.0493(12)	−0.0493(12)
4×4	−0.0492(11)	−0.0487(13)	−0.0487(12)
RGEVP	−0.0496(11)	−0.0492(12)	−0.0492(12)

TABLE XXXI. Results for the $I = 2$ scattering length times pion mass $m_\pi a_0$ calculated on the 32^3 lattice using the phase shift of the ground state shown in Table XXII and Eq. (34).

	Fit range		
GEVP type	4–9	5–9	6–9
2×2	−0.0538(41)	−0.0539(42)	−0.0532(43)
3×3	−0.0538(42)	−0.0539(42)	−0.0533(43)
4×4	−0.0531(44)	−0.0532(44)	−0.0525(45)
RGEVP	−0.0537(42)	−0.0537(42)	−0.0531(44)

TABLE XXXII. Results for the $I = 0$ scattering length times pion mass $m_\pi a_0$ calculated on the 24^3 lattice using Eq. (34).

	Fit range		
GEVP type	3–8	4–8	5–8
3×3	0.1902(52)	0.2001(72)	0.2069(98)
4×4	0.1904(53)	0.1986(72)	0.2044(95)
5×5	0.1937(53)	0.2023(73)	0.2080(95)
RGEVP	0.1885(48)	0.2038(70)	0.2083(91)

TABLE XXXIII. Results for the $I = 0$ scattering length times pion mass $m_\pi a_0$ calculated on the 32^3 lattice using Eq. (34).

	Fit range		
GEVP type	4–9	5–9	6–9
3×3	0.1871(91)	0.193(11)	0.203(17)
4×4	0.183(12)	0.190(14)	0.200(21)
5×5	0.180(13)	0.188(15)	0.199(22)
RGEVP	0.185(13)	0.195(15)	0.200(21)

TABLE XXXIV. Effective energy of the $I = 2$ two-pion ground state on the 24^3 lattice for various GEVP methods and input time parameters: δ_t, $t - t_0$, and t. The values are shown in lattice units. The rebasing matrix is calculated as $4 \times 4 \to 3 \times 3$ at $t_0 = 4$. The dashes (—) mean that the effective energy could not be evaluated because of one of the following possible reasons: 1. Correlators at $t + \delta_t + 1$ that are needed for calculating effective energy are not computed. 2. The ratio of corresponding GEVP eigenvalues $\lambda_0(t, t_0)/\lambda_0(t + 1, t_0)$ is negative for at least one jackknife sample.

GEVP type	δ_t	$t - t_0$	$t = 4$	$t = 6$	$t = 8$	$t = 4$ w DR	$t = 6$ w DR	$t = 8$ w DR
2×2	2	1	0.2845(28)	0.2817(27)	0.2812(29)	0.28139(41)	0.28121(43)	0.28121(45)
2×2	5	1	0.2833(12)	0.2810(12)	0.2810(13)	0.28135(35)	0.28123(36)	0.28126(37)
2×2	8	1	0.28268(98)	0.28121(94)	⋯	0.28130(35)	0.28120(35)	⋯
2×2	2	2	0.2845(28)	0.2817(27)	0.2812(29)	0.28139(41)	0.28121(43)	0.28121(45)
2×2	5	2	0.2833(12)	0.2810(12)	0.2810(13)	0.28135(35)	0.28123(36)	0.28126(37)
2×2	8	2	0.28268(98)	0.28121(94)	⋯	0.28130(35)	0.28120(35)	⋯
2×2	2	3	0.2846(28)	0.2817(27)	0.2812(29)	0.28139(41)	0.28121(43)	0.28121(45)
2×2	5	3	0.2833(12)	0.2810(12)	0.2810(13)	0.28135(35)	0.28123(36)	0.28126(37)
2×2	8	3	0.28268(98)	0.28121(94)	⋯	0.28131(35)	0.28120(35)	⋯
2×2	2	4	⋯	0.2817(27)	0.2812(29)	⋯	0.28121(43)	0.28121(45)
2×2	5	4	⋯	0.2810(12)	0.2810(13)	⋯	0.28123(36)	0.28126(37)
2×2	8	4	⋯	0.28121(94)	⋯	⋯	0.28120(35)	⋯
3×3	2	1	0.2845(28)	0.2817(27)	0.2812(29)	0.28137(41)	0.28121(43)	0.28122(45)
3×3	5	1	0.2833(12)	0.2810(12)	0.2810(13)	0.28134(35)	0.28123(36)	0.28126(37)
3×3	8	1	0.28268(98)	0.28121(94)	⋯	0.28130(35)	0.28120(35)	⋯
3×3	2	2	0.2845(28)	0.2817(27)	0.2812(29)	0.28137(41)	0.28121(43)	0.28121(45)
3×3	5	2	0.2833(12)	0.2810(12)	0.2810(13)	0.28134(35)	0.28123(36)	0.28126(37)
3×3	8	2	0.28268(98)	0.28121(94)	⋯	0.28130(35)	0.28120(35)	⋯
3×3	2	3	0.2845(28)	0.2817(27)	0.2812(29)	0.28137(41)	0.28121(43)	0.28121(45)
3×3	5	3	0.2833(12)	0.2810(12)	0.2810(13)	0.28134(35)	0.28123(36)	0.28126(37)
3×3	8	3	0.28268(98)	0.28121(94)	⋯	0.28130(35)	0.28120(35)	⋯
3×3	2	4	⋯	0.2817(27)	0.2812(29)	⋯	0.28121(43)	0.28121(45)
3×3	5	4	⋯	0.2810(12)	0.2810(13)	⋯	0.28123(36)	0.28126(37)
3×3	8	4	⋯	0.28121(94)	⋯	⋯	0.28120(35)	⋯
4×4	2	1	0.2845(28)	0.2817(27)	0.2812(29)	0.28135(41)	0.28119(43)	0.28122(45)
4×4	5	1	0.2833(12)	0.2810(12)	0.2810(13)	0.28133(35)	0.28122(36)	0.28125(37)
4×4	8	1	0.28267(98)	0.28121(94)	⋯	0.28129(35)	0.28120(35)	⋯
4×4	2	2	0.2845(28)	0.2817(27)	0.2812(29)	0.28135(41)	0.28123(43)	0.28122(45)
4×4	5	2	0.2833(12)	0.2811(12)	0.2810(13)	0.28133(35)	0.28123(36)	0.28126(37)
4×4	8	2	0.28267(98)	0.28121(94)	⋯	0.28129(35)	0.28120(35)	⋯
4×4	2	3	0.2845(28)	0.2817(27)	0.2812(29)	0.28135(41)	0.28123(43)	0.28121(45)
4×4	5	3	0.2833(12)	0.2811(12)	0.2810(13)	0.28133(35)	0.28123(36)	0.28126(37)
4×4	8	3	0.28267(98)	0.28121(94)	⋯	0.28129(35)	0.28120(35)	⋯
4×4	2	4	⋯	0.2817(27)	0.2812(29)	⋯	0.28123(43)	0.28121(45)
4×4	5	4	⋯	0.2811(12)	0.2810(13)	⋯	0.28124(36)	0.28125(37)
4×4	8	4	⋯	0.28122(94)	⋯	⋯	0.28121(35)	⋯
RGEVP	2	1	0.2845(28)	0.2817(27)	0.2812(29)	0.28134(41)	0.28126(43)	0.28123(45)
RGEVP	5	1	0.2833(12)	0.2811(12)	0.2810(13)	0.28133(35)	0.28125(36)	0.28125(37)
RGEVP	8	1	0.28267(98)	0.28122(94)	⋯	0.28129(35)	0.28121(35)	⋯
RGEVP	2	2	0.2845(28)	0.2817(27)	0.2812(29)	0.28134(41)	0.28124(43)	0.28122(45)
RGEVP	5	2	0.2833(12)	0.2811(12)	0.2810(13)	0.28133(35)	0.28124(36)	0.28125(37)
RGEVP	8	2	0.28267(98)	0.28122(94)	⋯	0.28129(35)	0.28121(35)	⋯
RGEVP	2	3	0.2845(28)	0.2817(27)	0.2812(29)	0.28136(41)	0.28122(43)	0.28121(45)
RGEVP	5	3	0.2833(12)	0.2810(12)	0.2810(13)	0.28134(35)	0.28123(36)	0.28125(37)
RGEVP	8	3	0.28267(98)	0.28121(94)	⋯	0.28129(35)	0.28120(35)	⋯
RGEVP	2	4	⋯	0.2817(27)	0.2812(29)	⋯	0.28123(43)	0.28121(45)
RGEVP	5	4	⋯	0.2810(12)	0.2810(13)	⋯	0.28123(36)	0.28125(37)
RGEVP	8	4	⋯	0.28121(94)	⋯	⋯	0.28120(35)	⋯

TABLE XXXV. Same as Table XXXIV, but for the $I = 2$ two-pion first excited state on the 24^3 lattice. The rebasing matrix is calculated as $4 \times 4 \to 3 \times 3$ at $t_0 = 4$.

GEVP type	δ_t	$t - t_0$	$t = 4$	$t = 6$	$t = 8$	$t = 4$ w DR	$t = 6$ w DR	$t = 8$ w DR
2×2	2	1	0.6117(20)	0.6059(21)	0.6048(33)	0.60974(53)	0.60821(78)	0.6068(17)
2×2	5	1	0.6102(13)	0.6059(14)	0.6065(22)	0.60941(43)	0.60833(58)	0.6085(11)
2×2	8	1	0.6101(13)	0.6059(13)	⋯	0.60935(40)	0.60810(51)	⋯
2×2	2	2	0.6117(20)	0.6059(21)	0.6048(33)	0.60974(53)	0.60821(78)	0.6068(17)
2×2	5	2	0.6102(13)	0.6059(14)	0.6065(22)	0.60940(43)	0.60833(58)	0.6085(11)
2×2	8	2	0.6101(13)	0.6059(13)	⋯	0.60935(40)	0.60810(51)	⋯
2×2	2	3	0.6117(20)	0.6059(21)	0.6048(33)	0.60974(53)	0.60821(78)	0.6068(17)
2×2	5	3	0.6102(13)	0.6059(14)	0.6065(22)	0.60940(43)	0.60833(58)	0.6085(11)
2×2	8	3	0.6101(13)	0.6059(13)	⋯	0.60935(40)	0.60810(51)	⋯
2×2	2	4	⋯	0.6059(21)	0.6048(33)	⋯	0.60821(78)	0.6068(17)
2×2	5	4	⋯	0.6059(14)	0.6065(22)	⋯	0.60833(58)	0.6085(11)
2×2	8	4	⋯	0.6059(13)	⋯	⋯	0.60810(51)	⋯
3×3	2	1	0.6111(20)	0.6054(21)	0.6049(33)	0.60913(53)	0.60775(79)	0.6069(16)
3×3	5	1	0.6097(13)	0.6056(14)	0.6066(22)	0.60887(43)	0.60803(58)	0.6086(11)
3×3	8	1	0.6095(13)	0.6056(13)	⋯	0.60882(40)	0.60779(52)	⋯
3×3	2	2	0.6111(20)	0.6054(21)	0.6050(33)	0.60913(53)	0.60775(79)	0.6070(16)
3×3	5	2	0.6097(13)	0.6056(14)	0.6066(22)	0.60887(43)	0.60803(58)	0.6086(11)
3×3	8	2	0.6095(13)	0.6056(13)	⋯	0.60882(40)	0.60779(52)	⋯
3×3	2	3	0.6111(20)	0.6054(21)	0.6049(33)	0.60913(53)	0.60775(79)	0.6069(16)
3×3	5	3	0.6097(13)	0.6056(14)	0.6066(22)	0.60887(43)	0.60803(58)	0.6086(11)
3×3	8	3	0.6095(13)	0.6056(13)	⋯	0.60882(40)	0.60779(52)	⋯
3×3	2	4	⋯	0.6054(21)	0.6050(33)	⋯	0.60774(79)	0.6070(16)
3×3	5	4	⋯	0.6056(14)	0.6066(22)	⋯	0.60803(58)	0.6086(11)
3×3	8	4	⋯	0.6056(13)	⋯	⋯	0.60779(52)	⋯
4×4	2	1	0.6111(20)	0.6054(21)	0.6047(33)	0.60908(53)	0.60771(79)	0.6067(17)
4×4	5	1	0.6096(13)	0.6056(14)	0.6065(22)	0.60881(42)	0.60797(58)	0.6085(11)
4×4	8	1	0.6095(13)	0.6055(13)	⋯	0.60877(39)	0.60773(52)	⋯
4×4	2	2	0.6111(20)	0.6053(21)	0.6048(33)	0.60908(53)	0.60770(79)	0.6068(17)
4×4	5	2	0.6096(13)	0.6056(14)	0.6065(22)	0.60881(42)	0.60797(58)	0.6085(11)
4×4	8	2	0.6095(13)	0.6055(13)	⋯	0.60877(39)	0.60773(52)	⋯
4×4	2	3	0.6111(20)	0.6053(21)	0.6048(33)	0.60908(53)	0.60770(79)	0.6068(17)
4×4	5	3	0.6096(13)	0.6056(14)	0.6065(22)	0.60881(42)	0.60797(58)	0.6085(11)
4×4	8	3	0.6095(13)	0.6055(13)	⋯	0.60877(39)	0.60773(52)	⋯
4×4	2	4	⋯	0.6053(21)	0.6048(33)	⋯	0.60770(79)	0.6068(17)
4×4	5	4	⋯	0.6056(14)	0.6065(22)	⋯	0.60797(58)	0.6085(11)
4×4	8	4	⋯	0.6055(13)	⋯	⋯	0.60773(52)	⋯
RGEVP	2	1	0.6111(20)	0.6054(21)	0.6048(33)	0.60908(53)	0.60771(79)	0.6068(17)
RGEVP	5	1	0.6096(13)	0.6056(14)	0.6065(22)	0.60881(42)	0.60797(58)	0.6085(11)
RGEVP	8	1	0.6095(13)	0.6055(13)	⋯	0.60877(39)	0.60774(52)	⋯
RGEVP	2	2	0.6111(20)	0.6053(21)	0.6048(33)	0.60908(53)	0.60770(79)	0.6068(17)
RGEVP	5	2	0.6096(13)	0.6056(14)	0.6065(22)	0.60881(42)	0.60797(58)	0.6085(11)
RGEVP	8	2	0.6095(13)	0.6055(13)	⋯	0.60877(39)	0.60773(52)	⋯
RGEVP	2	3	0.6111(20)	0.6053(21)	0.6048(33)	0.60909(53)	0.60770(79)	0.6068(17)
RGEVP	5	3	0.6096(13)	0.6056(14)	0.6065(22)	0.60881(42)	0.60797(58)	0.6085(11)
RGEVP	8	3	0.6095(13)	0.6055(13)	⋯	0.60877(39)	0.60773(52)	⋯
RGEVP	2	4	⋯	0.6053(21)	0.6048(33)	⋯	0.60769(79)	0.6068(17)
RGEVP	5	4	⋯	0.6056(14)	0.6065(22)	⋯	0.60797(58)	0.6085(11)
RGEVP	8	4	⋯	0.6055(13)	⋯	⋯	0.60773(52)	⋯

TABLE XXXVI. Same as Table XXXIV, but for the $I = 2$ two-pion second excited state on the 24^3 lattice. The rebasing matrix is calculated as $4 \times 4 \to 3 \times 3$ at $t_0 = 4$.

GEVP type	δ_t	$t - t_0$	$t = 4$	$t = 6$	$t = 8$	$t = 4$ w DR	$t = 6$ w DR	$t = 8$ w DR
3×3	2	1	0.8153(29)	0.8136(66)	0.798(14)	0.8168(18)	0.8159(51)	0.805(12)
3×3	5	1	0.8142(23)	0.8095(52)	0.7997(94)	0.8162(13)	0.8129(41)	0.8077(74)
3×3	8	1	0.8146(22)	0.8116(52)	⋯	0.8165(14)	0.8150(39)	⋯
3×3	2	2	0.8153(29)	0.8136(66)	0.798(14)	0.8168(18)	0.8159(51)	0.805(12)
3×3	5	2	0.8142(23)	0.8095(52)	0.7997(94)	0.8162(13)	0.8129(41)	0.8077(74)
3×3	8	2	0.8146(22)	0.8116(52)	⋯	0.8165(14)	0.8150(39)	⋯
3×3	2	3	0.8153(29)	0.8136(66)	0.798(14)	0.8168(18)	0.8159(51)	0.805(12)
3×3	5	3	0.8142(22)	0.8095(52)	0.7997(94)	0.8162(13)	0.8129(41)	0.8077(74)
3×3	8	3	0.8146(22)	0.8116(52)	⋯	0.8165(14)	0.8150(39)	⋯
3×3	2	4	⋯	0.8136(66)	0.798(14)	⋯	0.8159(51)	0.805(12)
3×3	5	4	⋯	0.8095(52)	0.7997(94)	⋯	0.8129(41)	0.8077(74)
3×3	8	4	⋯	0.8116(52)	⋯	⋯	0.8150(39)	⋯
4×4	2	1	0.8136(29)	0.8140(66)	0.798(15)	0.8150(17)	0.8163(51)	0.805(12)
4×4	5	1	0.8130(22)	0.8098(52)	0.8000(94)	0.8150(12)	0.8133(41)	0.8080(74)
4×4	8	1	0.8134(22)	0.8119(51)	⋯	0.8153(13)	0.8154(39)	⋯
4×4	2	2	0.8135(29)	0.8143(66)	0.798(14)	0.8150(18)	0.8166(51)	0.805(12)
4×4	5	2	0.8130(22)	0.8101(52)	0.7998(95)	0.8150(12)	0.8136(41)	0.8078(74)
4×4	8	2	0.8134(22)	0.8122(51)	⋯	0.8153(13)	0.8157(39)	⋯
4×4	2	3	0.8135(29)	0.8143(66)	0.799(14)	0.8150(18)	0.8166(51)	0.806(12)
4×4	5	3	0.8130(22)	0.8102(52)	0.8002(94)	0.8150(12)	0.8136(40)	0.8082(74)
4×4	8	3	0.8134(22)	0.8122(51)	⋯	0.8153(13)	0.8157(39)	⋯
4×4	2	4	⋯	0.8143(66)	0.800(14)	⋯	0.8167(51)	0.807(11)
4×4	5	4	⋯	0.8103(52)	0.8006(95)	⋯	0.8137(41)	0.8085(75)
4×4	8	4	⋯	0.8123(51)	⋯	⋯	0.8158(39)	⋯
RGEVP	2	1	0.8135(29)	0.8147(66)	0.801(14)	0.8150(18)	0.8171(51)	0.808(12)
RGEVP	5	1	0.8130(22)	0.8105(52)	0.8016(96)	0.8150(12)	0.8139(40)	0.8096(78)
RGEVP	8	1	0.8134(22)	0.8126(51)	⋯	0.8153(13)	0.8160(39)	⋯
RGEVP	2	2	0.8135(29)	0.8145(66)	0.801(14)	0.8150(18)	0.8168(51)	0.808(12)
RGEVP	5	2	0.8130(22)	0.8103(52)	0.8014(96)	0.8150(12)	0.8138(40)	0.8094(77)
RGEVP	8	2	0.8134(22)	0.8124(51)	⋯	0.8153(13)	0.8159(39)	⋯
RGEVP	2	3	0.8137(29)	0.8141(66)	0.800(14)	0.8152(18)	0.8164(51)	0.807(11)
RGEVP	5	3	0.8131(22)	0.8099(52)	0.8008(95)	0.8151(13)	0.8134(40)	0.8088(76)
RGEVP	8	3	0.8135(22)	0.8120(51)	⋯	0.8154(13)	0.8155(39)	⋯
RGEVP	2	4	⋯	0.8141(66)	0.800(14)	⋯	0.8164(51)	0.807(11)
RGEVP	5	4	⋯	0.8099(52)	0.8008(95)	⋯	0.8134(40)	0.8088(76)
RGEVP	8	4	⋯	0.8120(51)	⋯	⋯	0.8154(39)	⋯

TABLE XXXVII. Same as Table XXXIV, but for the $I = 2$ two-pion third excited state on the 24^3 lattice.

GEVP type	δ_t	$t - t_0$	$t = 4$	$t = 6$	$t = 8$	$t = 4$ w DR	$t = 6$ w DR	$t = 8$ w DR
4×4	2	1	0.9653(70)	0.940(21)	0.841(60)	0.9700(57)	0.948(17)	0.845(60)
4×4	5	1	0.9620(58)	0.940(17)	0.905(53)	0.9670(43)	0.946(13)	0.909(54)
4×4	8	1	0.9603(57)	0.936(17)	⋯	0.9654(41)	0.943(13)	⋯
4×4	2	2	0.9653(70)	0.940(21)	0.841(60)	0.9700(57)	0.948(17)	0.845(61)
4×4	5	2	0.9620(58)	0.939(17)	0.905(53)	0.9670(43)	0.946(13)	0.910(54)
4×4	8	2	0.9603(57)	0.935(17)	⋯	0.9655(41)	0.942(13)	⋯
4×4	2	3	0.9653(70)	0.940(21)	0.840(61)	0.9700(57)	0.948(17)	0.844(61)
4×4	5	3	0.9620(58)	0.939(17)	0.905(53)	0.9670(43)	0.946(13)	0.909(54)
4×4	8	3	0.9603(57)	0.935(17)	⋯	0.9655(42)	0.942(13)	⋯
4×4	2	4	⋯	0.940(21)	0.839(61)	⋯	0.948(17)	0.843(61)
4×4	5	4	⋯	0.939(17)	0.904(53)	⋯	0.946(13)	0.909(54)
4×4	8	4	⋯	0.935(17)	⋯	⋯	0.942(13)	⋯

TABLE XXXVIII. Same as Table XXXIV, but for the $I = 0$ two-pion ground state on the 24^3 lattice. The rebasing matrix is calculated as $5 \times 5 \to 3 \times 3$ at $t_0 = 4$.

GEVP type	δ_t	$t - t_0$	$t = 3$	$t = 5$	$t = 7$	$t = 3$ w DR	$t = 5$ w DR	$t = 7$ w DR
3×3	2	1	0.2790(28)	0.2694(29)	0.2711(32)	0.27281(51)	0.27011(74)	0.2700(15)
3×3	5	1	0.2752(12)	0.2700(13)	0.2708(14)	0.27166(44)	0.26999(60)	0.27079(73)
3×3	8	1	0.27437(96)	0.2705(10)	0.2705(11)	0.27156(39)	0.27060(47)	0.27012(66)
3×3	2	2	0.2793(28)	0.2696(29)	0.2711(31)	0.27311(49)	0.27022(68)	0.2700(15)
3×3	5	2	0.2755(12)	0.2701(13)	0.2708(14)	0.27193(43)	0.27004(58)	0.27080(74)
3×3	8	2	0.27457(96)	0.2705(10)	0.2705(11)	0.27176(39)	0.27060(47)	0.27013(65)
3×3	2	3	⋯	0.2697(29)	0.2712(31)	⋯	0.27038(63)	0.2700(13)
3×3	5	3	⋯	0.2702(13)	0.2708(14)	⋯	0.27018(55)	0.27079(74)
3×3	8	3	⋯	0.2705(10)	0.2705(11)	⋯	0.27063(46)	0.27015(64)
3×3	2	4	⋯	0.2701(29)	0.2714(31)	⋯	0.27073(59)	0.2702(11)
3×3	5	4	⋯	0.2705(13)	0.2708(14)	⋯	0.27050(51)	0.27078(74)
3×3	8	4	⋯	0.2707(10)	0.2705(11)	⋯	0.27078(46)	0.27015(63)
4×4	2	1	0.2789(28)	0.2695(29)	0.2698(40)	0.27275(52)	0.27012(74)	0.2686(27)
4×4	5	1	0.2752(12)	0.2700(13)	0.2708(14)	0.27163(44)	0.26995(61)	0.27081(76)
4×4	8	1	0.27434(96)	0.2705(10)	0.2700(14)	0.27153(39)	0.27061(47)	0.2696(10)
4×4	2	2	0.2792(28)	0.2696(29)	0.2707(33)	0.27307(50)	0.27022(68)	0.2695(16)
4×4	5	2	0.2754(12)	0.2700(13)	0.2708(15)	0.27189(44)	0.27000(59)	0.27084(80)
4×4	8	2	0.27455(96)	0.2705(10)	0.2702(12)	0.27173(40)	0.27060(47)	0.26984(82)
4×4	2	3	⋯	0.2697(29)	0.2711(31)	⋯	0.27038(64)	0.2699(13)
4×4	5	3	⋯	0.2702(13)	0.2708(15)	⋯	0.27015(55)	0.27081(78)
4×4	8	3	⋯	0.2705(10)	0.2703(12)	⋯	0.27063(47)	0.27001(71)
4×4	2	4	⋯	0.2701(29)	0.2713(31)	⋯	0.27072(60)	0.2701(11)
4×4	5	4	⋯	0.2705(13)	0.2708(15)	⋯	0.27048(51)	0.27079(78)
4×4	8	4	⋯	0.2707(10)	0.2704(12)	⋯	0.27078(47)	0.27002(68)
5×5	2	1	0.2789(28)	0.2694(29)	0.2694(49)	0.27275(52)	0.27008(77)	0.2682(38)
5×5	5	1	0.2752(12)	0.2700(13)	0.2706(14)	0.27163(44)	0.26996(60)	0.27064(72)
5×5	8	1	0.27435(96)	0.2706(10)	0.2698(16)	0.27153(39)	0.27065(47)	0.2695(12)
5×5	2	2	0.2792(28)	0.2695(29)	0.2705(34)	0.27306(50)	0.27019(68)	0.2693(18)
5×5	5	2	0.2754(12)	0.2700(13)	0.2707(14)	0.27189(44)	0.27000(58)	0.27075(77)
5×5	8	2	0.27455(96)	0.2705(10)	0.2701(13)	0.27173(40)	0.27061(46)	0.26977(90)
5×5	2	3	⋯	0.2697(29)	0.2711(31)	⋯	0.27038(64)	0.2700(12)
5×5	5	3	⋯	0.2702(13)	0.2707(14)	⋯	0.27015(55)	0.27074(76)
5×5	8	3	⋯	0.2705(10)	0.2703(12)	⋯	0.27063(47)	0.27001(73)
5×5	2	4	⋯	0.2701(29)	0.2713(31)	⋯	0.27073(60)	0.2701(11)
5×5	5	4	⋯	0.2705(13)	0.2707(14)	⋯	0.27048(51)	0.27076(77)
5×5	8	4	⋯	0.2707(10)	0.2704(12)	⋯	0.27077(47)	0.27003(69)
RGEVP	2	1	0.2792(28)	0.2694(29)	0.2719(29)	0.27301(49)	0.27010(78)	0.27073(97)
RGEVP	5	1	0.2753(12)	0.2700(13)	0.2707(14)	0.27173(43)	0.27001(60)	0.27073(71)
RGEVP	8	1	0.27454(96)	0.2706(10)	0.2709(11)	0.27172(39)	0.27070(47)	0.27055(62)
RGEVP	2	2	0.2792(28)	0.2696(29)	0.2717(30)	0.27306(49)	0.27022(67)	0.2706(10)
RGEVP	5	2	0.2755(12)	0.2700(13)	0.2708(14)	0.27196(42)	0.27001(59)	0.27079(75)
RGEVP	8	2	0.27459(96)	0.2705(10)	0.2706(11)	0.27178(38)	0.27062(46)	0.27028(68)
RGEVP	2	3	⋯	0.2697(29)	0.2713(30)	⋯	0.27035(65)	0.2702(12)
RGEVP	5	3	⋯	0.2702(13)	0.2708(14)	⋯	0.27013(53)	0.27077(76)
RGEVP	8	3	⋯	0.2705(10)	0.2704(12)	⋯	0.27061(46)	0.27008(70)
RGEVP	2	4	⋯	0.2700(29)	0.2713(31)	⋯	0.27067(59)	0.2701(12)
RGEVP	5	4	⋯	0.2704(13)	0.2707(14)	⋯	0.27035(49)	0.27071(74)
RGEVP	8	4	⋯	0.2706(10)	0.2703(12)	⋯	0.27070(45)	0.26999(70)

TABLE XXXIX. Same as Table XXXIV, but for the $I = 0$ two-pion first excited state on the 24^3 lattice. The rebasing matrix is calculated as $5 \times 5 \to 3 \times 3$ at $t_0 = 3$.

GEVP type	δ_t	$t - t_0$	$t = 3$	$t = 5$	$t = 7$	$t = 3$ w DR	$t = 5$ w DR	$t = 7$ w DR
3×3	2	1	0.5415(65)	0.497(44)	0.498(49)	0.5356(63)	0.499(44)	0.498(49)
3×3	5	1	0.5279(84)	0.512(18)	0.543(21)	0.5240(83)	0.513(18)	0.544(21)
3×3	8	1	0.5331(53)	0.5315(72)	0.528(18)	0.5294(53)	0.5331(72)	0.529(18)
3×3	2	2	0.5457(46)	0.499(33)	0.502(54)	0.5398(43)	0.501(34)	0.502(54)
3×3	5	2	0.5336(56)	0.511(20)	0.546(20)	0.5296(54)	0.512(20)	0.546(20)
3×3	8	2	0.5345(44)	0.5325(74)	0.529(18)	0.5309(43)	0.5341(75)	0.530(18)
3×3	2	3	⋯	0.503(25)	0.505(62)	⋯	0.505(25)	0.506(62)
3×3	5	3	⋯	0.509(20)	0.551(19)	⋯	0.511(20)	0.552(19)
3×3	8	3	⋯	0.5329(79)	0.531(17)	⋯	0.5345(80)	0.532(17)
3×3	2	4	⋯	0.511(15)	0.499(62)	⋯	0.513(15)	0.499(62)
3×3	5	4	⋯	0.508(16)	0.555(19)	⋯	0.510(16)	0.556(19)
3×3	8	4	⋯	0.5304(81)	0.533(17)	⋯	0.5320(81)	0.534(17)
4×4	2	1	0.5411(63)	0.497(52)	0.393(75)	0.5352(61)	0.499(52)	0.393(74)
4×4	5	1	0.5270(76)	0.498(16)	0.523(46)	0.5231(75)	0.500(16)	0.524(46)
4×4	8	1	0.5303(50)	0.5268(89)	0.463(61)	0.5267(49)	0.5284(89)	0.463(61)
4×4	2	2	0.5444(48)	0.499(36)	0.433(62)	0.5385(45)	0.501(36)	0.433(62)
4×4	5	2	0.5320(54)	0.500(16)	0.526(40)	0.5281(52)	0.501(16)	0.527(40)
4×4	8	2	0.5319(44)	0.5270(87)	0.483(43)	0.5282(43)	0.5286(87)	0.484(43)
4×4	2	3	⋯	0.503(24)	0.460(59)	⋯	0.505(24)	0.460(59)
4×4	5	3	⋯	0.500(16)	0.532(34)	⋯	0.502(16)	0.533(34)
4×4	8	3	⋯	0.5272(87)	0.495(35)	⋯	0.5288(87)	0.495(34)
4×4	2	4	⋯	0.511(15)	0.464(53)	⋯	0.513(15)	0.464(53)
4×4	5	4	⋯	0.501(14)	0.536(31)	⋯	0.502(14)	0.537(31)
4×4	8	4	⋯	0.5257(86)	0.499(31)	⋯	0.5273(86)	0.500(30)
5×5	2	1	0.5411(62)	0.474(94)	0.4(1.6)	0.5352(60)	0.476(94)	0.4(1.6)
5×5	5	1	0.5268(80)	0.499(16)	0.508(42)	0.5229(79)	0.501(16)	0.509(42)
5×5	8	1	0.5304(50)	0.5274(87)	0.450(82)	0.5267(49)	0.5290(87)	0.451(82)
5×5	2	2	0.5441(48)	0.485(60)	0.44(11)	0.5382(45)	0.487(60)	0.44(11)
5×5	5	2	0.5320(53)	0.501(14)	0.519(35)	0.5281(52)	0.503(14)	0.520(35)
5×5	8	2	0.5319(44)	0.5275(84)	0.476(54)	0.5283(43)	0.5290(85)	0.477(54)
5×5	2	3	⋯	0.498(32)	0.48(11)	⋯	0.500(32)	0.48(11)
5×5	5	3	⋯	0.501(15)	0.530(31)	⋯	0.502(15)	0.530(31)
5×5	8	3	⋯	0.5274(85)	0.491(41)	⋯	0.5290(85)	0.491(41)
5×5	2	4	⋯	0.510(15)	0.474(65)	⋯	0.512(15)	0.474(65)
5×5	5	4	⋯	0.501(14)	0.536(29)	⋯	0.502(14)	0.536(29)
5×5	8	4	⋯	0.5257(86)	0.494(36)	⋯	0.5273(86)	0.495(36)
RGEVP	2	1	0.5409(62)	0.490(57)	0.487(43)	0.5350(60)	0.492(57)	0.487(43)
RGEVP	5	1	0.5268(79)	0.506(16)	0.541(27)	0.5229(79)	0.508(16)	0.542(27)
RGEVP	8	1	0.5303(50)	0.5275(98)	0.529(21)	0.5267(49)	0.5291(98)	0.530(21)
RGEVP	2	2	0.5459(43)	0.487(56)	0.523(65)	0.5400(40)	0.489(56)	0.524(65)
RGEVP	5	2	0.5325(57)	0.508(23)	0.548(21)	0.5286(56)	0.510(23)	0.549(21)
RGEVP	8	2	0.5320(48)	0.531(12)	0.556(21)	0.5284(47)	0.532(12)	0.556(21)
RGEVP	2	3	⋯	0.497(32)	0.548(85)	⋯	0.499(32)	0.548(85)
RGEVP	5	3	⋯	0.498(20)	0.558(24)	⋯	0.500(20)	0.559(24)
RGEVP	8	3	⋯	0.526(10)	0.532(32)	⋯	0.527(10)	0.532(32)
RGEVP	2	4	⋯	0.510(17)	0.509(55)	⋯	0.512(17)	0.509(55)
RGEVP	5	4	⋯	0.501(14)	0.544(38)	⋯	0.502(13)	0.545(38)
RGEVP	8	4	⋯	0.5244(88)	0.507(32)	⋯	0.5260(88)	0.507(32)

TABLE XL. Same as Table XXXIV, but for the $I = 0$ two-pion second excited state on the 24^3 lattice. The rebasing matrix is calculated as $5 \times 5 \to 3 \times 3$ at $t_0 = 1$.

GEVP type	δ_t	$t - t_0$	$t = 3$	$t = 5$	$t = 7$	$t = 3$ w DR	$t = 5$ w DR	$t = 7$ w DR
3×3	2	1	0.672(44)	0.599(96)	1.13(94)	0.666(44)	0.601(96)	1.14(94)
3×3	5	1	0.656(51)	0.78(25)	⋯	0.652(51)	0.78(25)	⋯
3×3	8	1	0.743(81)	1.5(1.3)	⋯	0.739(81)	1.5(1.3)	⋯
3×3	2	2	0.668(46)	0.60(11)	1.13(94)	0.662(47)	0.60(11)	1.14(94)
3×3	5	2	0.650(54)	0.78(25)	⋯	0.646(54)	0.78(25)	⋯
3×3	8	2	0.741(83)	1.5(1.3)	⋯	0.737(83)	1.5(1.3)	⋯
3×3	2	3	⋯	0.59(12)	1.13(93)	⋯	0.59(12)	1.14(93)
3×3	5	3	⋯	0.78(25)	⋯	⋯	0.78(25)	⋯
3×3	8	3	⋯	1.5(1.3)	⋯	⋯	1.5(1.3)	⋯
3×3	2	4	⋯	0.58(13)	1.13(92)	⋯	0.59(13)	1.14(92)
3×3	5	4	⋯	0.78(26)	⋯	⋯	0.78(26)	⋯
3×3	8	4	⋯	1.5(1.3)	⋯	⋯	1.5(1.3)	⋯
4×4	2	1	0.672(36)	0.60(12)	0.618(61)	0.666(36)	0.60(12)	0.626(61)
4×4	5	1	0.655(42)	0.655(27)	0.650(58)	0.650(42)	0.658(27)	0.656(58)
4×4	8	1	0.698(19)	0.715(23)	0.515(50)	0.694(19)	0.718(23)	0.521(50)
4×4	2	2	0.682(26)	0.59(13)	0.66(13)	0.676(26)	0.60(13)	0.66(13)
4×4	5	2	0.656(37)	0.668(32)	0.665(58)	0.651(37)	0.670(32)	0.671(58)
4×4	8	2	0.694(19)	0.720(22)	0.500(58)	0.690(20)	0.723(22)	0.506(58)
4×4	2	3	⋯	0.59(13)	0.69(16)	⋯	0.59(13)	0.70(16)
4×4	5	3	⋯	0.677(43)	0.677(63)	⋯	0.679(43)	0.683(63)
4×4	8	3	⋯	0.730(22)	0.496(61)	⋯	0.732(22)	0.501(62)
4×4	2	4	⋯	0.60(12)	0.71(17)	⋯	0.60(12)	0.71(17)
4×4	5	4	⋯	0.663(51)	0.693(69)	⋯	0.665(51)	0.698(69)
4×4	8	4	⋯	0.733(23)	0.498(63)	⋯	0.735(23)	0.503(63)
5×5	2	1	0.668(44)	0.58(12)	0.69(22)	0.662(44)	0.58(12)	0.70(22)
5×5	5	1	0.643(59)	0.656(26)	0.599(65)	0.638(59)	0.658(26)	0.605(65)
5×5	8	1	0.698(21)	0.709(22)	0.514(50)	0.694(22)	0.711(22)	0.520(50)
5×5	2	2	0.684(26)	0.57(15)	0.75(25)	0.678(26)	0.57(15)	0.75(25)
5×5	5	2	0.653(44)	0.676(35)	0.619(63)	0.649(44)	0.679(35)	0.625(63)
5×5	8	2	0.695(20)	0.717(21)	0.503(56)	0.691(20)	0.720(20)	0.508(56)
5×5	2	3	⋯	0.57(17)	0.77(23)	⋯	0.57(17)	0.77(23)
5×5	5	3	⋯	0.685(45)	0.649(59)	⋯	0.688(45)	0.654(59)
5×5	8	3	⋯	0.729(21)	0.499(59)	⋯	0.732(21)	0.504(60)
5×5	2	4	⋯	0.58(15)	0.78(25)	⋯	0.58(15)	0.79(25)
5×5	5	4	⋯	0.666(51)	0.672(62)	⋯	0.668(51)	0.677(63)
5×5	8	4	⋯	0.733(23)	0.500(62)	⋯	0.735(23)	0.505(62)
RGEVP	2	1	0.7045(98)	0.696(31)	0.616(49)	0.6985(100)	0.698(31)	0.624(50)
RGEVP	5	1	0.684(12)	0.650(34)	0.96(26)	0.679(12)	0.652(34)	0.97(26)
RGEVP	8	1	0.697(13)	0.751(60)	1.01(46)	0.693(13)	0.753(60)	1.02(46)
RGEVP	2	2	0.690(15)	0.662(41)	0.654(99)	0.684(15)	0.663(41)	0.663(99)
RGEVP	5	2	0.660(24)	0.667(80)	2.2(3.6)	0.656(24)	0.669(80)	2.2(3.6)
RGEVP	8	2	0.696(22)	0.80(11)	⋯	0.691(22)	0.81(11)	⋯
RGEVP	2	3	⋯	0.634(59)	0.72(18)	⋯	0.636(59)	0.73(18)
RGEVP	5	3	⋯	0.69(13)	⋯	⋯	0.70(13)	⋯
RGEVP	8	3	⋯	0.79(11)	⋯	⋯	0.79(11)	⋯
RGEVP	2	4	⋯	0.595(97)	0.88(44)	⋯	0.596(97)	0.89(44)
RGEVP	5	4	⋯	0.69(14)	⋯	⋯	0.69(14)	⋯
RGEVP	8	4	⋯	0.755(70)	1.19(76)	⋯	0.757(70)	1.20(76)

TABLE XLI. Same as Table XXXIV, but for the $I = 0$ two-pion third excited state on the 24^3 lattice. The rebasing matrix is calculated as $5 \times 5 \to 3 \times 3$ at $t_0 = 1$.

GEVP type	δ_t	$t - t_0$	$t = 3$	$t = 5$	$t = 7$	$t = 3$ w DR	$t = 5$ w DR	$t = 7$ w DR
4×4	2	1	0.788(49)	0.84(14)	⋯	0.782(49)	0.84(14)	⋯
4×4	5	1	0.812(69)	1.7(1.9)	⋯	0.808(69)	1.7(1.9)	⋯
4×4	8	1	0.93(19)	⋯	−0.37(30)	0.93(19)	⋯	−0.37(30)
4×4	2	2	0.775(62)	0.84(15)	⋯	0.769(62)	0.84(15)	⋯
4×4	5	2	0.806(79)	1.7(1.9)	⋯	0.802(79)	1.7(1.9)	⋯
4×4	8	2	0.94(19)	⋯	⋯	0.93(19)	⋯	⋯
4×4	2	3	⋯	0.84(16)	⋯	⋯	0.84(16)	⋯
4×4	5	3	⋯	1.7(1.9)	⋯	⋯	1.7(1.9)	⋯
4×4	8	3	⋯	⋯	⋯	⋯	⋯	⋯
4×4	2	4	⋯	0.82(19)	⋯	⋯	0.82(19)	⋯
4×4	5	4	⋯	1.7(1.9)	⋯	⋯	1.7(1.9)	⋯
4×4	8	4	⋯	⋯	⋯	⋯	⋯	⋯
5×5	2	1	0.767(60)	0.79(27)	⋯	0.761(60)	0.79(27)	⋯
5×5	5	1	0.785(77)	1.8(2.4)	⋯	0.780(77)	1.8(2.4)	⋯
5×5	8	1	0.92(24)	⋯	1.1(6.6)	0.92(24)	⋯	1.1(6.6)
5×5	2	2	0.764(77)	0.81(18)	⋯	0.758(77)	0.81(18)	⋯
5×5	5	2	0.784(99)	0.97(24)	⋯	0.779(99)	0.98(24)	⋯
5×5	8	2	0.93(22)	1.01(14)	1.2(2.0)	0.93(22)	1.01(14)	1.2(2.0)
5×5	2	3	⋯	0.81(19)	⋯	⋯	0.81(19)	⋯
5×5	5	3	⋯	1.10(27)	1.5(1.6)	⋯	1.10(27)	1.5(1.6)
5×5	8	3	⋯	1.00(14)	1.2(2.0)	⋯	1.01(14)	1.2(2.0)
5×5	2	4	⋯	0.80(23)	⋯	⋯	0.80(23)	⋯
5×5	5	4	⋯	1.19(34)	1.5(1.6)	⋯	1.20(34)	1.5(1.6)
5×5	8	4	⋯	1.00(13)	1.2(2.0)	⋯	1.00(13)	1.2(2.0)

TABLE XLII. Same as Table XXXIV, but for the $I = 0$ two-pion fourth excited state on the 24^3 lattice.

GEVP type	δ_t	$t - t_0$	$t = 3$	$t = 5$	$t = 7$	$t = 3$ w DR	$t = 5$ w DR	$t = 7$ w DR
5×5	2	1	0.906(30)	0.81(21)	⋯	0.903(31)	0.82(21)	⋯
5×5	5	1	0.879(22)	0.79(17)	1.5(1.6)	0.878(22)	0.80(17)	1.5(1.6)
5×5	8	1	0.893(28)	⋯	−0.2(6.3)	0.892(28)	⋯	−0.2(6.3)
5×5	2	2	0.891(38)	0.79(12)	⋯	0.887(39)	0.80(12)	⋯
5×5	5	2	0.864(26)	1.6(2.6)	1.5(1.6)	0.863(26)	1.6(2.6)	1.5(1.6)
5×5	8	2	0.881(36)	⋯	⋯	0.879(37)	⋯	⋯
5×5	2	3	⋯	0.77(13)	⋯	⋯	0.78(13)	⋯
5×5	5	3	⋯	1.5(2.6)	⋯	⋯	1.5(2.6)	⋯
5×5	8	3	⋯	⋯	⋯	⋯	⋯	⋯
5×5	2	4	⋯	0.75(15)	⋯	⋯	0.76(15)	⋯
5×5	5	4	⋯	1.4(2.6)	⋯	⋯	1.4(2.6)	⋯
5×5	8	4	⋯	⋯	⋯	⋯	⋯	⋯

TABLE XLIII. Same as Table XXXIV, but for the $I = 2$ two-pion ground state on the 32^3 lattice. Only results with DR are shown. The rebasing matrix is calculated as $4 \times 4 \to 3 \times 3$ at $t_0 = 5$.

GEVP type	δ_t	$t - t_0$	$t = 5$	$t = 7$	$t = 9$	$t = 11$	$t = 13$
2×2	2	1	0.21049(69)	0.21075(52)	0.21076(65)	0.21030(64)	0.20982(62)
2×2	5	1	0.21070(49)	0.21068(45)	0.21046(51)	0.21001(49)	0.20982(51)
2×2	8	1	0.21060(46)	0.21055(41)	0.21032(47)	0.21011(45)	0.20993(45)
2×2	11	1	0.21050(45)	0.21047(42)	0.21038(46)	⋯	⋯
2×2	2	3	0.21049(69)	0.21074(52)	0.21077(65)	0.21031(64)	0.20985(63)
2×2	5	3	0.21070(49)	0.21068(45)	0.21046(51)	0.21000(49)	0.20982(51)
2×2	8	3	0.21060(46)	0.21055(41)	0.21032(47)	0.21011(45)	0.20994(45)
2×2	11	3	0.21050(45)	0.21047(42)	0.21038(46)	⋯	⋯
3×3	2	1	0.21051(69)	0.21075(52)	0.21073(65)	0.21030(65)	0.20990(66)
3×3	5	1	0.21070(49)	0.21068(45)	0.21045(51)	0.21001(49)	0.20983(51)
3×3	8	1	0.21060(46)	0.21055(41)	0.21031(47)	0.21011(45)	0.20992(45)
3×3	11	1	0.21050(45)	0.21047(42)	0.21037(46)	⋯	⋯
3×3	2	3	0.21051(69)	0.21075(52)	0.21075(65)	0.21031(65)	0.20986(64)
3×3	5	3	0.21070(49)	0.21067(45)	0.21045(51)	0.21000(49)	0.20982(51)
3×3	8	3	0.21060(46)	0.21055(41)	0.21031(47)	0.21011(45)	0.20993(45)
3×3	11	3	0.21050(45)	0.21047(42)	0.21037(46)	⋯	⋯
4×4	2	1	0.21056(69)	0.21075(52)	0.21081(67)	0.21010(82)	0.2089(21)
4×4	5	1	0.21071(49)	0.21068(45)	0.21048(51)	0.21001(49)	0.2089(11)
4×4	8	1	0.21061(46)	0.21055(41)	0.21033(47)	0.21011(45)	0.20952(72)
4×4	11	1	0.21052(45)	0.21047(42)	0.21038(47)	⋯	⋯
4×4	2	3	0.21052(69)	0.21076(53)	0.21077(65)	0.21020(67)	0.20995(84)
4×4	5	3	0.21071(49)	0.21068(45)	0.21046(51)	0.20999(50)	0.20958(60)
4×4	8	3	0.21061(46)	0.21055(41)	0.21032(47)	0.21011(45)	0.20977(48)
4×4	11	3	0.21051(45)	0.21047(42)	0.21038(46)	⋯	⋯
RGEVP	2	1	0.21051(69)	0.21075(52)	0.21073(65)	0.21029(65)	0.20991(66)
RGEVP	5	1	0.21069(49)	0.21068(45)	0.21045(51)	0.21000(49)	0.20984(51)
RGEVP	8	1	0.21059(46)	0.21055(41)	0.21031(47)	0.21011(45)	0.20993(46)
RGEVP	11	1	0.21050(45)	0.21047(42)	0.21037(46)	⋯	⋯
RGEVP	2	3	0.21050(69)	0.21075(52)	0.21076(65)	0.21029(65)	0.20987(63)
RGEVP	5	3	0.21070(49)	0.21067(45)	0.21045(51)	0.21000(49)	0.20984(51)
RGEVP	8	3	0.21060(46)	0.21055(41)	0.21032(47)	0.21011(45)	0.20994(45)
RGEVP	11	3	0.21050(45)	0.21047(42)	0.21037(46)	⋯	⋯

TABLE XLIV. Same as Table XXXIV, but for the $I = 2$ two-pion first excited state on the 32^3 lattice. Only results with DR are shown. The rebasing matrix is calculated as $4 \times 4 \to 3 \times 3$ at $t_0 = 5$.

GEVP type	δ_t	$t - t_0$	$t = 5$	$t = 7$	$t = 9$	$t = 11$	$t = 13$
2×2	2	1	0.45634(84)	0.4580(12)	0.4550(15)	0.4589(21)	0.4499(33)
2×2	5	1	0.45660(55)	0.45714(76)	0.45536(100)	0.4559(14)	0.4524(21)
2×2	8	1	0.45675(52)	0.45697(70)	0.45584(90)	0.4570(12)	0.4543(19)
2×2	11	1	0.45663(51)	0.45697(68)	0.45585(85)	⋯	⋯
2×2	2	3	0.45634(84)	0.4580(12)	0.4550(15)	0.4589(21)	0.4498(33)
2×2	5	3	0.45660(55)	0.45715(76)	0.45535(100)	0.4559(14)	0.4524(21)
2×2	8	3	0.45675(52)	0.45697(70)	0.45584(90)	0.4570(12)	0.4543(19)
2×2	11	3	0.45662(51)	0.45697(68)	0.45584(85)	⋯	⋯
3×3	2	1	0.45589(82)	0.4576(11)	0.4549(15)	0.4588(21)	0.4499(33)
3×3	5	1	0.45624(54)	0.45690(75)	0.45523(97)	0.4558(14)	0.4522(21)
3×3	8	1	0.45638(51)	0.45672(69)	0.45572(87)	0.4569(12)	0.4543(19)
3×3	11	1	0.45626(50)	0.45671(67)	0.45572(82)	⋯	⋯
3×3	2	3	0.45590(82)	0.4577(11)	0.4548(15)	0.4587(21)	0.4499(33)
3×3	5	3	0.45625(54)	0.45691(75)	0.45522(96)	0.4558(14)	0.4522(21)
3×3	8	3	0.45638(51)	0.45672(69)	0.45572(86)	0.4569(12)	0.4543(19)
3×3	11	3	0.45626(50)	0.45672(67)	0.45572(82)	⋯	⋯

(Table continued)

TABLE XLIV. *(Continued)*

GEVP type	δ_t	$t - t_0$	$t = 5$	$t = 7$	$t = 9$	$t = 11$	$t = 13$
4×4	2	1	0.45582(80)	0.4576(11)	0.4550(15)	0.4587(21)	0.4507(48)
4×4	5	1	0.45619(54)	0.45689(74)	0.45529(95)	0.4555(14)	0.4501(29)
4×4	8	1	0.45633(50)	0.45670(69)	0.45576(86)	0.4565(12)	0.4529(23)
4×4	11	1	0.45621(49)	0.45669(67)	0.45574(81)	...	...
4×4	2	3	0.45583(80)	0.4577(11)	0.4548(15)	0.4588(21)	0.4497(34)
4×4	5	3	0.45620(53)	0.45690(74)	0.45521(96)	0.4557(14)	0.4509(23)
4×4	8	3	0.45633(50)	0.45670(68)	0.45569(86)	0.4567(12)	0.4533(21)
4×4	11	3	0.45621(49)	0.45669(66)	0.45568(81)	...	...
RGEVP	2	1	0.45582(81)	0.4577(11)	0.4548(15)	0.4587(21)	0.4498(33)
RGEVP	5	1	0.45619(54)	0.45689(74)	0.45516(96)	0.4557(14)	0.4520(21)
RGEVP	8	1	0.45633(51)	0.45670(68)	0.45566(86)	0.4568(12)	0.4541(19)
RGEVP	11	1	0.45620(50)	0.45669(66)	0.45564(82)	...	...
RGEVP	2	3	0.45583(81)	0.4577(11)	0.4548(15)	0.4586(21)	0.4498(33)
RGEVP	5	3	0.45620(54)	0.45689(74)	0.45517(96)	0.4557(14)	0.4521(21)
RGEVP	8	3	0.45633(51)	0.45670(69)	0.45567(86)	0.4568(12)	0.4542(19)
RGEVP	11	3	0.45621(50)	0.45669(66)	0.45565(82)	...	...

TABLE XLV. Same as Table XXXIV, but for the $I = 2$ two-pion second excited state on the 32^3 lattice. Only results with DR are shown. The rebasing matrix is calculated as $4 \times 4 \to 3 \times 3$ at $t_0 = 5$.

GEVP type	δ_t	$t - t_0$	$t = 5$	$t = 7$	$t = 9$	$t = 11$	$t = 13$
3×3	2	1	0.6146(19)	0.6142(36)	0.6294(72)	0.601(18)	0.614(37)
3×3	5	1	0.6154(14)	0.6185(27)	0.6249(52)	0.611(12)	0.635(28)
3×3	8	1	0.6152(14)	0.6166(25)	0.6240(47)	0.608(11)	0.645(27)
3×3	11	1	0.6154(13)	0.6171(25)	0.6253(47)	...	...
3×3	2	3	0.6145(19)	0.6142(36)	0.6294(72)	0.601(18)	0.615(37)
3×3	5	3	0.6154(14)	0.6185(27)	0.6249(52)	0.611(12)	0.635(28)
3×3	8	3	0.6152(14)	0.6166(25)	0.6240(47)	0.608(11)	0.645(27)
3×3	11	3	0.6154(13)	0.6171(25)	0.6253(47)	...	...
4×4	2	1	0.6141(19)	0.6125(35)	0.6290(71)	0.601(18)	0.60(37)
4×4	5	1	0.6147(14)	0.6173(26)	0.6248(53)	0.611(12)	0.638(28)
4×4	8	1	0.6146(13)	0.6156(25)	0.6238(48)	0.608(11)	0.645(27)
4×4	11	1	0.6147(13)	0.6159(24)	0.6250(48)	...	...
4×4	2	3	0.6142(19)	0.6126(35)	0.6290(72)	0.601(18)	0.602(50)
4×4	5	3	0.6147(14)	0.6173(26)	0.6249(53)	0.611(12)	0.635(28)
4×4	8	3	0.6146(13)	0.6155(25)	0.6238(48)	0.608(11)	0.644(26)
4×4	11	3	0.6148(13)	0.6159(24)	0.6250(48)	...	...
RGEVP	2	1	0.6141(19)	0.6129(35)	0.6290(71)	0.601(18)	0.620(37)
RGEVP	5	1	0.6147(14)	0.6174(26)	0.6249(53)	0.612(12)	0.636(27)
RGEVP	8	1	0.6145(13)	0.6156(25)	0.6238(48)	0.608(11)	0.644(26)
RGEVP	11	1	0.6147(13)	0.6160(24)	0.6250(48)	...	...
RGEVP	2	3	0.6141(19)	0.6125(35)	0.6290(72)	0.602(18)	0.622(37)
RGEVP	5	3	0.6147(14)	0.6173(26)	0.6250(54)	0.612(12)	0.636(27)
RGEVP	8	3	0.6145(13)	0.6155(25)	0.6239(48)	0.608(11)	0.644(26)
RGEVP	11	3	0.6147(13)	0.6159(24)	0.6251(48)	...	...

TABLE XLVI. Same as Table XXXIV, but for the $I = 2$ two-pion third excited state on the 32^3 lattice. Only results with DR are shown.

GEVP type	δ_t	$t - t_0$	$t = 5$	$t = 7$	$t = 9$	$t = 11$	$t = 13$
4×4	2	1	0.7231(40)	0.7203(94)	0.759(23)	0.697(74)	0.64(45)
4×4	5	1	0.7247(29)	0.7267(72)	0.736(17)	0.667(52)	0.635(96)
4×4	8	1	0.7240(28)	0.7248(70)	0.738(17)	0.694(51)	0.70(11)
4×4	11	1	0.7235(28)	0.7248(67)	0.745(17)	⋯	⋯
4×4	2	3	0.7231(40)	0.7202(95)	0.759(23)	0.697(74)	0.64(13)
4×4	5	3	0.7246(29)	0.7267(72)	0.736(17)	0.666(52)	0.636(98)
4×4	8	3	0.7239(28)	0.7248(70)	0.738(17)	0.694(51)	0.70(11)
4×4	11	3	0.7234(28)	0.7248(67)	0.745(17)	⋯	⋯

TABLE XLVII. Same as Table XXXIV, but for the $I = 0$ two-pion ground state on the 32^3 lattice. Only results with DR are shown. The rebasing matrix is calculated as: $5 \times 5 \to 4 \times 4$ at $t_0 = 1$, $4 \times 4 \to 3 \times 3$ at $t_0 = 2$, and $3 \times 3 \to 2 \times 2$ at $t_0 = 4$.

GEVP type	δ_t	$t - t_0$	$t = 4$	$t = 7$	$t = 9$	$t = 11$
3×3	2	1	0.20359(73)	0.20313(96)	0.2020(14)	0.20(11)
3×3	5	1	0.20304(55)	0.20252(93)	0.2017(15)	0.2022(35)
3×3	8	1	0.20287(49)	0.20269(60)	0.2020(98)	0.2013(16)
3×3	11	1	0.20280(47)	0.20226(64)	0.2011(68)	⋯
3×3	2	3	0.20397(75)	0.20319(94)	0.2023(10)	0.201(50)
3×3	5	3	0.20325(56)	0.20261(75)	0.2017(14)	0.202(18)
3×3	8	3	0.20308(51)	0.20265(60)	0.2018(12)	0.2013(31)
3×3	11	3	0.20291(48)	0.20228(61)	0.202(33)	⋯
4×4	2	1	0.20356(74)	0.20314(97)	0.201(19)	0.207(27)
4×4	5	1	0.20302(56)	0.20255(100)	0.2015(24)	0.2025(16)
4×4	8	1	0.20285(51)	0.20262(77)	0.203(12)	0.20(37)
4×4	11	1	0.20274(49)	0.2022(27)	0.2012(19)	⋯
4×4	2	3	0.20395(75)	0.2033(10)	0.2022(12)	0.201(42)
4×4	5	3	0.20322(57)	0.20264(78)	0.2016(12)	0.202(42)
4×4	8	3	0.20305(52)	0.20260(63)	0.202(27)	0.2012(16)
4×4	11	3	0.20287(49)	0.20234(67)	0.201(19)	⋯
5×5	2	1	0.20356(74)	0.20318(97)	0.205(77)	⋯
5×5	5	1	0.20303(57)	0.2025(10)	0.20(16)	⋯
5×5	8	1	0.20285(51)	0.2025(29)	0.2017(48)	0.2014(15)
5×5	11	1	0.20273(50)	0.2022(58)	0.2011(12)	⋯
5×5	2	3	0.20395(75)	0.2033(10)	0.2022(13)	0.194(57)
5×5	5	3	0.20322(57)	0.20263(79)	0.2013(17)	0.202(40)
5×5	8	3	0.20305(52)	0.20253(71)	0.203(20)	0.2013(15)
5×5	11	3	0.20286(49)	0.20236(72)	0.201(11)	⋯
RGEVP	2	1	0.20361(78)	0.20355(99)	0.2017(16)	0.2022(36)
RGEVP	5	1	0.20307(59)	0.20277(81)	0.2015(14)	0.2021(18)
RGEVP	8	1	0.20286(53)	0.20253(67)	0.2018(11)	0.2013(15)
RGEVP	11	1	0.20273(49)	0.20235(66)	0.20118(100)	⋯
RGEVP	2	3	0.20374(78)	0.20328(97)	0.2021(11)	0.2015(60)
RGEVP	5	3	0.20317(59)	0.20263(75)	0.2017(13)	0.2020(27)
RGEVP	8	3	0.20297(55)	0.20261(60)	0.20184(99)	0.201(13)
RGEVP	11	3	0.20273(51)	0.20232(66)	0.202(12)	⋯

TABLE XLVIII. Same as Table XXXIV, but for the $I = 0$ two-pion first excited state on the 32^3 lattice. Only results with DR are shown. The rebasing matrix is calculated as $5 \times 5 \to 4 \times 4$ at $t_0 = 1$, $4 \times 4 \to 3 \times 3$ at $t_0 = 2$, and $3 \times 3 \to 2 \times 2$ at $t_0 = 4$.

GEVP type	δ_t	$t - t_0$	$t = 4$	$t = 7$	$t = 9$	$t = 11$
3×3	2	1	0.4057(70)	0.43(11)	0.27(77)	0.38(60)
3×3	5	1	0.397(17)	0.31(12)	0.25(30)	0.15(56)
3×3	8	1	0.379(29)	0.31(16)	0.09(21)	0.01(22)
3×3	11	1	0.382(36)	0.28(14)	0.08(16)	⋯
3×3	2	3	0.4083(38)	0.413(71)	0.26(36)	0.31(84)
3×3	5	3	0.4065(53)	0.32(12)	0.24(26)	0.15(36)
3×3	8	3	0.3994(66)	0.32(16)	0.10(23)	0.01(22)
3×3	11	3	0.4006(67)	0.28(15)	0.08(17)	⋯
4×4	2	1	0.4049(64)	0.46(11)	0.38(34)	0.0(2.1)
4×4	5	1	0.396(19)	0.31(15)	0.24(40)	0.3(2.2)
4×4	8	1	0.376(40)	0.27(25)	−0.08(38)	−0.04(46)
4×4	11	1	0.38(18)	0.25(19)	−0.02(26)	⋯
4×4	2	3	0.4060(43)	0.43(19)	0.22(56)	0.4(1.1)
4×4	5	3	0.4062(53)	0.31(15)	0.22(35)	0.2(2.8)
4×4	8	3	0.3993(63)	0.29(24)	−0.03(36)	−0.05(30)
4×4	11	3	0.4005(61)	0.25(19)	0.00(24)	⋯
5×5	2	1	0.4054(70)	0.457(81)	0.39(52)	⋯
5×5	5	1	0.396(22)	0.31(14)	0.29(47)	⋯
5×5	8	1	0.38(12)	0.27(27)	−0.2(3.9)	−0.1(1.7)
5×5	11	1	0.40(36)	0.25(44)	−0.0(1.1)	⋯
5×5	2	3	0.4056(45)	0.43(19)	0.22(59)	0.4(1.6)
5×5	5	3	0.4062(53)	0.31(14)	0.22(43)	0.3(2.6)
5×5	8	3	0.3994(63)	0.29(26)	−0.10(52)	−0.08(55)
5×5	11	3	0.4004(60)	0.24(21)	−0.01(29)	⋯
RGEVP	2	1	0.4036(60)	0.436(19)	0.361(44)	0.357(87)
RGEVP	5	1	0.4071(51)	0.401(17)	0.351(36)	0.397(92)
RGEVP	8	1	0.3970(65)	0.397(21)	0.391(42)	0.418(88)
RGEVP	11	1	0.3976(79)	0.404(22)	0.346(44)	⋯
RGEVP	2	3	0.441(35)	0.417(95)	0.26(17)	0.29(28)
RGEVP	5	3	0.404(46)	0.32(11)	0.25(20)	0.22(27)
RGEVP	8	3	0.374(57)	0.31(13)	0.13(18)	0.03(20)
RGEVP	11	3	0.367(89)	0.25(17)	0.05(16)	⋯

TABLE XLIX. Same as Table XXXIV, but for the $I = 0$ two-pion second excited state on the 32^3 lattice. Only results with DR are shown. The rebasing matrix is calculated as $5 \times 5 \to 4 \times 4$ at $t_0 = 1$ and $4 \times 4 \to 3 \times 3$ at $t_0 = 2$.

GEVP type	δ_t	$t - t_0$	$t = 4$	$t = 7$	$t = 9$	$t = 11$
3×3	2	1	0.489(54)	0.458(74)	0.29(75)	0.35(60)
3×3	5	1	0.457(52)	0.432(49)	0.38(11)	0.39(49)
3×3	8	1	0.436(44)	0.402(25)	0.400(31)	0.432(54)
3×3	11	1	0.420(41)	0.419(18)	0.399(23)	⋯
3×3	2	3	0.486(57)	0.48(11)	0.30(25)	0.43(72)
3×3	5	3	0.447(64)	0.426(64)	0.384(98)	0.389(88)
3×3	8	3	0.415(68)	0.389(48)	0.391(55)	0.433(53)
3×3	11	3	0.401(72)	0.416(24)	0.397(27)	⋯
4×4	2	1	0.50(48)	0.459(86)	0.47(77)	0.3(1.6)
4×4	5	1	0.453(68)	0.433(54)	0.37(18)	0.3(3.1)
4×4	8	1	0.428(59)	0.396(35)	0.398(40)	0.425(24)
4×4	11	1	0.40(23)	0.420(18)	0.396(38)	⋯
4×4	2	3	0.519(22)	0.51(19)	0.30(26)	0.5(1.1)
4×4	5	3	0.465(70)	0.432(71)	0.38(15)	0.4(4.4)

(Table continued)

TABLE XLIX. *(Continued)*

GEVP type	δ_t	$t - t_0$	$t = 4$	$t = 7$	$t = 9$	$t = 11$
4×4	8	3	0.431(93)	0.380(69)	0.389(73)	0.435(32)
4×4	11	3	0.41(12)	0.421(25)	0.395(36)	⋯
5×5	2	1	0.57(58)	0.58(100)	⋯	⋯
5×5	5	1	0.448(78)	0.430(43)	0.5(1.1)	⋯
5×5	8	1	0.42(16)	0.396(38)	0.40(30)	0.4(1.1)
5×5	11	1	0.37(44)	0.41(45)	0.4(1.0)	⋯
5×5	2	3	0.519(21)	0.51(19)	0.30(26)	⋯
5×5	5	3	0.463(77)	0.430(62)	0.37(21)	0.4(6.4)
5×5	8	3	0.43(10)	0.379(73)	0.391(80)	0.436(29)
5×5	11	3	0.41(13)	0.422(23)	0.396(37)	⋯
RGEVP	2	1	0.533(10)	0.576(52)	0.41(12)	0.48(61)
RGEVP	5	1	0.523(11)	0.475(36)	0.454(54)	0.42(17)
RGEVP	8	1	0.487(19)	0.437(50)	0.35(36)	0.29(85)
RGEVP	11	1	0.467(32)	0.418(19)	0.400(25)	⋯
RGEVP	2	3	0.485(61)	0.49(13)	0.27(29)	0.45(86)
RGEVP	5	3	0.440(83)	0.436(93)	0.36(15)	0.4(1.1)
RGEVP	8	3	0.403(89)	0.381(66)	0.391(65)	0.444(70)
RGEVP	11	3	0.375(96)	0.421(30)	0.391(36)	⋯

TABLE L. Same as Table XXXIV, but for the $I = 0$ two-pion third excited state on the 32^3 lattice. Only results with DR are shown. The rebasing matrix is calculated as $5 \times 5 \to 4 \times 4$ at $t_0 = 1$.

GEVP type	δ_t	$t - t_0$	$t = 4$	$t = 7$	$t = 9$	$t = 11$
4×4	2	1	0.53(51)	0.78(35)	−0.4(1.5)	⋯
4×4	5	1	0.574(38)	0.68(29)	0.54(87)	0.6(3.7)
4×4	8	1	0.570(36)	0.58(13)	0.55(17)	⋯
4×4	11	1	0.554(22)	0.67(16)	0.53(18)	⋯
4×4	2	3	0.505(80)	0.76(33)	−0.0(1.2)	⋯
4×4	5	3	0.552(63)	0.68(28)	0.55(89)	0.6(5.5)
4×4	8	3	0.544(52)	0.57(15)	0.51(27)	⋯
4×4	11	3	0.519(41)	0.66(16)	0.50(23)	⋯
5×5	2	1	0.41(55)	0.5(1.0)	0.1(5.5)	⋯
5×5	5	1	0.571(44)	0.630(94)	⋯	⋯
5×5	8	1	0.567(42)	0.58(10)	0.5(1.4)	⋯
5×5	11	1	0.549(27)	0.641(70)	0.56(16)	⋯
5×5	2	3	0.48(10)	0.71(14)	0.43(31)	⋯
5×5	5	3	0.547(73)	0.64(11)	0.73(33)	⋯
5×5	8	3	0.540(60)	0.57(10)	0.52(22)	1.16(84)
5×5	11	3	0.514(47)	0.648(86)	0.54(17)	⋯
RGEVP	2	1	0.666(16)	0.686(88)	0.66(60)	0.3(8.2)
RGEVP	5	1	0.605(29)	0.630(99)	0.67(35)	1.0(3.3)
RGEVP	8	1	0.584(33)	0.577(80)	0.54(15)	1.4(2.4)
RGEVP	11	1	0.563(25)	0.65(11)	0.53(15)	⋯
RGEVP	2	3	0.500(83)	0.78(36)	−0.1(1.4)	⋯
RGEVP	5	3	0.548(68)	0.71(36)	0.5(1.1)	0.5(5.1)
RGEVP	8	3	0.541(54)	0.58(17)	0.51(30)	⋯
RGEVP	11	3	0.516(44)	0.67(18)	0.50(24)	⋯

TABLE LI. Same as Table XXXIV, but for the $I = 0$ two-pion fourth excited state on the 32^3 lattice. Only results with DR are shown.

GEVP type	δ_t	$t - t_0$	$t = 4$	$t = 7$	$t = 9$	$t = 11$
5×5	2	1	0.670(16)	1.8(2.5)	⋯	⋯
5×5	5	1	0.668(26)	2.1(8.2)	⋯	⋯
5×5	8	1	0.685(30)	1.3(2.0)	⋯	⋯
5×5	11	1	0.681(24)	1.4(1.7)	⋯	⋯
5×5	2	3	0.648(27)	1.7(2.4)	⋯	⋯
5×5	5	3	0.666(31)	2.1(8.2)	⋯	⋯
5×5	8	3	0.683(34)	1.3(2.1)	⋯	⋯
5×5	11	3	0.675(29)	1.4(1.7)	⋯	⋯
RGEVP	2	1	0.670(16)	1.8(2.5)	⋯	⋯
RGEVP	5	1	0.668(26)	2.1(8.2)	⋯	⋯
RGEVP	8	1	0.685(30)	1.3(2.0)	⋯	⋯
RGEVP	11	1	0.681(24)	1.4(1.7)	⋯	⋯
RGEVP	2	3	0.648(27)	1.7(2.4)	⋯	⋯
RGEVP	5	3	0.666(31)	2.1(8.2)	⋯	⋯
RGEVP	8	3	0.683(34)	1.3(2.1)	⋯	⋯
RGEVP	11	3	0.675(29)	1.4(1.7)	⋯	⋯

[1] T. Blum *et al.*, Phys. Rev. D **91**, 074502 (2015).
[2] Z. Bai *et al.* (RBC, UKQCD Collaborations), Phys. Rev. Lett. **115**, 212001 (2015).
[3] R. Abbott *et al.* (RBC, UKQCD Collaborations), Phys. Rev. D **102**, 054509 (2020).
[4] T. Blum, P. A. Boyle, V. Gülpers, T. Izubuchi, L. Jin, C. Jung, A. Jüttner, C. Lehner, A. Portelli, and J. T. Tsang (RBC, UKQCD Collaborations), Phys. Rev. Lett. **121**, 022003 (2018).
[5] M. Bruno, T. Izubuchi, C. Lehner, and A. S. Meyer, Proc. Sci. LATTICE2019 (**2019**) 239.
[6] M. Luscher, Nucl. Phys. **B354**, 531 (1991).
[7] Y. Kuramashi, M. Fukugita, H. Mino, M. Okawa, and A. Ukawa, Phys. Rev. Lett. **71**, 2387 (1993).
[8] T. Yamazaki *et al.* (*CP*-PACS Collaboration), Phys. Rev. D **70**, 074513 (2004).
[9] S. Aoki *et al.* (*CP*-PACS Collaboration), Phys. Rev. D **71**, 094504 (2005).
[10] S. R. Beane, P. F. Bedaque, K. Orginos, and M. J. Savage (NPLQCD Collaboration), Phys. Rev. D **73**, 054503 (2006).
[11] S. R. Beane, T. C. Luu, K. Orginos, A. Parreno, M. J. Savage, A. Torok, and A. Walker-Loud, Phys. Rev. D **77**, 014505 (2008).
[12] X. Feng, K. Jansen, and D. B. Renner, Phys. Lett. B **684**, 268 (2010).
[13] S. R. Beane, E. Chang, W. Detmold, H. W. Lin, T. C. Luu, K. Orginos, A. Parreno, M. J. Savage, A. Torok, and A. Walker-Loud (NPLQCD Collaboration), Phys. Rev. D **85**, 034505 (2012).
[14] J. J. Dudek, R. G. Edwards, and C. E. Thomas, Phys. Rev. D **86**, 034031 (2012).
[15] Z. Fu, Phys. Rev. D **87**, 074501 (2013).
[16] J. Bulava, B. Fahy, B. Hörz, K. J. Juge, C. Morningstar, and C. H. Wong, Nucl. Phys. **B910**, 842 (2016).
[17] R. A. Briceno, J. J. Dudek, R. G. Edwards, and D. J. Wilson, Phys. Rev. Lett. **118**, 022002 (2017).
[18] L. Liu *et al.*, Phys. Rev. D **96**, 054516 (2017).
[19] Z. Fu and X. Chen, Phys. Rev. D **98**, 014514 (2018).
[20] C. Culver, M. Mai, A. Alexandru, M. Döring, and F. X. Lee, Phys. Rev. D **100**, 034509 (2019).
[21] J. Bijnens, G. Colangelo, G. Ecker, J. Gasser, and M. E. Sainio, Phys. Lett. B **374**, 210 (1996).
[22] J. Bijnens, G. Colangelo, G. Ecker, J. Gasser, and M. E. Sainio, Nucl. Phys. **B508**, 263 (1997); **B517**, 639(E) (1998).
[23] M. Fischer, B. Kostrzewa, L. Liu, F. Romero-López, M. Ueding, and C. Urbach, Eur. Phys. J. C **81**, 436 (2021).
[24] T. Blum *et al.* (RBC, UKQCD Collaborations), Phys. Rev. D **104**, 114506 (2021).
[25] A. S. Meyer *et al.* (RBC, UKQCD Collaborations), arXiv:2304.03313.
[26] L. Maiani and M. Testa, Phys. Lett. B **245**, 585 (1990).
[27] N. H. Christ, C. Kelly, and D. Zhang, Phys. Rev. D **101**, 014506 (2020).
[28] B. Ananthanarayan, G. Colangelo, J. Gasser, and H. Leutwyler, Phys. Rep. **353**, 207 (2001).
[29] G. Colangelo, J. Gasser, and H. Leutwyler, Phys. Lett. B **488**, 261 (2000).
[30] G. Colangelo, J. Gasser, and H. Leutwyler, Nucl. Phys. **B603**, 125 (2001).

[31] R. Garcia-Martin, R. Kaminski, J. R. Pelaez, J. Ruiz de Elvira, and F. J. Yndurain, Phys. Rev. D **83**, 074004 (2011).
[32] R. Garcia-Martin, R. Kaminski, J. R. Pelaez, and J. Ruiz de Elvira, Phys. Rev. Lett. **107**, 072001 (2011).
[33] S. M. Roy, Phys. Lett. **36B**, 353 (1971).
[34] M. Luscher and U. Wolff, Nucl. Phys. **B339**, 222 (1990).
[35] B. Blossier, M. Della Morte, G. von Hippel, T. Mendes, and R. Sommer, J. High Energy Phys. 04 (2009) 094.
[36] T. Blum *et al.* (RBC, UKQCD Collaborations), Phys. Rev. D **93**, 074505 (2016).
[37] J. Tu, Ph.D. thesis, Columbia University, 2020.
[38] T. Blum, T. Izubuchi, and E. Shintani, Phys. Rev. D **88**, 094503 (2013).
[39] E. Shintani, R. Arthur, T. Blum, T. Izubuchi, C. Jung, and C. Lehner, Phys. Rev. D **91**, 114511 (2015).
[40] J. Foley, K. Jimmy Juge, A. O'Cais, M. Peardon, S. M. Ryan, and J.-I. Skullerud, Comput. Phys. Commun. **172**, 145 (2005).
[41] M. Peardon, J. Bulava, J. Foley, C. Morningstar, J. Dudek, R. G. Edwards, B. Joo, H.-W. Lin, D. G. Richards, and K. J. Juge (Hadron Spectrum Collaboration), Phys. Rev. D **80**, 054506 (2009).
[42] R. Aaij *et al.* (LHCb Collaboration), Phys. Rev. Lett. **122**, 211803 (2019).
[43] A. Soni, in *37th International Symposium on Lattice Field Theory (Lattice 2019) Wuhan, Hubei, China, 2019* (2020), arXiv:2001.10014.
[44] R. J. Sobie, Nucl. Phys. B, Proc. Suppl. **253–255**, 99 (2014).
[45] D. C. Moore and G. T. Fleming, Phys. Rev. D **73**, 014504 (2006); **74**, 079905(E) (2006).
[46] K. Rummukainen and S. A. Gottlieb, Nucl. Phys. **B450**, 397 (1995).
[47] T. Yamazaki *et al.* (*CP*-PACS Collaboration), Phys. Rev. D **70**, 074513 (2004).
[48] D. Renfrew, T. Blum, N. Christ, R. Mawhinney, and P. Vranas, Proc. Sci. LATTICE2008 (**2008**) 048.
[49] M. Abramczyk, S. Aoki, T. Blum, T. Izubuchi, H. Ohki, and S. Syritsyn, Phys. Rev. D **96**, 014501 (2017).
[50] Y. Aoki *et al.* (Flavour Lattice Averaging Group (FLAG)), Eur. Phys. J. C **82**, 869 (2022).
[51] M. A. Clark, C. Jung, and C. Lehner, EPJ Web Conf. **175**, 14023 (2018).
[52] G. Parisi, Phys. Rep. **103**, 203 (1984).
[53] M. Tomii, T. Blum, D. Hoying, T. Izubuchi, L. Jin, C. Jung, and A. Soni, Proc. Sci. LATTICE2021 (**2022**) 394.
[54] V. Cirigliano, H. Gisbert, A. Pich, and A. Rodríguez-Sánchez, J. High Energy Phys. 02 (2020) 032.